Scuola Internazionale Superiore di Studi Avanzati – Trieste

Activation of nicotinic receptors protects brainstem motoneurons from excitotoxic death

Thesis submitted for the degree of

"Doctor Philosophiae"

Candidate:

Silvia Corsini

Supervisor:

Prof. Andrea Nistri

SISSA - Via Bonomea 265 - 34136 TRIESTE - ITALY

Notes

The work described in this thesis was carried out at SISSA, Trieste, between November 2012 and November 2016. Data reported in the present thesis have been published or are under review as indicated.

Corsini S, Tortora M, and Nistri A (2016). Nicotinic receptor activation contrasts pathophysiological bursting and neurodegeneration evoked by glutamate uptake block on rat hypoglossal motoneurons. *J Physiol* 594, 6777-6798.

Tortora M, Corsini S, and Nistri A (2017) Nicotinic receptors modulate the onset of reactive oxygen species production and mitochondrial dysfunction evoked by glutamate uptake block in the rat hypoglossal nucleus. *Neuroscience letters* 639, 43-48.

Corsini S, Tortora M, Rauti R and Nistri A (2017). Nicotine protects rat hypoglossal motoneurons from excitotoxic death via downregulation of connexin 36. Under review in *Cell death and Disease*.

Data reported in Corsini et al. (2016 and 2017) and Tortora et al. (2017) arises from my own experiments and data analysis (electrophysiology, immunohistochemistry, Western Blot, Real Time/PCR, MTT-mitochondrial toxicity test, and calcium imaging) and in collaboration with Maria Tortora (immunohistochemistry, ROS evaluation, MTT, and Western Blot) and Dr. Rossana Rauti (calcium imaging). Finally, I collaborated with Filippo Ghezzi and Andrea Nistri to the conception and design of the work “Electrophysiological characterization of the M-current in rat hypoglossal motoneurons” published by *Neuroscience* (340, 62-75).

Contents

Abbreviations 7

Abstract 9

1. Amyotrophic lateral sclerosis 11

1.1. Epidemiology and clinical features 11

1.1.1. Motoneuron degeneration pathogenesis 13

1.1.2. Excitotoxicity 13

1.1.3. Mitochondrial dysfunction 14

1.1.4. Oxidative stress 15

1.1.5. Protein misfolding and aggregations 16

1.1.6. Other ALS causes 16

2. Hypoglossal nucleus 18

2.1. Location, organization and function of the hypoglossal nucleus 18

2.2. Hypoglossal motoneuron receptors and intrinsic properties 22

2.2.1. Synaptic transmission in HMs 22

2.2.2. Intrinsic properties of HMs 24

2.3. Hypoglossal motoneurons in pathological conditions and excitotoxicity studies 27

3. Nicotinic ACh receptors 29

3.1. Cholinergic systems in the brain 29

3.1.1. ACh receptor subtypes 31

3.2. Nicotinic ACh receptors 31

3.2.1. nAChR genes and molecular structure 31

3.2.2. nAChR life cycle 34

3.2.3. nAChR desensitization and upregulation 35

3.2.4. nAChR localization and their function 37

3.2.5. nAChR distribution in the brain and expression during development and aging 38

3.2.5.1. nAChRs in the nucleus hypoglossus 39

3.2.6. nAChR role in normal brain function and mental disorders..... 39

3.3. Nicotine..... 42

Aims of the study.....45

Nicotinic receptor activation contrasts pathophysiological bursting and neurodegeneration evoked by glutamate uptake block on rat hypoglossal motoneurons

Nicotinic receptors modulate the onset of reactive oxygen species production and mitochondrial dysfunction evoked by glutamate uptake block in the rat hypoglossal nucleus

Nicotine protects rat hypoglossal motoneurons from excitotoxic death via downregulation of connexin 36

Discussions.....47

1. Outlook for present and future studies 51

1.1. Current animal model in use 51

1.1.1. Canine neurodegenerative myelopathy 51

1.1.2. Transgenic animals 52

1.2. Limitations of the current models..... 53

1.2.1. nAChR positive allosteric modulators 54

1.3. Concluding remarks..... 55

References.....56

Abbreviations

ACh, acetylcholine
AD, Alzheimer's disease
ALS, amyotrophic lateral sclerosis
AMPA, 5-methyl-4-isoxazole propionate
AP5, (2R)-amino-5phosphonovaleric acid
ATF6, activating transcription factor 6
CNS, central nervous system
CPGs, central pattern generators
Cx36, connexin 36
DHβE, dihydro-beta-erythroidine
DNQX, 6,7-dinitroquinoxaline-2,3-dione
EAATs, excitatory amino acid transporters
ER, endoplasmic reticulum
fALS, familial amyotrophic lateral sclerosis
FUS, fusion in malignant liposarcoma
HMs, hypoglossal motoneurons
IRE1, inositol-requiring enzyme 1
Kin, knock-in
Ko, knock-out
mAChRs, muscarinic acetylcholine receptors
mGluR, metabotropic glutamatergic receptors
MLA, methyllycaconitine
nAChRs, nicotinic acetylcholine receptors
NMDA, N-methyl-D-aspartate
PAMs, positive allosteric modulators
PD, Parkinson's disease
PERK, protein kinase RNA-like ER kinase
Rho 123, rhodamine 123

RNS, reactive nitrogen species

ROS, reactive oxygen species

sALS, sporadic amyotrophic lateral sclerosis

SOD1, superoxide dismutase 1

TBOA, DL-threo-β-benzyloxyaspartate

TDP-43, TAR DNA binding-protein

UPR, unfolded protein response

Abstract

Amyotrophic lateral sclerosis (ALS) is a neurodegenerative disease characterized by progressive muscular paralysis reflecting patchy motoneuron degeneration. The exact causes are still unknown, but it is thought to be a complex interplay among multiple pathological mechanisms, such as excitotoxicity, mitochondrial dysfunction, increased reactive oxygen species, and endoplasmic reticulum stress. High levels of glutamate have been detected in the cerebrospinal fluid of ALS patients due to decreased function of the excitatory aminoacid transporter (EAAT) proteins, responsible for glutamate re-uptake. We, therefore, hypothesize that glutamate-induced excitotoxicity is one major provoking mechanism of ALS. During disease progression, the hypoglossal nucleus is one of the most affected motor nuclei due to some peculiarities of its motoneurons, like Ca^{2+} permeable AMPA receptors, low Ca^{2+} buffer capacity and poor EAAT expression. Thus, these characteristics make hypoglossal motoneurons (HMs) readily vulnerable to glutamate excitotoxicity. To investigate the early pathological mechanisms activated by excitotoxic stress, we used an established *in vitro* model of the neonatal rat brainstem slice containing the nucleus hypoglossus in which excitotoxicity is induced by the glutamate uptake blocker DL-threo-β-benzyloxyaspartate, TBOA. Because the activation of nicotinic acetylcholine receptors (nAChRs) by nicotine has manifested neuroprotective function in certain brain neurons, we investigated if nicotine could arrest the progression of the excitotoxic damage to highly vulnerable HMs. On about 50% of HMs, TBOA evoked intense network bursting activity and large Ca^{2+} transients that were inhibited by 1-10 µM nicotine, whereas nAChR antagonists facilitated burst emergence in non-bursting cells. Moreover, nicotine inhibited glutamatergic transmission and enhanced GABA and glycine release. The strong neuroprotection given by nicotine prevented cell loss after 4h of continuous TBOA exposure. This neuroprotective action was due to block of downstream processes of neurotoxixcity such as impaired energy metabolism, increased intracellular reactive oxygen species, upregulated genes involved in the endoplasmic reticulum stress, and increased level of the apoptotic inducing factor (AIF). We hypothesised that the neuroprotective role of nicotine was mediated by its effect on gap junctions and, in particular, on connexin 36, which supports excitotoxicity spread. Moreover, nicotine

raised the expression levels of the heat shock protein 70 (Hsp70), a protective molecule that binds AIF preventing its nuclear translocation associated with cell death. Our results suggest that activation of nAChRs should be a potential target for inhibiting excitotoxic damage of motoneurons at an early stage of the neurodegenerative process.

Introduction

1. Amyotrophic lateral sclerosis

Amyotrophic lateral sclerosis (ALS), also known as Lou Gehrig's disease or Charcot disease, is a neurodegenerative disease characterized by progressive muscular paralysis reflecting the loss of cortical, brainstem, and spinal motoneurons. ALS symptoms were firstly described by Charles Bell (1774 – 1842) in 1824, but it was the French neurobiologist and physician Jean-Martin Charcot (1825 – 1893) to connect the clinical signs and the neuropathology features in the 1860s (Rowland LP, 2001). ALS leads to death due to respiratory failure after a progressive muscular paralysis (Orsini et al., 2015).

1.1. Epidemiology and clinical features

ALS is classified as a rare disease inasmuch the incidence ranges between 1.5 to 2.5 for 100,000 patients per year in Europe and North America. Nevertheless, there are some geographic loci of the Western Pacific where prevalence of ALS is 50 - 100 times higher than elsewhere in the world, like the Kii Peninsula of Japan, the islands of Guam and Rota, and southern West New Guinea (Hermosura and Garruto, 2007; Wijesekera and Leigh, 2009). From the first symptoms the mean survival is of about 36 months but it could varies considerably between few months to 10 -15 years (Soriani and Desnuelle, 2009).

About 90% of the patients are affected by the sporadic form of ALS (sALS) in which onset usually occurs in the age range of 55 – 65, with a mean of 64 years; and a slight male prevalence (M:F ratio ~1.5:1), probably connected to possible protective hormonal factors in women (Calvo et al., 2014; Orsini et al., 2015). About two thirds of sALS patients manifest a spinal form of the disease, which firstly affects lower motoneurons either distally or proximally in the upper and/or lower limbs (Orsini et al., 2015; Wijesekera and Leigh, 2009). First symptoms are asymmetric and characterized by weakness and wasting of the muscles, which evolve in spasticity of the weakened limbs affecting manual dexterity and gait (Wijesekera and Leigh, 2009; Zarei et al., 2015). Patients who manifest dysarthria as first symptom followed by dysphagia present the

bulbar sALS form which affects about the 30% of patients (Wijesekera and Leigh, 2009; Zarei et al., 2015). Limbs weakness can occur simultaneously or within 2 years (Wijesekera and Leigh, 2009).

The familiar form of ALS (fALS) is manifested in 5-10% of the cases, with a pathological and clinical presentation similar to sALS (Zarei et al., 2015). In this case, the mean age of onset is about a decade earlier compared with sALS and the disease connected with both autosomal dominant and recessive pattern of inheritance affects equally males and females (Wijesekera and Leigh, 2009). Till now, researchers have discovered more than 20 gene mutations involved in fALS and sALS, where the most frequent is C9ORF72 (Calvo et al., 2014).

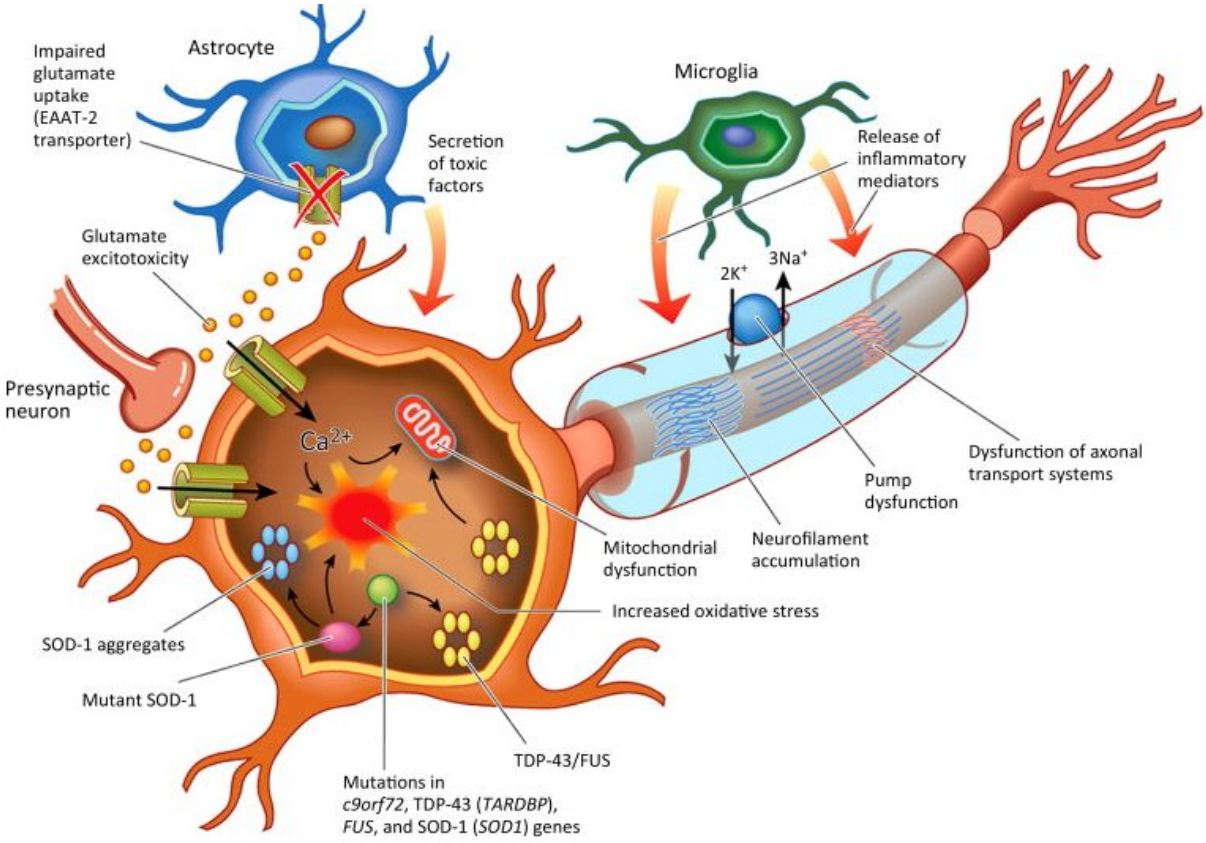

Figure 1. Schematic representation of the diverse pathological process that may contribute in motoneuron degeneration pathogenesis (from Vucic and Kiernan, 2010).

1.1.1. Motoneuron degeneration pathogenesis

In ALS patients, motoneuron degeneration causes remain unknown for the majority of cases, most likely they are due with a vast and complex interplay among multiple and interconnected mechanisms (Fig. 1).

1.1.2. Excitotoxicity

The major excitatory neurotransmitter in the central nervous system (CNS) is glutamate, which is virtually involved in most activities of the brain (Lewerenz and Maher, 2015; Miladinovic et al., 2015). Once released into the synaptic cleft, in addition to metabotropic receptor activation, glutamate binds to postsynaptic ionotropic receptors (AMPA, kainate, and NMDA), which mediate sodium and calcium influx into the cell, leading to plasma membrane depolarization and action potential generation (Lewerenz and Maher, 2015; Van Den Bosch et al., 2006). Increases of glutamate levels in the extracellular space to a concentration of 2-5 µM are able to induce neuronal dysfunction and death, a process called excitotoxicity (Fig. 2; Dong et al., 2009; Van Den Bosch et al., 2006). Excitotoxicity can be activated by an increase of the neurotransmitter release or by a deficit in the glutamate uptake system (Van Den Bosch et al., 2006). Glutamate re-uptake is mediated by the excitatory amino acid transporters (EAATs), located on astrocytes, oligodendrocites and neurons (Miladinovic et al., 2015). The isoform GLT-1/EAAT2, which is found on the astrocytic plasma membrane, is the most abundant and widely expressed throughout the CNS and responsible for about 90% of glutamate re-uptake (Miladinovic et al., 2015; Van Den Bosch et al., 2006). In autopsied ALS patients a pronounced EAAT2 reduction in the grey matter has been observed with significant loss of motoneurons (Rothstein et al., 1992, 1995; Sasaki et al., 2000). Moreover, probably as a consequence of the downregulation of the EAAT2, in the CSF of ALS patients glutamate levels are increased (Rothstein et al., 1990).

Although excitotoxicity could affect any kind of neuron, several data highlight a particular vulnerability of hypoglossal motoneurons (HMs; Van Den Bosch et al., 2006) due to expression of GluR2-lacking AMPA receptors (Laslo et al., 2001), large amount of intracellular free Ca^{2+} (Ladewig et al., 2003), and relatively low levels of glutamate transporters (Rothstein et al., 1992) and Ca^{2+} binding proteins (Medina et al., 1996). Moreover, gap junctions play a pivotal role and

are the fundamental determinants for spreading excitotoxicity and the following cell death (Belousov and Fontes, 2014).

Glutamate dysfunctions are not limited to ALS, but are involved in other central pathologies such as neurodegenerative diseases (Alzheimer's disease, Parkinson's disease and Hungtingon's disease), and neurodevelopment and psychiatric disorders (Dong et al., 2009; Lewerenz and Maher, 2015; Miladinovic et al., 2015).

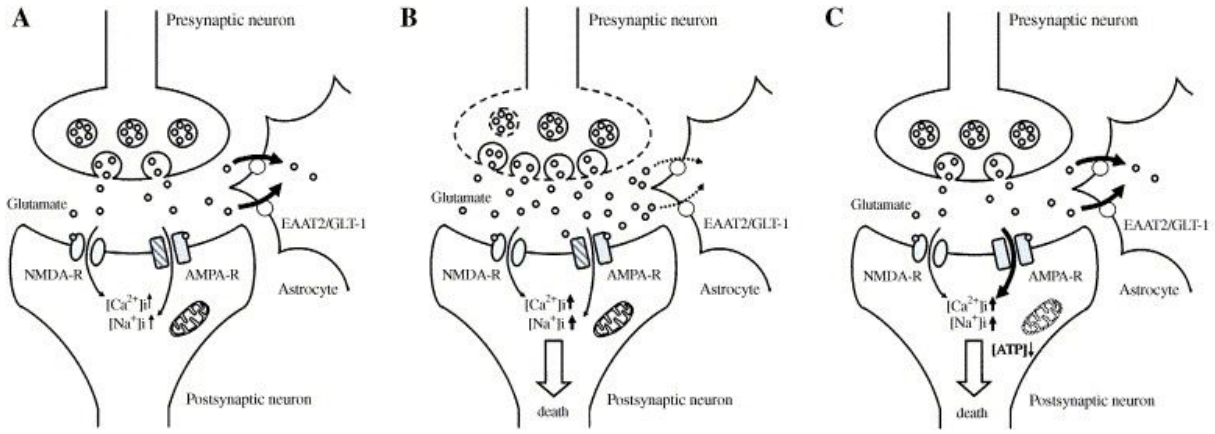

Figure 2. Glutamatergic neurotransmission and excitotoxicity. A, in normal condition, presynaptic glutamate release activates AMPA and NMDA receptors due with Na^+ and Ca^{2+} ions influx, depolarization of the postsynaptic neuron and action potential stimulation. B, Increased concentration of extracellular glutamate induces classical excitotoxicity. Thus, it can be induced by deficit in glutamate re-uptake by the EAAT2/GLT-1 transporters (located on astrocytes) or by an increase of glutamate release. Excessive stimulation of AMPA and NMDA receptors increased intracellular concentration of Na^+ and Ca^{2+} ions, which can results in neuronal death. Neuronal disintegration causes a further increase of extracellular glutamate and amplifies the excitotoxic damage. C, Slow excitotoxicity is induced by an increase in the sensitivity of the postsynaptic neurons to glutamate stimulation, although unchanged concentrations of extracellular glutamate. This alteration can be caused by changes in glutamate receptor properties, resulting in higher intracellular Ca^{2+} concentration, or by mitochondrial distress, compromising energetically neurons (from Van Den Bosch et al., 2006).

1.1.3. Mitochondrial dysfunction

Mitochondria are pivotal organelles in the cell, playing a complex role not only in energy metabolism but also in the storage of calcium ions. Together with the endoplasmic reticulum (ER) they are the most important buffers for calcium homeostasis. Moreover, mitochondria are

key organelles in the activation of apoptosis mechanisms through the release of cytochrome c (Fukunaga et al., 2015).

Like in other neurodegenerative disorders, in ALS there are some peculiar mitochondrial configurations or alterations, suggesting a possible association between mitochondrial dysfunction and degeneration (Sasaki and Iwata, 2007; Schon and Przedborski, 2011). In particular, the majority of abnormalities were observed in mitochondria located in motoneuron dendrites (Vinsant et al., 2013). Many studies have associated mitochondrial alteration with the misfolded protein superoxide dismutase 1 (SOD1), one of the genes that have been found to be mutated in ALS patients (Sasaki and Iwata, 2007; Vinsant et al., 2013). SOD1 was the first mutated gene associated to fALS and by now more than 150 mutations have been identified in this gene (Rosen et al., 1993; Vehviläinen et al., 2014). Its role is correlated with the elimination of the reactive oxygen species (ROS), which are linked to dysfunction of mitochondria and induction of apoptosis (Fukunaga et al., 2015). In the last two decades, SOD1 mutations have been extensively studied, contributing significantly to the understanding of ALS pathology, even if less than 1% of ALS patients express SOD1 mutations (Carrì et al., 2015). Disease pathogenesis might be directly associated with mitochondrial deficits in the respiratory chain, ATP production and calcium uptake (Carrì et al., 2015; Palomo and Manfredi, 2015; Schon and Przedborski, 2011).

1.1.4. Oxidative stress

The oxidative stress, a process tightly connected with mitochondrial dysfunction, is the mechanism generated by an imbalance between an excessive generation of ROS or reactive nitrogen species (RNS) and the antioxidant cell system (Kim et al., 2015). ROS are a group of oxygen-derived molecules, such as superoxide radical anion (O_2^-), hydroperoxyl radical (HO_2), and hydrogen peroxide (H_2O_2), which have cytotoxic effects (Chiurchiù et al., 2016; Kim et al., 2015). ROS formation could be induced either by exogenous sources, like chemicals, radiation, and atmospheric pollutants, or endogenously by mitochondria, ER, and peroxisomes (Chiurchiù et al., 2016; Kim et al., 2015). Mitochondrial ROS production is related to the respiratory chain complexes, whereas ER production of ROS is connected with protein folding and lipid biosynthesis (Kim et al., 2015). The antioxidant system is driven by SOD which transforms the

superoxide O_2^- into H_2O_2 that may be further reduced to H_2O by glutathione peroxidases, catalases, and peroxiredoxins (Kim et al., 2015; Vehviläinen et al., 2014). At physiological levels, ROS/RNS regulate important functions, but increased concentrations could induce molecule damage in living organisms (Niedzielska et al., 2015). Many studies have revealed the increase of different ROS/RNS biomarkers in ALS patients suggesting their association with disease progression; conversely, divergent results have been obtained with antioxidant biomarkers (D'Amico et al., 2013; Niedzielska et al., 2015; Pollari et al., 2014).

1.1.5. Protein misfolding and aggregations

A hallmark of ALS are intra-cytoplasmic inclusions which may have a role in pathogenesis or induction of cytotoxicity (Blokhuis et al., 2013; Ciechanover and Kwon, 2015; Kabashi and Durham, 2006; Wijesekera and Leigh, 2009). These inclusions are the result of aberrant protein sequestration resulting from pathological or physiological processes that, in the ER, alter the normal protein folding or induce ER stress (Doyle et al., 2011; Kabashi and Durham, 2006). In case of ER stress, the cell activates a series of pro-survival pathways, that collectively are called the unfolded protein response (UPR) (Doyle et al., 2011; Hetz et al., 2013). Initially UPR blocks the normal protein synthesis and activates processes capable of managing the increase of unfolded proteins and restore homeostasis, but if the cell is highly damaged UPR induces apoptosis (Doyle et al., 2011; Hetz et al., 2013). Three are the main sensors of ER stress in mammals: the activating transcription factor 6 (ATF6, α and β isoforms); the inositol-requiring enzyme 1 (IRE1, α and β); and the protein kinase RNA-like ER kinase (PERK). In ALS patients UPR sensors are increased, but it remains unclear if they are addressed leading to induce or are neuroprotective (Doyle et al., 2011; Matus et al., 2013).

1.1.6. Other ALS causes

As previously reported, a small percentage of the disease is hereditary. fALS is due, in the majority of the cases, to an autosomal dominant transmission (Shaw, 2005). Among more than 20 discovered mutations, only four genes covered more than 50% of fALS cases: SOD1, C9orf72, fusion on malignant liposarcoma (FUS), and TAR DNA binding-protein (TDP-43; Turner et al., 2013; Zarei et al., 2015).

SOD1 was the first mutantion discovered at the beginning of 1990s; its discovery significantly helped research through the development of the first ALS animal model (Turner et al., 2013). This mutation, which induces a toxic gain of function instead of an antioxidant function impairment, affects about 20% of fALS patients (Orsini et al., 2015; Wijesekera and Leigh, 2009).

C9orf72 mutations, discovered about five years ago, are more widespread inducing the disease in up to 40% of fALS and 6% of sALS (Calvo et al., 2014; Turner et al., 2013). Its role is involved in RNA metabolism (Calvo et al., 2014).

FUS and TDP-43 are each responsible for about 5% of fALS (Calvo et al., 2014; Orsini et al., 2015). Both are involved in processes regulating gene expression and control, such as transcription, RNA splicing, transport, and translation (Zarei et al., 2015).

Other cellular mechanisms which may be involved in the pathogenesis of motoneuron degeneration in ALS are: impaired axonal transport, neurofilament aggregation, inflammatory dysfunction, and deficits in signaling pathways such as neurotrophic factors (Wijesekera and Leigh, 2009; Zarei et al., 2015).

2. Hypoglossal nucleus

2.1. Location, organization and function of the hypoglossal nucleus

The hypoglossal motor nucleus, or XII cranial nucleus, is located bilaterally in the medulla oblongata immediately beneath the base of the forth ventricle and close to the midline (Fig. 3 and 4; Krammer et al., 1979). Several studies have been performed on cats, rats and monkeys to understand the cytoarchitecture of the nucleus. Two different neuronal populations have been

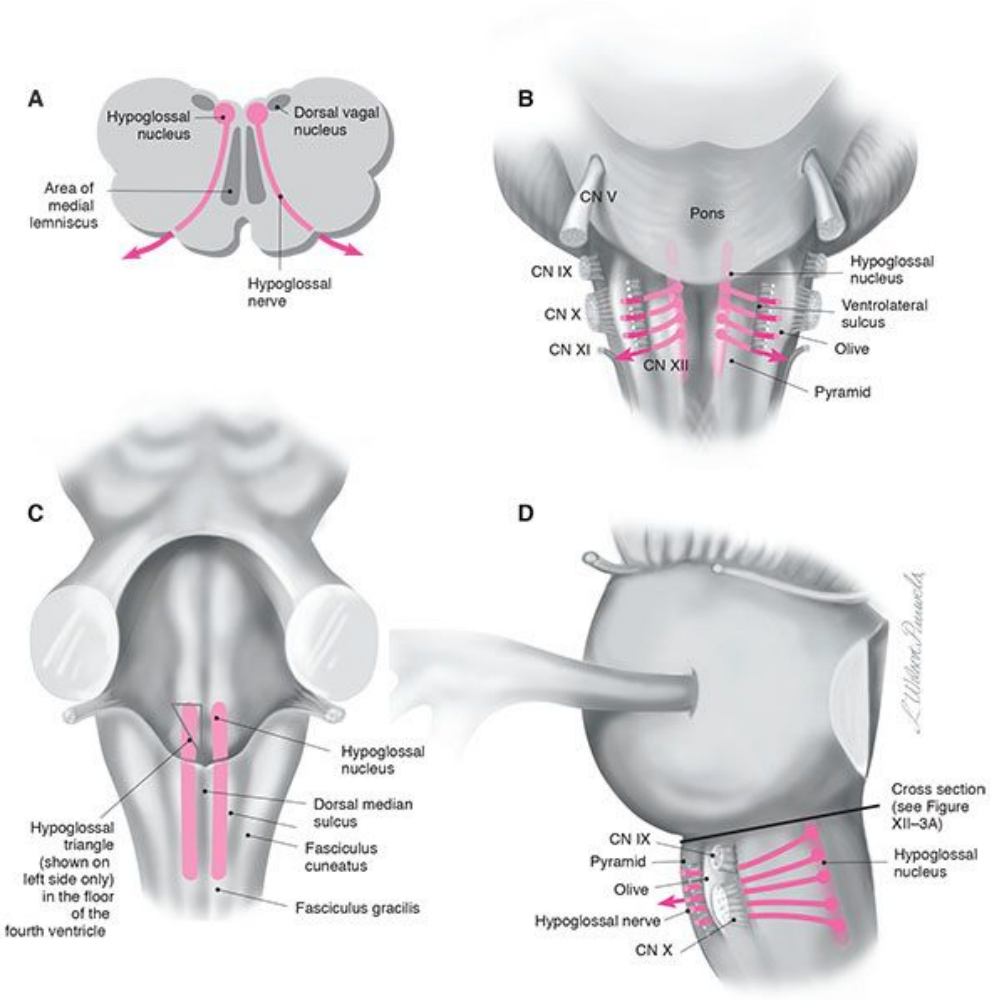

Figure 3. Views of the XII nucleus. A, Cross-section through the medulla-open portion. B, ventral view. C, Dorsal view. D, lateral view. From Wilson-Pauwels et al., 2002.

observed: group I and group II (Boone and Aldes, 1984; Cooper, 1981; Lowe, 1980; Takasu and Hashimoto, 1988). The group I includes all the motoneurons within the hypoglossal nucleus that are large multipolar cells with extended soma diameters (> 20 µm) and a variety of shapes: mainly triangular, but also bulbous, quadrangular, fusiform, and oval (Boone and Aldes, 1984; Cooper, 1981). Primal dendrites, generally 4 or 5 which divide in secondary branches, are widespread extensively within the ipsilateral and controlateral hypoglossal nucleus and into the adjacent reticular formation (Boone and Aldes, 1984; Cooper, 1981). Group II is formed by small, round or oval shaped interneurons with a diameter < 18 µm (Boone and Aldes, 1984; Cooper, 1981; Lowe, 1980; Takasu and Hashimoto, 1988). Dendrites have less branching compared with group I neurons and their cell bodies distribution is limited to the most ventral and dorsolateral region of the XII nucleus (Boone and Aldes, 1984; Takasu and Hashimoto, 1988). In accordance with their GABA-like immunoreactivity (Takasu and Hashimoto, 1988; Takasu et al., 1987) and electrophysiological properties (Peever et al., 2002; Takata, 1993), these small neurons are thought to be GABAergic interneurons with inhibitory functions.

The primary source of the inputs to the hypoglossal nucleus originated from the caudal part of the reticular formation, a set of interconnected nuclei located throughout the brainstem, and in particular from the dorsal medullary reticulum column, immediately ventral to the nucleus of the solitary tract (Borke et al., 1983; Cunningham and Sawchenko, 2000). The dorsal medullary reticulum column largely and bilaterally innervates the nucleus hypoglossus: the dorsal and the ventral subdivisions innervate the protractor and retractor muscles of the tongue (Cunningham and Sawchenko, 2000; Dobbins and Feldman, 1995). Other afferents to the XII nucleus originate from the spinal V complex, or the nucleus of the solitary tract, both with ipsilateral predominance (Borke et al., 1983), and other brainstem and forebrain regions (Lowe, 1980; Peever et al., 2002; Rekling et al., 2000). Moreover, inspiratory inputs are generated also by interneurons within the hypoglossal nucleus itself which participate in the transmission and the control of the respiratory drive (Peever et al., 2002).

Group I axons constitute the hypoglossal nerve which emerges from the preolivary sulcus of the medulla, passes into the hypoglossal canal and innervate the hypoglossus, styloglossus, geniohyoid and genioglossus muscles, forming the extrinsic musculature and all the intrinsic muscle of the tongue (Fig. 4 and 5). Extrinsic muscles alter the shape and position of the tongue,

whereas intrinsic muscles only control the shape. The myotopical organization of HMs within the nucleus controls the functional movement of the tongue (Fig. 4). In particular, in the rat, protractor muscles are innervated by HMs located in the ventrolateral subdivision of the XII nuclei (Aldes, 1995), HMs in the dorsal part are responsible for retraction (McClung and Goldberg, 2000), and intrinsic muscles receive inputs from neurons located in the middle third of the nucleus (Fig. 4; Gestreau et al., 2005; Sokoloff, 2000).

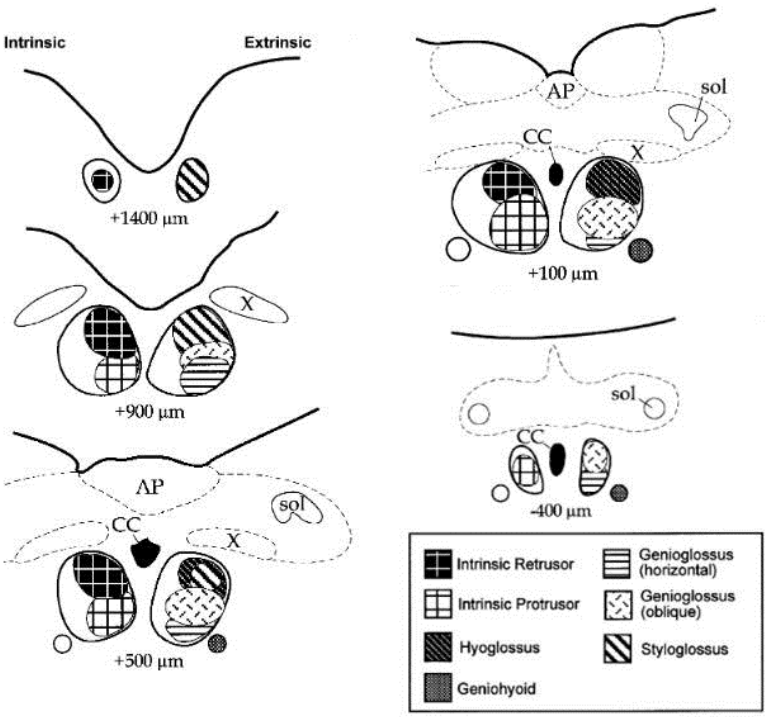

Figure 4. Myotropic organization of the hypoglossal nucleus. Schematic representation of the dorsomedial medulla at five distinct levels (rostral to caudal) expressed in µm relative to the obex. The approximate location of the HMs supplying both the intrinsic (left side) and extrinsic (righ sige) tongue muscle. Abbreviations: X, dorsal motor nucleus of the vagus; sol, tractus solitaries; AP, area postrema; CC, central canal (modified from Gestreau et al., 2005).

The innervations of tongue musculature should be functional from birth and participate in several oropharyngeal behaviors such as breathing, mastication, vocalization, swallowing, suckling and protective reflexes like coughing (Gestreau et al., 2005). Muscles contract in different combination, either synergistically or antagonistically, depending on the required movement. For example, during inspiration, the activity of the genioglossus, laryngeal, and pharyngeal muscles

are enhanced to increase airway patency and stability (Feldman and Del Negro, 2006; Peever et al., 2002); this stimulation is inhibited during swallowing to prevent

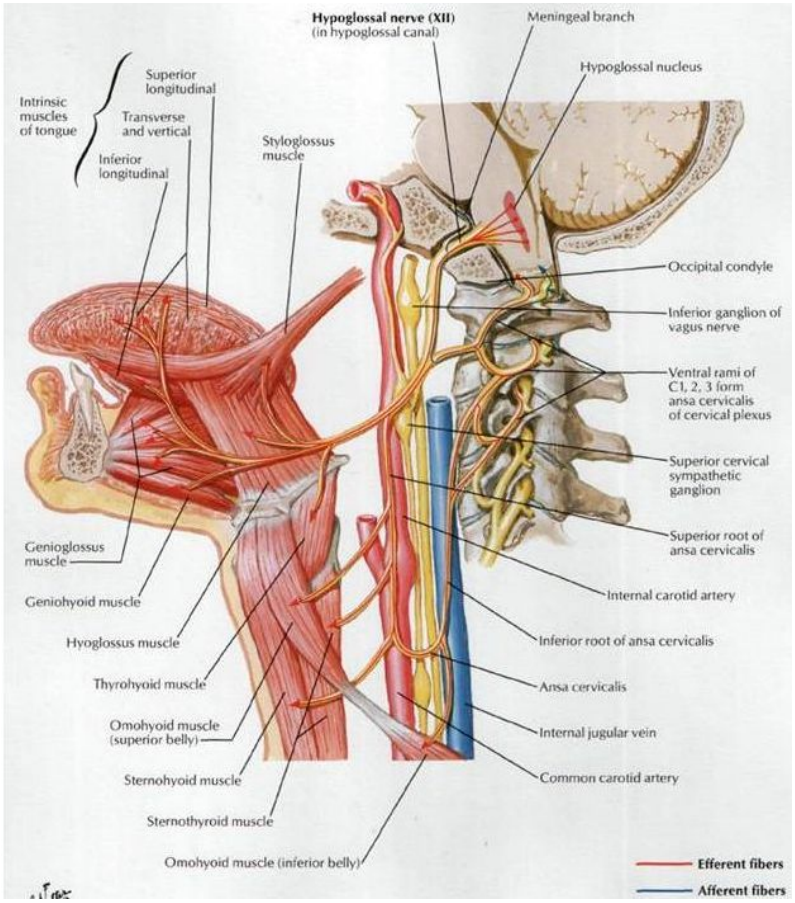

Figure 5. Hypoglossal nerve. From Netter, 2006.

food aspiration (Gestreau et al., 2005). As previously reported (Gestreau et al., 2005; Roda et al., 2002) HMs are not a homogeneous population, but rather present distinct functional pools. Roda ad collaborators (2002) analyzed simultaneously the discharge patterns of HMs during breathing, swallowing and coughing *in vivo*; their results show that some cells are active only with one behavior (swallowing), others receive inputs during breathing and swallowing, and a third population receives a synaptic drive in relation to the three tested behaviors. These results propose that common subsets of neurons in the hypoglossal nucleus are active during multiple behaviors. HMs do not provide directly rhythmic discharge, as they are not endowed with

spontaneous activity; the multiple behaviors controlled by HMs are driven by central pattern generators (CPGs), a group of functionally connected neurons located at the level of the brainstem. Neurons forming CPGs are wired together to produce rhythmic motor discharges even in absence of commands from higher centres or sensory afferents (Marder and Calabrese, 1996). Different CPGs for breathing (Suzue, 1984), swallowing (Suzue, 1984) and mastication (Nakamura and Katakura, 1995) have been identified.

2.2. Hypoglossal motoneuron receptors and intrinsic properties

2.2.1. Synaptic transmission in HMs

Synaptic transmission in the hypoglossal nucleus is mediated by glutamate, as excitatory input, and GABA and glycine, as inhibitory neurotrasmitters (Berger, 2000; Quitadamo et al., 2005; Rekling et al., 2000).

Glutamate is the main excitatory neurotransmitter and mediates about 70% of synaptic transmission within the central nervous system through three ionotropic and eight metabotropic receptors. The ionotropic receptors are ligated-coupled ion channels, classified into 5-methyl-4-isoxazole propionate (AMPA), kainate, and N-methyl-D-aspartate (NMDA) receptors; each one of them is composed of four subunits encoded by different genes. Each combination presents different channel properties in cation permeability; for example in AMPA receptors the sole presence of one GluR2 subunits facilitates Na^+ permeability, whereas GluR2 lacking receptors are highly Ca^{2+} permeable (Martínez-Lozada and Ortega, 2015; Sommer et al., 1991), as the ones in the hypoglossal nucleus (Essin et al., 2002; García Del Caño et al., 1999). AMPA and kainate receptors have fast activation and deactivation time, followed by a rapid and strong desensitization phase. NMDA receptors present a slower deactivation kinetic followed by a slow and modest desensitization (Traynelis et al., 2010). Electrophysiological (Berger et al., 1998; Funk et al., 1993; O'Brien et al., 1997) and immunohistochemical (García Del Caño et al., 1999; Williams et al., 1996) experiments have demonstrated the presence of all three types of ionotropic receptors at HM glutamatergic synapses. In neonatal rat, synaptic transmission is mainly mediated by AMPA and kainate receptors (Funk et al., 1993), a condition changed during

adulthood where also NMDA receptors are involved (Steenland et al., 2008). During the post natal period NMDA receptors are not directly involved in fast synaptic transmission, while their block inhibits dendritic branching and somatic growth of motoneurons (Kalb, 1994). Their activation triggers bursting behavior in a percentage of HMs, which resembles the pattern involved in suckling (Sharifullina et al., 2008).

Metabotropic glutatergic receptors (mGluR) are coupled with G-proteins and classified in three groups: group I (mGluR 1 and mGluR 5) stimulates phospholipase C due to intracellular Ca^{2+} release, whereas group II (mGluR 2 and mGluR 3) and group III (mGluR 4, mGluR 6, mGluR 7, and mGluR8) inhibit adenylate cyclase and negatively modulate synaptic glutamate release (Pomierny-Chamioło et al., 2014). Moreover, mGluR activation can lead to oscillatory activity in forebrain networks (Cobb et al., 2000; Hughes et al., 2002; Whittington et al., 1995), including synchronization of inhibitory transmission networks (Whittington et al., 1995). In the hypoglossal nucleus, where only the mGluR 1 has been detected (Hay et al., 1999), these channels modulate excitability and facilitate glycinergic inhibitory neurotransmission (Donato and Nistri, 2000; Donato et al., 2003; Pomierny-Chamioło et al., 2014; Sharifullina et al., 2004). Moreover, application of the selective group I mGluR agonist, dihydroxyphenylglycine – DHPG, induces persistent and regular oscillations, characterized by large outward slow current alternated by fast, repeated inward current. This phenomenon requires transmission through AMPA receptors and neurons electrically coupled via gap junctions (Sharifullina et al., 2005). This characteristic behavior suggests a potential role of mGluR 1 in facilitating rhythmic firing, such the one required during suckling behavior (Sharifullina et al., 2005).

In the hypoglossal nucleus, the inhibitory transmission is mediated by GABAergic and glycinergic synapses originating from respiratory centers like the pre Bötzinger complex (Paton and Richter, 1995), reticular formation neurons (Li et al., 1997) and hypoglossal interneurons (Peever et al., 2002). Glycine receptors are blocked by strychnine, while GABA receptors, which mainly belong to the $GABA_A$ class, are reversibly blocked by bicuculline (Barnard et al., 1993; Donato and Nistri, 2000). Both inhibitory receptors are Cl^- channels, which during the period between late embryonic and early postnatal period shift their response from depolarizing to hyperpolarizing, in relation to the change in intracellular chloride concentrations induced by the

maturation of Cl^- transporters (Singer and Berger, 2000). Nonetheless, a study on rat spinal and hypoglossal motoneurons have revealed that, already at birth, GABA and glycine are playing an inhibitory role at synaptic level (Marchetti et al., 2002). Both receptors have been detected immunohistochemically and electrophysiologically in the nucleus hypoglossus (Donato and Nistri, 2000; Muller et al., 2004; Rekling et al., 2000; Singer et al., 1998). Although both neurotransmitters might be released at the same synapse, about 70% of the inhibitory inputs are mediated by glycinergic receptors in neonatal rats (Donato and Nistri, 2000; Singer and Berger, 2000). Moreover, glycinergic currents are faster and manifest higher frequency and amplitude in comparison to GABAergic ones (Donato and Nistri, 2000).

In addition, a receptors for neuromodulators affecting motoneuronal excitability through pre- and post-synaptic mechanisms are expressed on HMs, including: norepinephrine (Parkis et al., 1995), serotonine (Berger et al., 1992), substance P (Yasuda et al., 2001), and thyrotropin-releasing hormone (Rekling, 1990). Also the cholinergic system is widespread in the hypoglossal nucleus, affecting both excitatory and inhibitory transmission to HMs, and acting via nicotinic (Lamanauskas and Nistri, 2006; Pagnotta et al., 2005; Quitadamo et al., 2005) or muscarinic receptors (Bellingham and Berger, 1996; Pagnotta et al., 2005).

2.2.2. Intrinsic properties of HMs

HM motor output is not only regulated by synaptic inputs (excitatory, inhibitory, and modulatory), but also by the intrinsic motoneuron membrane properties, such as resting membrane potential and input resistance, and the type, location and density of ion channels along the cell membrane (Berger, 2000). Series of experiments has discovered a wide range of ion channels contributing to the intrinsic properties of HMs (Fig. 6). These could be activated by depolarization or hyperpolarization from the resting membrane potential of about –70 mV in HMs (Viana et al., 1994).

HMs have the classic voltage-dependent transient tetrodotoxin-sensitive sodium current ($I_{Na\,i}$) and the delayed rectifier tetraethylammonium-sensitive K^+ current (I_{Kdr}), both involved in shaping of the action potential. The first one is involved in the rapid depolarization phase (Fig. 6A), whereas the second one contributes to the falling phase and in the fast afterhyperpolarization (fAHP; Fig.

6A,B) (Haddad et al., 1990; Lape and Nistri, 1999, 2001; Mosfeldt Laursen and Rekling, 1989; Viana et al., 1993a).

HMs posses other K^+ currents such as the transient outward (I_A), Ca^{2+}-activated K^+ (large or small conductance, $I_{KCa(BK)}$ or $I_{KCa(SK)}$ respectively) and the recently observed M-current (I_M). I_A is activated by depolarization and plays a role in affecting the duration of the action potential (Fig. 6A) and in the initial adaptation of firing occurring after injection of depolarizing current steps (Fig. 6C; Lape and Nistri, 1999; Mosfeldt Laursen and Rekling, 1989; Viana et al., 1993a). The voltage dependet-$I_{KCa(BK)}$, is activated by influx of Ca^{2+} during an action potential and is involved in the falling phase of the action potential (Fig. 6A) and in the repetitive firing behavior (Mosfeldt Laursen and Rekling, 1989; Rekling et al., 2000; Viana et al., 1993a). Although $I_{KCa(SK)}$ is activated due to Ca^{2+} influx, such current is voltage independent and mediates the medium afterhyperpolarization (mAHP) (Lape and Nistri, 2000; Mosfeldt Laursen and Rekling, 1989; Rekling et al., 2000; Viana et al., 1993a). Recently, our laboratory has reported I_M in HMs, where it regulates cell excitability depressing neuronal firing (Ghezzi et al., 2016).

HMs also express low- and high- threshold calcium channels, LVA (I_{CaLVA}; T-type) and HVA (I_{CaHVA}; N-, P/Q- and L-types), respectively. Ca^{2+} conductances are involved in the repolarization of the action potential, the spike afterdepolarization and afterhypolarization (Fig. 6A: Umemiya and Berger, 1994; Viana et al., 1993b). The mixed cationic Na^+/K^+ hyperpolarization-activated current (I_h) contributes to the resting membrane potential stabilization and underlies rebound depolarization and hyperpolarizations (Fig. 6B; Bayliss et al., 1994; Viana et al., 1994). Moreover, the persistent inward currents mediated by Na^+ (I_{NaP}) and/or Ca^{2+} (I_{CaP}), which is activated below spike threshold, accelerate subthreshold membrane depolarization to spike threshold, integrating synaptic inputs and prolonging rhythmic discharges (Fig. 6A, B; Del Negro et al., 2005; Lamanauskas and Nistri, 2008; Rekling et al., 2000).

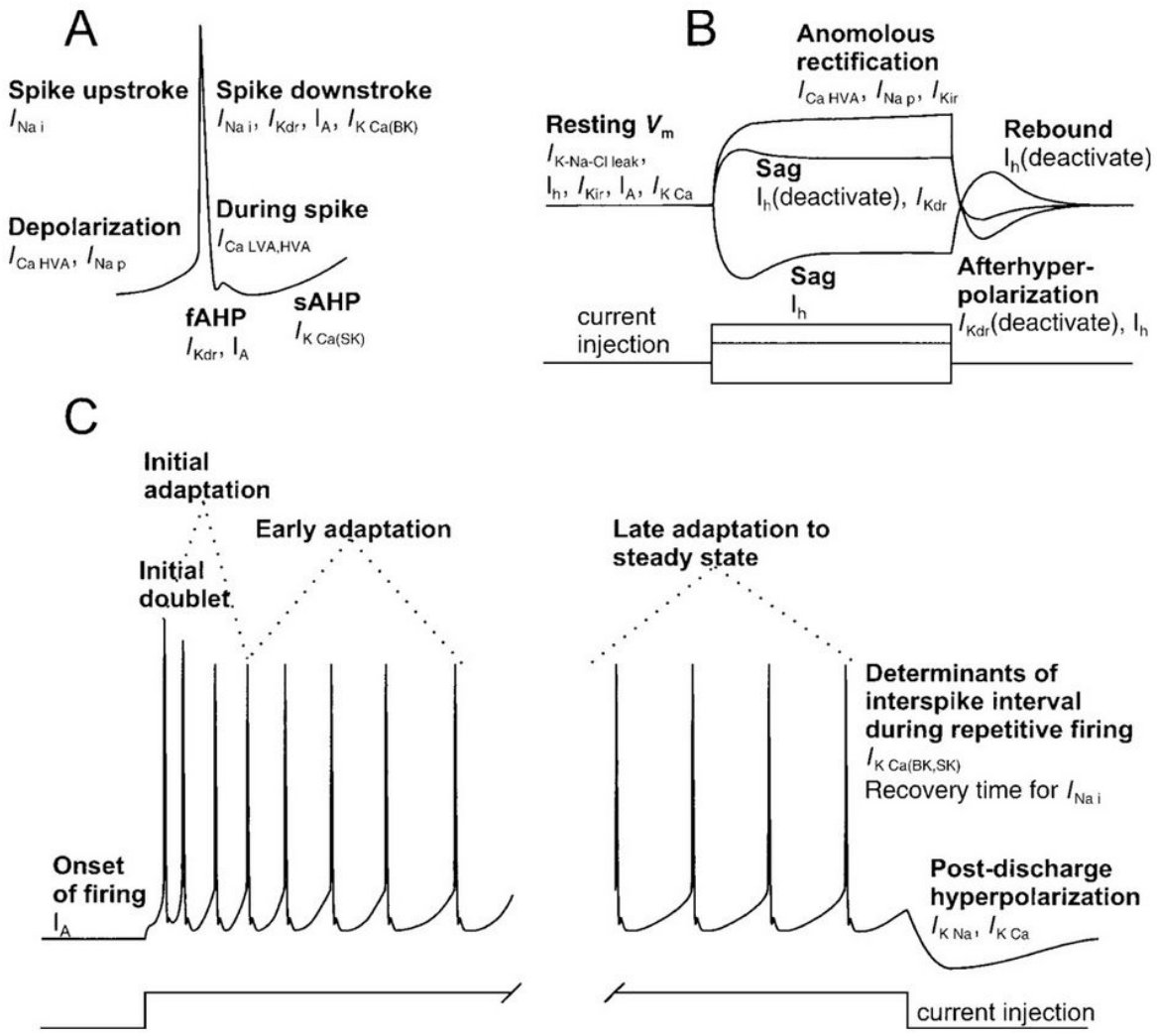

Figure 6. Supra- and subthreshold membrane behavior of motoneurons. A, action potential waveform underlined by involved ion currents. B, subthreshold membrane behavior induced by a short-lasting depolarizing/hyperpolarizing square current pulse. C, different phase of adaptation in case of repetitive firing and postdischarge hyperpolarization during a long-lasting current pulse (from Rekling et al., 2000).

HM repetitive firing patterns change markedly during development due to variation in some conductances. Neurons in the neonatal rat manifest two different behaviors: HMs < P4 show a decrementing or adapting firing pattern, whereas, during the second postnatal week, HMs trigger incrementing or accelerating firing pattern (Viana et al., 1995). In adults (> P21) the

decrementing firing pattern reappears and is followed by three distinct phases of adaptation (Sawczuk et al., 1995; Viana et al., 1995). The modulation of the firing pattern of rat HMs has been shown to be caused by a decrease in the AHP duration (Viana et al., 1994, 1995), a reduction of the LVA calcium current (Umemiya and Berger, 1994; Viana et al., 1993b), and an increase in I_h expression (Bayliss et al., 1994; Viana et al., 1994).

To conclude, motoneuronal output is the outcome of synaptic input modulation by several factors, including motor unit subtype, location and type of synaptic terminals, distribution and character of active and passive membrane properties, neuromodulator effect on HMs and repetitive firing behavior.

2.3. Hypoglossal motoneurons in pathological conditions and excitotoxicity studies

As mentioned above, HMs are highly involved in ALS onset; in particular they are severely damaged in the bulbar form of the disease, but also patients manifesting the limb-onset ALS eventually develop bulbar symptoms, as respiratory failure is the primary cause of death in ALS (Orsini et al., 2015; Wijesekera and Leigh, 2009; Zarei et al., 2015). Little is known about the early ALS pathogenesis in HMs. Thus, our laboratory has developed a simple *in vitro* model of excitotoxicity using the glutamate uptake inhibitor TBOA (Sharifullina and Nistri, 2006). TBOA application recreates the early stage of the disease gradually increasing the extracellular glutamate concentration without affecting glutamatergic receptors and carriers (Anderson et al., 2001). Glutamate uptake inhibition induces a strong enhancement in excitatory synaptic transmission and (in a percentage of motoneurons) strong bursting activity supported by electrical coupling among neighbouring motoneurons (Cifra et al., 2009, 2011; Sharifullina and Nistri, 2006). The network origin of these bursts has been confirmed with TTX application, or the cell-permeable Ca^{2+} chelator BAPTA-AM, or the gap junction blocker carbenoxolone (Sharifullina and Nistri, 2006). Previous studies have reported that during normal synaptic transmission NMDA and mGlu receptors are not activated by glutamate (Huang and Bordey, 2004; Huang et al., 2004). In condition of excitotoxic stress, the increase in ambient glutamate recruits NMDA and mGlu receptors, which facilitate bursting by spreading membrane depolarization and increasing membrane resistance, thus making neurons electrotonically more compact and sensitive to excitatory inputs (Sharifullina and Nistri, 2006). The electrical activity induces an

irreversible increase in intracellular calcium concentration leading to the activation of a series of pathway which may cause motoneuron death (Sharifullina and Nistri, 2006). These early events are followed by an increased number of cells positive to propidium iodide, a dye penetrating disrupted cell membrane and binding DNA, or ATF-3, a motoneuronal distress marker (Nani et al., 2010). Damage is reduced by drugs suppressing bursting activity, such as carbenoxolone or riluzole (Cifra et al., 2011; Sharifullina and Nistri, 2006).

3. Nicotinic ACh receptors

3.1. Cholinergic systems in the brain

The cholinergic system includes all neurons which synthesize, store and release the neurotransmitter acetylcholine (ACh). It is one of the phylogenetically oldest and most important nervous pathways.

The ester ACh is synthesized from choline and the acetic acid acetyl-CoA by the enzyme choline acetyltransferase located in the cytosol. Choline is supplied from the extracellular space by high affinity active transport system, whereas acetyl-CoA is synthesized in mitochondria. After synthesis, ACh is released into the synaptic cleft, by exocytosis through the synaptic vescicles, where it may activate cholinergic receptors or be rapidly degradated by acetylcholinesterases to choline and acetate.

The cholinergic system has modulator functions and is made up of a series of substystems closely connected with different functions; in particular, eight major groups of cells, largely overlapping, have been discovered. Each group, which receives a large and complete set of sensory-based information, innervates only its own discrete area (Gotti and Clementi, 2004; Woolf, 1991). The major cholinergic subsystems are (Fig. 7; Gotti and Clementi, 2004; Woolf, 1991):

- *Magnocellular basal complex* (nucleus basalis): this is the most important group of cholinergic neurons, which provide the majority of cortical and hippocampal inputs.
- *Laterodorsal and peduncolopontine tegmental nuclei:* these represent the second most important cholinergic complex in the brain, innervating thalamus, substantia nigra, tectum, medial habenula, deep cerebellar nuclei, pontine reticular formation, raphe nuclei, medullary reticular formation, vestibular nuclei and locus coeruleus.
- *Striatum:* its cholinergic fibers originate from the cholinergic neurons located in the caudate nucleus, putamen and nucleus accumbens, and do not project beyond the striatum borders.
- *Lower brain system:* neurons located in the brainstem reticular formation and spinal intermediate grey matter which innervate the superior colliculus, cerebellar nuclei and cortex.

- *Habenula-interpeduncular system:* these neurons, that receive inputs from the thalamus, are located in the medial habenula and project, through the habenula-interpeduncular tract, to the interpeduncular nucleus. It is an important station through which the limbic system can influence the reticular formation of the brainstem.
- *Autonomic nervous system:* the preganglionic neurons in both the parasympathetic and sympathetic systems are cholinergic. The parasympathetic preganglionic cells, located in a series of nuclei in the encephalic trunk and spinal cord segment S2-S4, project to (or near) target organs. The sympathetic preganglionic cells are located in the column of the mediolateral gray matter of the spinal cord segment T1-L3, innervating paravertebral sympathetic ganglia.

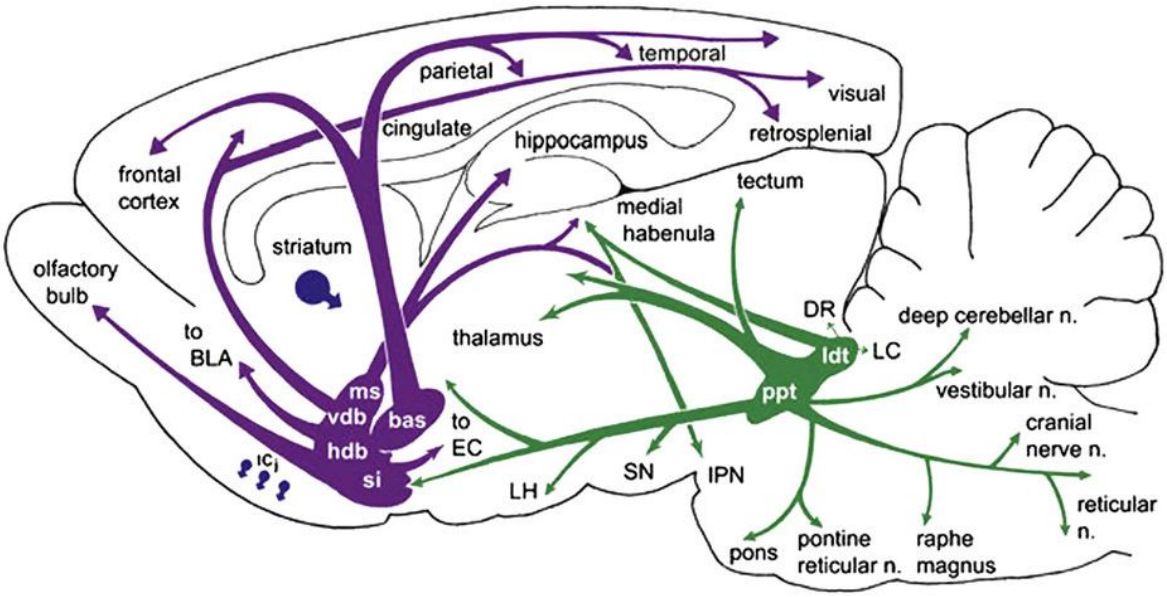

Figure 7. Central cholinergic pathways in the brain. bas, nucleus basalis; BLA, basolateral amygdale; DR, dorsal raphe; EC, enthorinal cortex; hdb, horizontal diagonal band nucleus; Icj, island of Cajella; IPN, interpeduncular nucleus; LC, locus ceruleus; ldt, laterodorsal tegmental nucleus; LH, lateral hypothalamus; ms, medial septal nucleus; PPN, pedunculopontine nucleus; si, substantia innominata; SN, substantia nigra; vdb, vertical diagonal band nucleus (from Perez-Lloret and Barrantes, 2016).

3.1.1. ACh receptor subtypes

ACh exerts its effects by binding to and activating two pharmacologically separated groups of receptors: sensitive to nicotine and sensitive to muscarine leading to the classification of nicotinic acetylcholine receptors (nAChRs) and muscarinic acetylcholine receptors (mAChRs), respectively. Both are expressed by either neuronal or nonneuronal cells throughout the body. These two different receptor families are structurally and functionally unrelated inasmuch nAChRs are ligand gated ion channels, while mAChRs are G-protein coupled receptors, which exert their action via GTP-binding proteins. The mAChR family, distributed throughout the central nervous system, includes five metabotropic receptors, M1-5; with M1, 3, and 5 coupling to $G\alpha_{q/11}$ subunits, leading to phospholipase C activation, and M2, and 4 coupling to $G\alpha_{i/o}$ subunits and inhibiting adenylyl cyclase (Scarr, 2012). Moreover, in addition to their canonical signal pathways, mAChRs are capable of activating multiple signal transduction pathways, altering cellular homeostasis of inositol triphosphate, phospholipase C, cAMP and free calcium.

3.2. Nicotinic ACh receptors

The heterogenous nAChR family of pentameric channels is involved in a wide range of physiological and pathophysiological processes. So far, seventeen vertebrate subunits (α1-10, β1-4, γ, δ, and ε) have been identified in the nervous system and muscles; nevertheless, only the subunits expressed in the mammalian central nervous system are reviewed in this work.

3.2.1. nAChR genes and molecular structure

In the mammalian nervous system have been cloned eleven genes (CHRNA2-CHRNA7, CHRNA9-CHRNA10, and CHRNB2-CHRNB4; Table 1), divided in two sub families of eight α type (α2-α7, and α9-α10) and three β type (β2- β4) (Hurst et al., 2013; Zoli et al., 2015). The α subunits are so called in homology to muscle α1 subunit when two adjacent cysteines are located at the N-terminal part (aminoacid position 192 and 193) as locus participating in the ACh binding site; those cysteines are not present in β subunits (Lindstrom et al., 1995; Zoli et al., 2015).

Table 1. Chromosomal localizations of genes coding for human neuronal nAChR subunits. Data taken from Hurst et al., 2013.

nAChR subunit	**Chromosomal localization**
CHRNA2	8p21
CHRNA3	15q24
CHRNA4	20q13.3
CHRNA5	15q24
CHRNA6	8p11.21
CHRNA7	15q14
CHRNA9	4p15.1
CHRNA10	11p15.5
CHRNB2	1q21.3
CHRNB3	8p11.22
CHRNB4	15q24

nAChRs belong to the gene superfamily of ligand gated ions family, that also includes $GABA_{A/C}$, glycine and serotonin ionotropic receptors (Zoli et al., 2015). As other members of this family characterized by cys-loop homology, all nAChR subunits have four putative membrane-spanning domains (M1, M2, M3, and M4; Fig. 8A), with a total length of less than 600 amino acids. Both N- and C- terminal parts are extracellular; the amino-terminal part, with an approximately length of 200 amino acid, presents glycosilation and the ligand-binding sites, whereas the intracellular loop linking M3 and M4 presents phosphorylation sites. The four α-helices transmembrane domains are packed around the central hydrophilic ion pore. M2 lines the pore, establishing the ion gate, selectivity, and channel conductivity, whereas, M4 is the one that mostly interacts with the lipid bilayer (Albuquerque et al., 2009; Zoli et al., 2015). Neuronal nAChRs have pentameric structure with a molecular weight in the 300 kDa range. The channel kinetics are determined by all five subunits, which may arrange in a variety of subtypes due to the diversity of the possible combinations. Thus, the subunit composition of the receptor determines the pharmacological characteristics of the binding site and the cation preference of the channel, which is permeable to Na^+, K^+, and in some cases, Ca^{2+} ions. The channel opens immediately (time constant about 20 μs) when at least two ACh molecules bind to the receptor. In the open state the nAChR channel has a pore diameter of 9-10 Å with a conductance in the range from 5 to 35 pS. The functional properties of each nAChR subtype overlap among the several isoforms making it very difficult to distinguish among them through the use of pharmacological agents (Zoli et al., 2015). Receptor subtypes can be pharmacologically divided into two major groups: α-bungarotoxin-sensitive,

which include channels made up of the α7, α9, and α10 subunits; and α-bungarotoxin insensitive, consisting of receptor made up by a heteromeric combinations of α2-6 and β2-4, that bind nicotine with high affinity (Changeux, 2010; Gotti and Clementi, 2004).

nAChRs can be subdivided in homopentamers or heteropentamers. The first ones are formed by five identical subunits, whereas the second ones result from the combination of different subunits (Fig. 8B). Homopentamers are the receptor simplest form with five identical ACh-binding sites located at the interface between two adjacent subunits. They are exemplified by α7 nAChRs, which are widely distributed in the central and peripheral nervous system. They are characterized by high calcium permeability and fast desensitization (Lindstrom et al., 1995; Yu and Role, 1998) and they are thought to be the closest form to the ancestor receptor. The homomeric form of the channel may also be composed also by α9 subunits. Two or more subunit types may associate to form heteropentamers. They display a broad spectrum of physiological and pharmacological properties and functions, in relation to the ratios of α and β subunits, but at least two α subunits including the binding sites should form the receptor. The ACh binding site, in heteromeric channels, has a principal and a complementary component; α2-α4 and α6 subunits carry the principal component, whereas β2 or β4 subunits the complementary site; in the homomeric receptors each subunit contributes to both components of the binding site (Fig. 8B). The α5 and β3 subunits are classified as auxiliary subunits inasmuch they carry neither the principal nor the complementary site (Gotti and Clementi, 2004). Thus, the α5, α6, and β3 subunits can form functional receptors only in combination with other subunits, therefore they are called “orphan” subunits. The α4β2-containing nAChR is the most widespread isoform in the central nervous system. It account for 90% of the high affinity neuronal nAChRs in mammalian brain and may presents different stoichiometry, $(\alpha4)_2(\beta2)_3$, $(\alpha4)_3(\beta2)_2$, and $(\alpha4)_2(\beta2)_2(\alpha5)$, yielding several configurations with different properties, including agonist sensitivity and calcium permeability (Albuquerque et al., 2009; Colombo et al., 2013; Hurst et al., 2013).

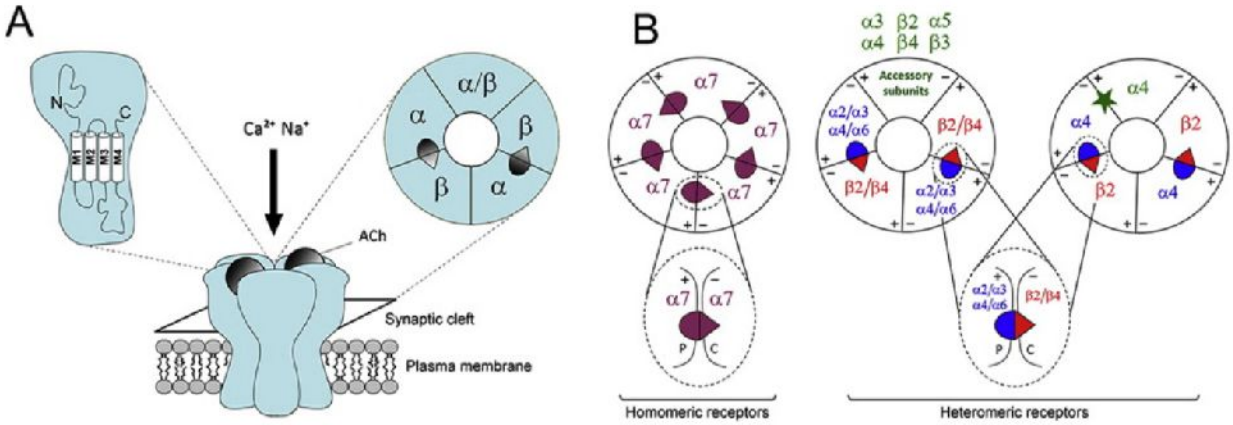

Figure 8. Structure of neuronal nAChRs. A, (left) diagram showing a single subunit composed of extracellular N- and C- termini and four hydrophobic transmembrane domain (M1-M4). (Middle) an assembled arrangement of nAChR subunits. (Right) organization and localization of ACh binding sites in a heteropentameric receptor. B, homopentameric and heteropentameric structures of nAChRs. (Left) homopentameric channel formed by the α7 subtype and (middle and right) example of heteropentameric structures. The primary component, indicates as P(+) is carried by α subunints, whereas complementary component C(-) by an α or non- αsubunit. The $(\alpha4)_3(\beta2)_2$ subtype has an additional binding site ate the α4α4 interface (star). Modified from Zoli et al., 2015.

3.2.2. nAChR life cycle

The first level of nAChR expression regulation is through the transcriptional control of subunit composition. Studies on cultured cells and tissues have shown cell-specific regulation of nAChR transcription, with qualitative and quantitative difference in receptor subunit composition during development (Albuquerque et al., 2009; Boulter et al., 1990; Witzemann et al., 1989). Transcription is finely regulated by signals provided by synaptic partners and soluble factors. Moreover, subunit genes with a closer chromosomal localization may form a unique gene cluster. For example, α3, α5, and β4 are often coexpressed in the central and peripheral nervous system (Table 1; Albuquerque et al., 2009; Rosenberg et al., 2002).

During receptor assembly, cells employ multiple mechanisms to ensure correct subunit association; in fact, the relatively few subtypes found do not match the substantial number of possible receptors. The proper stoichiometry that is assembled into the ER is ensured firstly by the regulation of the transcription, which is differently modulated by the state of development or stress of the cell. Secondly, the unique primary structure ensure proper folding and preferential

interactions between subunits: for example, mutations in the large cytoplasmic loop between M3 and M4 have been connected to a diminished or abolished expression of the mutated subunit (Mukherjee et al., 2009; Tsetlin et al., 2011). In detail, in addition to the Cys-loop domain, assembly is modulated by positively charged aminoacids at the end of the M4 fragment and by the interaction between residues in the lower part of the M1 and the fragment M2 (Tsetlin et al., 2011). Despite the several mechanisms for assembly control, about 80% of the synthesized subunits appear to be improperly associated or never leave the ER where they are degraded. Another important mechanism acting as modulator of nAChR expression involves chaperone proteins that (in addition to transporting receptors away from the ER) when associated with nAChR precursor subunits enhance and favor the folding into complete complexes and monitor the glycosilated state. Some of these chaperons are: calnexin, rapsyn, ERp75 and Bip, 14-3-3 β-protein and RIC-3 (Albuquerque et al., 2009). The pentameric receptors that exit the ER spend about 3h to reach the cell surface passing through the Golgi complex via COPII vescicles, a process relatively slow compared to the maturation phase that last about 30 min (Colombo et al., 2013; Sallette et al., 2005). Only a small percentage of receptors, about 15%, reach the cell surface, where their half-life has been estimated to be in the range of 10h (Arroyo-Jiménez et al., 1999; Sallette et al., 2005). Then, plasma membrane nAChRs are internalized to the lysosomal compartments where are degraded or re-exposed on the cell surface. The trafficking mechanism is complicated by the fact that receptors have to target specific sites in the cell membrane (Colombo et al., 2013).

3.2.3. nAChR desensitization and upregulation

Desensitization is the physiological loss of functional response upon continuous or repeated exposure to agonist (Fig. 9A). When nAChRs are exposed to ACh, they may manifest a decline in the response, whose onset is time, agonist, concentration, and nAChR subunit dependent (Giniatullin et al., 2005; Quick and Lester, 2002). Concerning desensitization, mammalian nervous system nAChRs can be divided in two main groups: α7-containing receptors that rapidly desensitize (in millisecond) or non α7-containing nAChRs that desensitize slowly (in seconds; Giniatullin et al., 2005; Quick and Lester, 2002). As previously reported, desensitization may change with agonist concentration (Fig. 9B). ‘Classical desensitization’ occurs when a medium to

high (µM to mM) concentration of ligand is applied that first activates the receptors and then desensitizes them with subsequent recovery after agonist removal; classical desensitization generally develops in the range of tens of milliseconds. Desensitization can be developed also without apparent receptor activation; this occurs with low agonist concentrations, a process that is referred to as 'high-affinity desensitization'. Both phenomena are nAChR subunit and agonist dependent (Giniatullin et al., 2005). Other local factors may modulate the response to desensitization: for example, substance P facilitates it by binding an allosteric site of the receptor, whereas intracellular messengers, such as Ca^{2+}, target the recovery phase (Giniatullin et al., 2005).

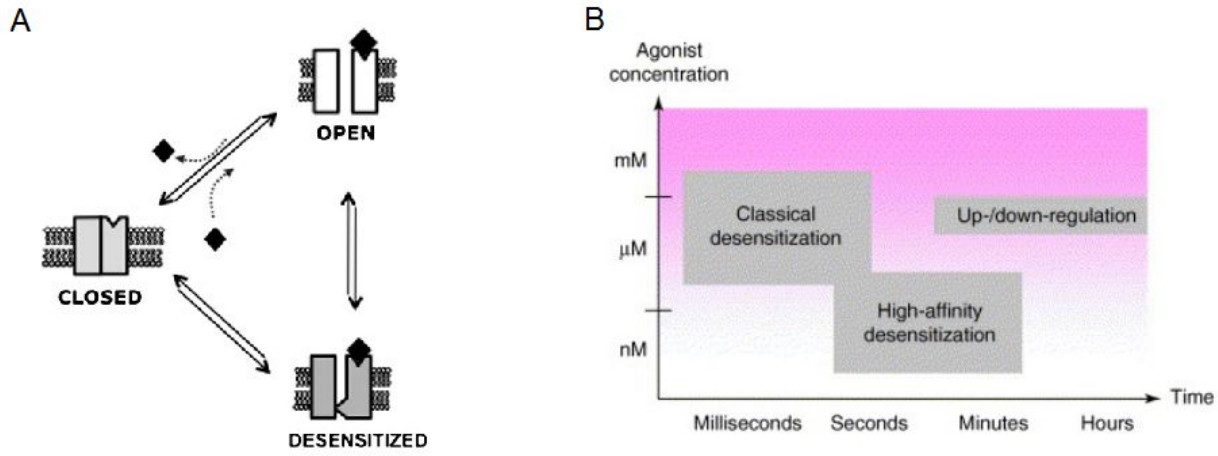

Figure 9. Modulation of responsiveness to agonist. A, minimal allosteric model illustrating functional states of ligand gated ion channels. The model consists in three functional states: in absence of ligand the state is closed, whereas when there is the bound of the agonist two functional states are possible (open and desensitized), but only the open state permits ions flux. B, relation between agonist concentration and exposure time. "Classical desensitization" is induced by relatively high (micromolar to millimolar) concentrations of the ligand. "High-affinity desensitization" is induced by low concentrations of agonists which directly desensitize the channel without open it. Long-lasting application of ligands induces nAChR upregulation or downregulation. Modified from Giniatullin et al., 2005, and Hurst et al., 2013.

Generally, a sustained (from minutes to hours) exposure of agonists to many plasma membrane receptors, such as ionotropic glutamate receptors and G-protein coupled receptors, causes a 'downregulation' of the receptor through its internalization. However, nAChRs may undergo

‘upregulation’ after a chronic exposure to the agonist nicotine (Albuquerque et al., 2009; Henderson and Lester, 2015; Hurst et al., 2013; Sallette et al., 2005; Srinivasan et al., 2011). Receptor increase is not limited to the plasma membrane but involves an increase in nAChR abundance in several organelles like the ER and Golgi complex. Moreover, upregulation is not limited to a change in receptor number, but also in its stoichiometry and trafficking (Henderson and Lester, 2015; Kuryatov et al., 2005; Sallette et al., 2005). Nicotine acts intracellularly by modulating maturational processes, matchmaking, and chaperoning but not by increasing trascription (Henderson and Lester, 2015; Hurst et al., 2013; Sallette et al., 2005). It has to be taken in consideration that upregulation is receptor-, region- and cell-specific; in fact, not all nAChRs are upregulated in response to nicotine, or they do so limitedly. For example, α4β2 receptors highly increase with low concentration (≤ 100 nM) of nicotine, whereas α4α6β2 nAChRs are not upregulated at all, and α3β4 receptors increase only when expose to high levels of nicotine (≥ 10 μM; Henderson and Lester, 2015).

3.2.4. nAChR localization and their function

nAChRs are widespread throughout the neuronal plasma membrane; their localization on neurons can be divided in: cell soma, dendrites, axon terminals, preterminal axon regions, and myelinated axons. Multiple mechanisms regulates the targeting processes to subcellular compartments but the intracellular loop between the transmembrane domains M3 and M4 of the receptor subunits is critical for their localization (Colombo et al., 2013).

The primary role of the somatodendritic nAChRs (α7, and (non-α6)α4β2; Champtiaux et al., 2003), that are not confined to cholinergic synapses, is to modulate the type IA current, a fast-inactivating whole cell current mediated principally by the α7 receptors, that have a low affinity for agonists, a brief open state (~ 100 μs), a large conductance (70-105 pS), and a high permeability to Ca^{2+} relative to Na^{+} (Albuquerque et al., 2009). Moreover, application of α7 receptor agonist in the somatodendritic area favors Na^{+} channel recruitment and action potential initiation (Alkondon et al., 1999).

The nAChRs localized on axon terminals facilitate neurotransmitter release, including GABA, glutamate, dopamine, serotonin, norepinephrine, and acetylcholine. Some of the subtypes

reported to be expressed in such areas are: α7, α4β2, α4α5β2, α6β3β2, and α6α4β3β2 (Champtiaux et al., 2003; Marchi et al., 2002; Salminen et al., 2004).

Receptors expressed in the preterminal axon regions and on myelinated axons regulate axon excitability, facilitating neurotransmitter release by increasing intracellular calcium concentrations or through the depolarization of the presynaptic bouton (Albuquerque et al., 2009; Hurst et al., 2013).

Recent studies have revealed that the distribution of nAChRs is not limitated to plasmamembrane, but include localization to the outher membrane of mitochondria (Gergalova et al., 2012; Lykhmus et al., 2014). In a tissue specific manner, brain mitochondria express several nicotinic receptor subtypes: α7β2, α4β2, and α3β2. These receptors, blocking the cytochrome c release, control various pathways due to mitochondrial type of apoptosis through the activation of intraorganelle kinases. nAChRs play a key role in defending mitochondria from any types of stress influence (Gergalova et al., 2012, 2014; Lykhmus et al., 2014).

3.2.5. nAChR distribution in the brain and expression during development and aging

The distribution of nAChRs has been consistently investigated at both mRNA and protein level. To accomplish the pleiotropic role in physiology and pathology, nAChRs are distributed on neuronal and non-neuronal cells. In the rodent brain, the most widespread receptor subtype is the α4β2, which may contain the α3β4 and α5 subunits. Also, the α7 nAChR is rather diffuse, in particular in the hippocampus, the hypothalamus, the cortex and the motor nuclei. Other receptors are limited to certain areas, such as the α6-containing receptors present in the locus coeruleus, the optic pathway, and the dopaminergic neurons; or the α9/α10- containing nAChRs expressed only extraneuronally in limited areas like the cochlea, the pituitary pars tuberalis and the olfactory epithelium. Also in the primate brain the α4β2 receptor is the main isoform; although the subtype α2β2 also has a substantial presence (Gotti and Clementi, 2004).

During development and aging, nAChR expression changes considerably in all animal species. Earliest detection of the receptor mRNA is at E11 in rat and after 5-7 weeks of gestational age in human brain (Zoli, 2000). In rat fetal brain, the α7 mRNA expression starts from E13 and increase until birth; then its level decreases in the postnatal days to adult expression levels. α2, α3, α4, α5, α6, β2, and β4 Subunit mRNA is present from the early days in rat; and their

distribution is not dissimilar from that of adult animals. During aging the expression of the several mRNA subunits slightly decreases, even with regional specificity; moreover, with aging the cholinergic system may present dysfunctions, contributing to neurodegenerative disease onset (Albuquerque et al., 2009; Gotti and Clementi, 2004).

3.2.5.1. nAChRs in the nucleus hypoglossus

As previously described, the hypoglossal nucleus receives cholinergic nerve terminals from the laterodorsal and peduncolopontine tegmental nuclei, even if they are not abundant and are distributed in an apparently scattered fashion (Rukhadze and Kubin, 2007; Woolf, 1991). Immunoistochemical experiments have detected the nicotinic α2, α3, α4, α5, α7, α9, β1 and β2 subunits in this nucleus (Quitadamo et al., 2005; Vivekanandarajah et al., 2016). Despite their presence, no spontaneous cholinergic events have been recorded, even when acetylcholinesterase blockers were applied or after the stimulation of the reticular formation. However, administration of dihydro-β-erythroidine (DHβE) or methyllycaconitine (MLA), selective antagonists of the α4 and α7 subunits respectively, significantly decreases the amplitude (but not the frequency) or the kinetics of the glutamatergic, miniature, and evoked post synaptic currents. When both antagonists are coapplied, significant decrease in both amplitude and frequency is recorded. Moreover, DHβE and MLA virtually suppress the currents evoked by nicotine indicating that the main contribution to glutamatergic currents into the nucleus hypoglossus by nAChRs is given by the α4β2 and α7 subtypes. It should be noted that the continuos presence of nicotine desensitizes these receptors (Quitadamo et al., 2005).

3.2.6. nAChR role in normal brain function and mental disorders

nAChRs are not essential for survival and basic behavior execution, rather they are involved in the implementation and fine control of sophisticated and complex behaviors. Fundamental contribution to study the functional role of nAChRs has been given by genetically engineered knock-out (Ko) or knock-in (Kin) mice. Due to multiorgan dysfunction, the α3 and double β2-β4 Ko mice usually die in the first week of life. α4 and β2 Ko mice manifest great reduction in antinociceptive and analgesic responses, whereas the α5 and β4 Ko show deficit in sympathetic and parasympathetic ganglionic transmission (Gotti and Clementi, 2004; Marubio et al., 1999).

Finally, the phenotype not expressing the α7 subunit manifests lack of nicotine-evoked fast desensitizing currents (Gotti and Clementi, 2004).

Nicotinic transmission is mainly involved in cognitive processes; in particular, nicotine improves task performances involving associative and spatial learning, attention, cognition, and working memory. Furthermore, nAChRs control many processes involved in locomotion. Moreover, nicotine capacity to modulate the dopaminergic system is thought to be connected with drug reinforcement; this additive property is achieved by increasing the release of dopamine that activates nAChRs of dopaminergic neurons (Changeux, 2010; Gotti and Clementi, 2004).

In addition to the above described effects, nAChRs play a pivotal role in a wide variety of diseases associated with the nervous system. These diseases could be divided into three major groups: age-related degenerative diseases, age-dependent disorders and age-indipendent disorders.

Degenerative diseases:

In some neurodegenerative diseases, the cholinergic pathways are consistently affected. In particular, the activity of choline acetyltransferase is decreased and the nucleus basalis of Meynert manifests degeneration. Epidemiological studies of Alzheimer's disease (AD) and Parkinson's disease (PD) patients highlight that tobacco smoking reduces the probability to develop such diseases, although smoking adversely affects cardiovascular and certain cerebrovascular functions (Gotti and Clementi, 2004).

- Alzheimer's disease: the age-related decline in nAChRs and neurons in the central nervous system together with the impairment of the limbic cholinergic system contributes to the onset of dementias including AD. nAChR subtypes are differentially affected during disease progression; in particular β-amyloid proteins principally accumulate in brain regions that express α4β2 and α7 nAChRs such as neocortex and hippocampus (Albuquerque et al., 2009; Dineley et al., 2015). In an advanced state of the disease, there is a decrease of about 50% of the α4β2 nAChR, while muscarinic receptors remain relatively intact (Dineley et al., 2015). Early treatments with acetylcholinesterase or nAChR agonist could have positive symptomatic effect on disease progression by

delaying decline of cognitive processes, although AD progression continues (Gotti and Clementi, 2004).

- Parkinson's disease: nAChRs play a pivotal role in dopaminergic neurons where α6β2 and α4β2 receptors promote the release of dopamine (Gotti and Clementi, 2004). Treatments with drugs that selectively target the receptors above mentioned may prove useful in the management of PD in which the nigro-striatal pathway is severely damaged (Quik and Wonnacott, 2011).

Age-dependent disorders:

- Attention-deficit hyperactivity disorder (ADHD): It is a multigenic neurobehavioral disorder characterized by hyperactivity, impulsivity, and difficulties in attending to tasks. This disease presents as risk factors early smoking and maternal smoking (Potter et al., 2014).
- Autism: this neurodevelopmental disorder is characterized by deficit in socialization and communication and becomes apparent in early childhood. Studies on post-mortem tissues of autistic patients revealend a decrease in mRNA expression of 50% of the α3, α4, and β2 nAChR subunits (Martin-Ruiz et al., 2004).
- Schizophrenia: it comprises cognitive deficit and disordered thoughts characterized by altered perception of reality. Its relation to nAChRs is suggested by the high prevalence of smoking among patients, which some consider to be a form of self-medication (deficit in α7 receptors has been observed). Symptoms appear to be improved or normalized after nicotine exposure (Dineley et al., 2015).
- Tourette syndrome: this familial, chronic neuropsychiatric disorder induces movement disturbances, inappropriate vocalizations and cacolalia. Although there is no evidence for direct involvement of nAChR in this disease, neuroprotective effects of nicotine have been observed in animal models, where nAChR agonists positively affected movement disorders perhaps modulating dopaminergic release from striatal and limbic cortical areas (Gotti and Clementi, 2004; Quik et al., 2014).

Age-independent disorders:

- Epilepsy and febrile convulsions: correlation between nAChRs and epilepsy has been observed in the autosomal dominant nocturnal frontal lobe form of epilepsy that is characterized by attacks arising during the non-rapid eye movement (non-REM) phase of sleep. A percentage of families presenting this disease carries mutations in genes coding for subunits of the heteromeric nAChRs, in particular the α4β2 subtype (Becchetti et al., 2015).
- Depression and anxiety: positive association between smoking cessation and mental illness has been reported. In humans, nicotine has antidepressant and mood stabilizer properties (Fluharty et al., 2016).

3.3. Nicotine

Nicotine is a potent alkaloid found in the Solanaceae family of plant, in particular in the leaves of Nicotiana rustica, Duboisia hopwoodii, Asclepias syriaca, and the tobacco plant Nicotina tabacum.

Nicotine is a weak base (pK_a = 8.0) and a tertiary amine consisting of a pyrrolidine and a pyridine ring. In tobacco, it is found as (S)-nicotine that binds stereoselectively nAChRs. (R)-nicotine, present in small quantities in cigarette smoke, is a nAChR agonist (Benowitz, 2009). In smokers, the nicotine peak concentration is tissue and body fluid specific: in blood plasma it is about 0.31 μM (between 10 and 50 ng/ml), in milk, due to a more acidic pH, the concentration is triple (mean value 100 ng/ml), in the brain is about 1 μM, and after smoking in lung fluids the value may reach the concentration of 60 μM (Clunes et al., 2008; Matta et al., 2006). When smoke from a cigarette is inhaled, nicotine is carried into the lungs where it is absorbed rapidly and reaches the brain within 8-10 s through arterial circulation. The absorbed nicotine through mucous membranes is rapidly distributed to tissues; in particular, it tends to accumulate in those rich of lipids. The half-life of nicotine is about 2 h, and the one of cotinine, the major nicotine metabolite, is about of 16 h (Benowitz, 2009). In man, nicotine is metabolized to six primary metabolites and several minor metabolites by the liver. As previously reported, the quantitatively (approximately 70 to 80%) most important metabolite is cotinine, produced by the liver enzyme CYP2A6. Only 5% of nicotine is excreted unchanged by the kidney. The metabolism and

clearance of nicotine and its metabolites have been reported to be affected by several factors such as age, sex, race, stress, and disease states (Matta et al., 2006). Further to nAChR activation, in specific brain regions, chronic exposure to nicotine increase the number of nAChRs due to post-trascriptional mechanisms, the process called up-regulation (Colombo et al., 2013; Henderson and Lester, 2015).

Aims of the study

The main goal of the present study was to investigate a putative protective role of nicotine against TBOA-induced excitotoxicity in an ALS model *in vitro*. To this purpose, we employed brainstem slices conteining the nucleus hypoglossus from neonatal Wistar rats. Nicotine was co-applied with TBOA at a concentration of 1 or 10 µM, similar to values reported in human fluids after smoking.

The questions we tried to answer during this thesis were the following ones:

1. Which are the downstream effects of the excitotoxicity? Is nicotine able to block them?
   This question led to study:
   - Electrophysiological characterization of bursting activity and synaptic transmission
   - Evaluation of the mitochondrial energy metabolism
   - Analysis of the reactive oxygen species production
   - Investigation of the endoplasmic reticulum stress response
2. What are the characteristics of the excitotoxic network propagation? And how do they change in the presence of nicotine?
   This question should shed light on:
   - the network mechanisms of excitation spread
   - the role of gap junctions in determining propagation and protection from excitototoxicity
3. Which are the cell death mechanisms activated by the increase of glutamate?

For Material & Methods and Results sections, please see enclosed papers.

JPn
Neuroscience
The Journal of Physiology

Nicotinic receptor activation contrasts pathophysiological bursting and neurodegeneration evoked by glutamate uptake block on rat hypoglossal motoneurons

Silvia Corsini, Maria Tortora and Andrea Nistri

Department of Neuroscience, International School for Advanced Studies (SISSA), Trieste, Italy

Key points

- Impaired uptake of glutamate builds up the extracellular level of this excitatory transmitter to trigger rhythmic neuronal bursting and delayed cell death in the brainstem motor nucleus hypoglossus.
- This process is the expression of the excitotoxicity that underlies motoneuron degeneration in diseases such as amyotrophic lateral sclerosis affecting bulbar motoneurons.
- In a model of motoneuron excitotoxicity produced by pharmacological block of glutamate uptake *in vitro*, rhythmic bursting is suppressed by activation of neuronal nicotinic receptors with their conventional agonist nicotine. Emergence of bursting is facilitated by nicotinic receptor antagonists.
- Following excitotoxicity, nicotinic receptor activity decreases mitochondrial energy dysfunction, endoplasmic reticulum stress and production of toxic radicals. Globally, these phenomena synergize to provide motoneuron protection.
- Nicotinic receptors may represent a novel target to contrast pathological overactivity of brainstem motoneurons and therefore to prevent their metabolic distress and death.

Abstract Excitotoxicity is thought to be one of the early processes in the onset of amyotrophic lateral sclerosis (ALS) because high levels of glutamate have been detected in the cerebrospinal fluid of such patients due to dysfunctional uptake of this transmitter that gradually damages brainstem and spinal motoneurons. To explore potential mechanisms to arrest ALS onset, we used an established *in vitro* model of rat brainstem slice preparation in which excitotoxicity is induced by the glutamate uptake blocker DL-threo-β-benzyloxyaspartate (TBOA). Because certain brain neurons may be neuroprotected via activation of nicotinic acetylcholine receptors (nAChRs) by nicotine, we investigated if nicotine could arrest excitotoxic damage to highly ALS-vulnerable hypoglossal motoneurons (HMs). On 50% of patch-clamped HMs, TBOA induced intense network bursts that were inhibited by 1–10 μM nicotine, whereas nAChR antagonists facilitated burst emergence in non-burster cells. Furthermore, nicotine inhibited excitatory transmission and enhanced synaptic inhibition. Strong neuroprotection by nicotine prevented the HM loss observed after 4 h of TBOA exposure. This neuroprotective action was due to suppression of downstream effectors of neurotoxicity such as increased intracellular levels of reactive oxygen species, impaired energy metabolism and upregulated genes involved in endoplasmic reticulum (ER) stress. In addition, HMs surviving TBOA toxicity often expressed UDP-glucose glycoprotein glucosyltransferase, a key element in repair of misfolded proteins: this phenomenon was absent after nicotine application, indicative of ER stress prevention. Our results suggest nAChRs to be potential targets for inhibiting excitotoxic damage of motoneurons at an early stage of the neurodegenerative process.

DOI: 10.1113/JP272591

(Received 8 April 2016; accepted after revision 21 June 2016; first published online 4 July 2016)
Corresponding author A. Nistri: SISSA, Via Bonomea 265, 34136 Trieste, Italy. Email: nistri@sissa.it

Abbreviations ALS, amyotrophic lateral sclerosis; AP5, (2R)-amino-5-phosphonovaleric acid; DHβE, dihydro-β-erythroidine; DHR 123, dihydrorhodamine 123; DNQX, 6,7-dinitroquinoxaline-2,3-dione; EAAT, excitatory amino acid transporter; ER, endoplasmic reticulum; fALS, familial amyotrophic lateral sclerosis; HM, hypoglossal motoneuron; MLA, methyllycaconitine; MTT, 3(4,5-dimethylthiazolyl-2)-2,5 diphenyl tetrazolium; nAChR, nicotinic acetylcholine receptor; Rho 123, rhodamine 123; R_{in}, input resistance; ROI, region of interest; ROS, reactive oxygen species; sALS, sporadic amyotrophic lateral sclerosis; sEPSC, spontaneous excitatory post synaptic current; sIPSC, spontaneous inhibitory post synaptic current; sPSC, spontaneous post synaptic current; TBOA, DL-threo-β-benzyloxyaspartate; UGGT, UDP-glucose glycoprotein glucosyltransferase; UPR, unfolded protein response; V_h, holding potential.

Introduction

Amyotrophic lateral sclerosis (ALS) is a fatal neurodegenerative disease characterized by progressive muscular paralysis. The vast majority of patients show the sporadic form of this syndrome affecting bulbar and/or spinal motoneurons (Aguilar *et al.* 2007; Poppe *et al.* 2014; Boylan, 2015). In the brainstem, hypoglossal motoneurons (HMs) are particularly vulnerable (Lewinski & Keller, 2005), leading to early dysarthria and dysphagia. A complex interplay among multiple mechanisms such as protein misfolding, mitochondrial dysfunction, oxidative stress and excitotoxicity are likely to foster and accompany motoneuron death (Shaw, 2005; Ngo & Steyn, 2015). These phenomena are associated with enhanced motoneuron excitability that may actually occur presymptomatically to indicate excitotoxicity (Gu *et al.* 2010), a deleterious process caused by overstimulation of glutamate receptors apparently due to deficit in glial glutamate re-uptake (Van Den Bosch *et al.* 2006). In support of the latter notion, large increases in glutamate levels (Spreux-Varoquaux *et al.* 2002) have been reported in the cerebrospinal fluid of ALS patients together with impaired glutamate transport of post-mortem tissue (Rothstein *et al.* 1992; Cleveland & Rothstein, 2001). Enhanced excitatory neurotransmission may also originate (or be aggravated by) from heightened network release of glutamate (Van Den Bosch *et al.* 2006). The latter process might be caused by loss of inhibitory inputs mediated by cholinergic fibres, an early event reported for ALS spinal motoneurons (Nagao *et al.* 1998). Identification of new treatments aiming at arresting disease progression therefore remains a top priority and requires an understanding of its underlying basic mechanisms.

Although continuous exposure to nicotine *in utero* and during the first week of life through breast milk alters cardiorespiratory rhythms (Hafström *et al.* 2005) and desensitizes nicotinic acetylcholine receptors (nAChRs), increasing the incidence of apnoea (Robinson *et al.* 2002; Pilarski *et al.* 2012), later in life nicotine might also provide neuroprotection in neurodegenerative diseases, neurodevelopmental disorders and neuropathic pain (Dineley *et al.* 2015). Cholinergic transmission, mediated by nAChRs, is widely distributed through the brain to regulate different physiological processes (Dani & De Biasi, 2001; Sharma & Vijayaraghavan, 2001, 2002; Zhou *et al.* 2002; Changeux, 2010; Wevers, 2011). nAChRs are predominantly located at neuronal cell bodies and presynaptic terminals (Gotti & Clementi, 2004), where they modulate neurotransmitter release (Dani & De Biasi, 2001; McKay *et al.* 2007; Wevers, 2011). Their prolonged agonist exposure increases receptor number and sensitivity (Bohnen & Frey, 2007; Henderson & Lester, 2015). In the brainstem the hypoglossal nucleus expresses α7 and $\alpha4\beta2$ nAChRs (Dominguez del Toro *et al.* 1994; Chamberlin *et al.* 2002; Dehkordi *et al.* 2005; Quitadamo *et al.* 2005; Wevers, 2011). Even if there is no detectable nicotinic synaptic transmission on HMs, the early consequence of nicotine application is facilitation of network excitatory and inhibitory neurotransmission, although onset of desensitization may later change this phenomenon (Quitadamo *et al.* 2005; Lamanauskas & Nistri, 2006). The role of endogenous ACh in modulating synaptic transmission on HMs is, however, complex because, in addition to the effects of nAChRs, ACh-sensitive muscarinic receptors are reported to inhibit glutamatergic transmission (Bellingham & Berger, 1996) and also to depress inhibitory synaptic transmission (Pagnotta *et al.* 2005). It is therefore clear that the functional impact of nAChR activity depends on a fine balance between the facilitatory and depressant actions of network cholinergic transmission (Quitadamo *et al.* 2005; Zhou *et al.* 2015). After excitotoxic insult, neuroprotection by both $\alpha4\beta2$ (Laudenbach *et al.* 2002; Nakamizo *et al.* 2005) and α7 (Laudenbach *et al.* 2002; Nakamizo *et al.* 2005; Riljak *et al.* 2011) subtypes is described with neuronal cultures (Nakamizo *et al.* 2005), and adult (Riljak *et al.* 2011) or neonatal (Laudenbach *et al.* 2002) animal models. Whether this approach is applicable to the excitotoxicity of HMs remains to be explored.

In recent years, our laboratory has developed a simple *in vitro* model of excitotoxic stress by applying the glutamate uptake inhibitor DL-threo-β-benzyloxyaspartate (TBOA)

to the nucleus hypoglossus motoneurons (Sharifullina & Nistri, 2006) as a useful tool to investigate the physiological and pathophysiological mechanisms of motoneuron excitability (Nistri *et al.* 2006). Inhibition of excitatory amino acid transporters (EAATs) reflects the pathological condition reported in familial and sporadic ALS (fALS and sALS) patients (Rothstein *et al.* 1995; Fray *et al.* 1998; Sasaki *et al.* 2000). The aim of the present study was to examine the effect of nAChR activation on HMs during excitotoxicity. To this end, we used nicotine as a selective, stable agonist on nAChRs. In particular, we focused on how nicotine could modify not only the electrophysiological consequences of glutamate uptake block, but also certain parameters essential for cell viability such as mitochondrial respiration, generation of reactive oxygen species (ROS), changes in gene expression and related intrinsic protection mechanisms.

Methods

Ethical approval

All experiments and treatment protocols were approved by the Scuola Internazionale Superiore di Studi Avanzati (SISSA) ethics committee (prot. 3599, 28 May 2012) and were carried out in accordance with the European Union rules for animal experimentation. All efforts were made to minimize the number of animals used for the present experiments and their suffering. Experiments were performed with *in vitro* brainstem slices removed from neonatal Wistar rats (postnatal days 2–6; P2–P6) rapidly decapitated under I.P. urethane anaesthesia (10% solution, 0.1 ml injection).

Slice preparation and drug application protocols

Details of all experimental procedures have been previously published (Sharifullina & Nistri, 2006; Nani *et al.* 2010). The brainstem was isolated in continuously oxygenated (95% O_2 and 5% CO_2) Krebs solution containing (in mM): 130 NaCl, 3 KCl, 1.5 NaH_2PO_4, 1 $CaCl_2$, 5 $MgCl_2$, 25 $NaHCO_3$ and 18.5 glucose (pH 7.4; 300–330 mosmol l^{-1}). Slices (250–450 μm thick) obtained with a vibrating tissue slicer (Vibracut, FTB, Weinheim, Germany) were transferred to an incubation chamber for 20 min at 32°C and then for at least 10 min at room temperature before use for patch clamp recording as detailed below.

For all other experiments that included longer slice maintenance *in vitro* (4–6 h), slices or isolated brainstems were incubated under resting conditions as above and subsequently kept in continuously oxygenated Krebs solution (sham), TBOA (50 μM), TBOA (50 μM) + nicotine (10 μM) or nicotine (10 μM) at room temperature and processed as indicated later.

Electrophysiological recordings

Single slices (300 μm thick) were placed in a small recording chamber and superfused (2–3 ml min^{-1}) with Krebs solution containing the following salt composition (in mM): 130 NaCl, 3 KCl, 1.5 NaH_2PO_4, 1.5 $CaCl_2$, 1 $MgCl_2$, 25 $NaHCO_3$ and 19.4 glucose (pH 7.4; 300–330 mosmol l^{-1}) at room temperature. Under ×40 magnification, the large soma of HMs (~25 μm) was clearly visible for patch clamp recording. Patch electrodes (3–4 MΩ resistance) were filled with an intracellular CsCl-based solution (in mM: 130 CsCl, 5 NaCl, 2 $MgCl_2$, 1 $CaCl_2$, 10 Hepes, 10 EGTA, 2 ATP-Mg salt and 2 glucose; pH 7.2 with CsOH, 300–330 mosmol l^{-1}) to reduce leak currents of cells clamped at −70 mV holding potential (V_h). Series resistance (R_s; 5–20 MΩ) was continuously monitored and compensated for; data were discarded when R_s exceeded 20% of the initial value. Recordings (obtained with Clampex 9.2 software, Molecular Devices, Sunnyvale, CA, USA) were filtered at 10 kHz and sampled at 10 kHz.

Electrophysiological data analysis

Electrophysiological data were analysed using Clampfit 10.0 (Molecular Devices). The template search function of the software was used to detect pharmacologically isolated excitatory and inhibitory spontaneous post synaptic currents (sPSCs). Cell input resistance (R_{in}) was calculated measuring the current response to 10 mV hyperpolarizing steps from V_h.

Immunohistochemistry

Immunohistochemical experiments were run to determine the effect of TBOA and nicotine on HM survival. For this, brainstem slices (450 μm) containing the hypoglossal nucleus were processed as described above. After 4 h of treatment, PBS containing 4% paraformaldehyde was used as fixative medium (4 h at 4°C) and 30% sucrose as cryoprotector (72 h at 4°C). Thereafter, slices were embedded in a mounting medium for cryostat sectioning and frozen for at least 12 h. Cryostat tissue sections (30 μm) were sequentially collected on histology slides, rinsed three times for 10 min in PBS, and treated with blocking solution (10% normal goat serum, 50% BSA, 3% Triton X-100 in PBS) for 3 h at room temperature. Slices were then incubated overnight at 4°C with the primary antibodies anti-SMI 32 (mouse monoclonal, 1:200 dilution; BioLegend, San Diego, CA, USA; validated in our previous studies, see Nani *et al.* 2010; Cifra *et al.* 2012) and anti-UDP-glucose glycoprotein glucosyltransferase 1 (UGGT; rabbit monoclonal, 1:500 dilution; Abcam, Cambridge, UK). The secondary antibodies AlexaFluor 488 and 594 (1:500

dilution; Molecular Probes, Invitrogen, Carlsbad, CA, USA) were applied for 2 h at room temperature. Primary and secondary antibodies were diluted in the antibody solution containing: 2% normal goat serum, 10% BSA and 1% Triton X-100 in PBS. After incubation with the secondary antibody, slices were rinsed and stained with the DNA dye DAPI (1:1000 dilutions in PBS) for 20 min at room temperature. Finally, slices were mounted with fluorescence mounting medium (Dako, Glostrup, Denmark) to reduce fading. Images were taken by either a Zeiss Axioskop2 microscope (Oberkochen, Germany) or a Nikon confocal microscope (Tokyo, Japan), using 1 μm z sectioning. SMI 32-immunopositive HMs were counted within a 67.2 mm^2 region of interest (ROI) for each nucleus section, using ImageJ software (version 1.44p, W. Rasband, National Institutes of Health, Bethesda, MD, USA).

MTT mitochondrial toxicity test

As described by Mosmann (1983), cell viability was tested with the MTT assay in accordance with previously reported methods (Mazzone *et al.* 2010). After 4 h treatment with various protocols as above, slices were incubated for 2 h at room temperature with 3(4,5-dimethylthiazolyl-2)-2,5 diphenyl tetrazolium (MTT) dissolved (0.5 mg ml^{-1}) in PBS (pH 7.4) and diluted to a final concentration of 0.5 mg ml^{-1} in Krebs solution. After this period, the medium was replaced with 0.5 ml of HCl and 0.04 M isopropanol, and the samples were slowly shaken in a roller drum at room temperature overnight. The dissolved tissues were then centrifuged at 10,000 *g* for 5 min and the absorbance values (wavelength = 550 nm) were evaluated with a Bio-Rad microplate reader (model 550, Bio-Rad Laboratories, Poole, UK).

Detection of intracellular ROS

Membrane-permeable dihydrorhodamine 123 (DHR 123; Molecular Probes, Invitrogen) was used to evaluate the generation of intracellular free oxygen radicals as previously reported (Cifra *et al.* 2009; Nani *et al.* 2010). Slices (250 μm) were incubated for 4 h using the protocols as reported, and then treated for 20 min with DHR 123 (5 μM) and Hoechst 33342 (10 mg ml^{-1} stock from Molecular Probes, Invitrogen; dilution 1:1000) diluted in Krebs solution. Finally, slices were washed and transferred to a small Petri dish containing Krebs solution to be analysed with a TCS SP2 Leica confocal microscope (20× objective and 2× magnification). To obtain fluorescence images of rhodamine 123 (Rho 123, the oxidized form of DHR 123) staining, slices were visualized by excitation at 514 nm and emission at 530–610 nm. For slice counterstaining, we used Hoechst 33342, a cell-permeable fluorescent dye which emits blue fluorescence once bound to double-stranded DNA. Images were acquired in 5 μm steps to a total 40 μm z-stack (corresponding to one HM plane) from each slice side for both hypoglossal nuclei. ImageJ software was used to measure Rho 123 fluorescence signal intensity and detect Hoechst 33342 and Rho 123 signal-positive voxels.

Western blot

Western blot analysis was performed on whole brainstem treated according to the protocols described above and previously published (Mladinic *et al.* 2014). Tissues were lysed in CHAPS buffer solution (0.5% CHAPS, 50 mM Tris pH 7.5, 1 mM EDTA, 150 mM NaCl, 10% glycerol plus protease inhibitors mixture; Complete, Roche Applied Science, Basel, Switzerland) and immunoblotted with rabbit anti-UGGT (1:7000, Abcam) and mouse anti-β-actin (1:2000, Sigma) antibodies. For signal detection we used the enhancer chemiluminescence light system (Amersham Bioscience, Piscataway, NJ, USA). The signal was recorded with the digital imaging system Alliance 4.7 (UVItec, Cambridge, UK) and quantified with the program Alliance LD2-77-WL (UVItec).

Real-time RT-PCR

As for Western blot, PCR experiments were performed on whole brainstem and RNA was extracted with the protocol described above using Trizol reagent (Invitrogen). After extracting RNA with a purpose-made kit (Ambion, Austin, TX, USA), cDNA was purified using the RNeasy Mini Kit (Qiagen, Hilden, Germany) and retrotranscribed with the iScript cDNA Synthesis Kit (Bio-Rad, Hercules, CA, USA). To study the unfolded protein response (UPR) we used the RT^2 Profiler PCR Array PARN 089ZD (Qiagen; http://www.sabiosciences.com/rt_pcr_product/HTML/PARN-089Z.html) (Kuny *et al.* 2012). All the analysed genes are listed in the Supporting Information, Table S1.

Drugs

The following drugs were used: (2R)-amino-5-phosphonovaleric acid (AP5, Tocris, Bristol, UK), 6,7-dinitroquinoxaline-2,3-dione (DNQX, Abcam), bicuculline methiodide (Tocris), dihydro-β-erythroidine (DHβE, Tocris), (TBOA, Tocris), methyllycaconitine (MLA, Sigma-Aldrich, Saint Louis, MO, USA), nicotine (Sigma-Aldrich) and strychnine hydrochloride (Tocris).

Statistical analysis

Results were collected from at least three different experiments and expressed as means ± standard error of the mean; *n* refers to the number of slices or brainstems for

each independent experiment. For statistical analysis, we used SigmaStat 3.5 (Systat Software, Chicago, IL, USA). A normality test was first used to distinguish between parametric and non-parametric data. For multiple groups, parametric data were compared with the one-way ANOVA, whereas non-parametric data were evaluated with the Kruskal–Wallis one-way ANOVA on ranks test. Student's *t*-test was applied to compare two parametric groups; otherwise non-parametric values were processed with the Mann–Whitney test. Groups of data were accepted as statistically different at $P \leq 0.05$.

Results

Nicotine inhibited bursts induced by TBOA

Figure 1*A* exemplifies how bath application of TBOA (50 μM) induced bursting activity that occurred in 51% of HMs (41/80) in accordance with previous data from our laboratory (Sharifullina & Nistri, 2006). This phenomenon is known to originate from extensive network excitation involving rhythmic intracellular Ca^{2+} waves, gap junction communication and activation of certain K^+ conductances (Sharifullina *et al.* 2005). Bursts disappear when TBOA is washed out within 20 min from onset; otherwise HMs are usually damaged (Sharifullina & Nistri, 2006). In the present study bursts had a mean amplitude of -545 ± 69 pA calculated from baseline current, duration of 43 ± 2 s and period of 94 ± 7 s ($n = 41$). It is noteworthy that, within a typical burst sequence of seven events, the second and third ones (Fig. 1*Da*) were the largest in amplitude followed by a gradual decrease. Regardless of a cell's ability to generate bursts, a significant rise in amplitude and frequency of spontaneous post-synaptic currents was observed in analogy to previous data (Sharifullina & Nistri, 2006).

To test the effect of nAChR ligands on bursting activity and other electrophysiological properties, we first established that TBOA could evoke bursting (at least two such events) and then applied the drug under investigation. Figure 1*B* exemplifies the effect of nicotine (1 μM), which switched off bursts within 3 min. A higher concentration (10 μM) of nicotine rapidly and fully blocked TBOA-evoked bursts (Fig. 1*C*). Figure 1*Da–c* summarizes average data for burst depression induced by 1 or 10 μM nicotine.

Nicotine-induced modulation of synaptic events

Regardless a cell's propensity to generate TBOA-elicited bursts, nicotine consistently exerted similar effects on spontaneous synaptic events that were measured in the interval between bursts or during the inward baseline current induced by TBOA on non-bursters (Sharifullina & Nistri, 2006). Thus, Fig. 1*E* and *F* shows that the two nicotine concentrations (1 and 10 μM) decreased average amplitude of sPSCs that returned to basal values within approximately 10 min. While these data collectively indicated that nicotine could depress bursting as well as synaptic transmission, we next inquired the mechanism of action underlying the observed phenomena. Recording a mixed population of synaptic events did not allow us to identify any discrete modulation by nicotine of excitatory or inhibitory synaptic transmission. In particular, because nicotine can facilitate synaptic inhibition (Jaiswal *et al.* 2016), it might have been possible that enhanced inhibition was one process to block bursting.

On HMs, synaptic inhibition is mediated by glycinergic (Singer *et al.* 1998) and GABAergic (Donato & Nistri, 2000) inputs that were investigated after blocking glutamatergic transmission. Hence, we antagonized AMPA and NMDA receptors with DNQX (10 μM) and AP5 (50 μM), and thus suppressed TBOA-induced bursts (Sharifullina & Nistri, 2006). In the presence of nicotine (10 μM), GABAergic events (Fig. 2*A*) unmasked with the glycine antagonist strychnine (0.4 μM; Donato & Nistri, 2000) were not significantly changed in amplitude (Fig. 2*A*, *C*; $n = 5$), while their frequency (Fig. 2*A*, *D*) rose significantly from 3 ± 0.7 to 7 ± 0.04 Hz ($P \leq 0.001$; $n = 5$). The GABA receptor blocker bicuculline (10 μM) was used to investigate glycinergic current changes in the presence of nicotine (10 μM). Also in this case the event amplitude remained unchanged (Fig. 2*B*, *C*; $n = 5$), while the event frequency was significantly increased from 2 ± 0.9 to 6 ± 1 Hz ($P = 0.042$; $n = 5$; Fig. 2*B*, *D*). While these data indicated that nicotine could facilitate inhibitory neurotransmission onto HMs, the impact of this phenomenon on bursting could not be directly assessed because bursts were pharmacologically prevented.

Next, we explored if nicotine modulated excitatory synaptic transmission after suppressing synaptic inhibition with bicuculline (10 μM) and strychnine (0.4 μM) (Donato & Nistri, 2000; Marchetti *et al.* 2002): with such a protocol the occurrence of TBOA-induced bursts becomes facilitated (Sharifullina & Nistri, 2006), as validated by the present observation that TBOA evoked bursts in all recorded cells ($n = 5$). Nicotine (10 μM) fully blocked bursting activity (Fig. 2*E*), yet it did not influence spontaneous excitatory postsynaptic current (sEPSC) amplitude recorded in the presence of TBOA + strychnine + bicuculline (Fig. 2*F*). Furthermore, sustained application of nicotine led to a late, significant decrease in the average sEPSC frequency, suggesting depressed release of glutamate (Fig. 2*G*; $n = 4$) probably due to nAChR desensitization (Quitadamo *et al.* 2005). In these tests (Fig. 2*F*, *G*) we analysed for each drug protocol applied to each slice approximately 3000 synaptic events in control Krebs, a value that fell to about 1500 at the end of the TBOA plus nicotine application.

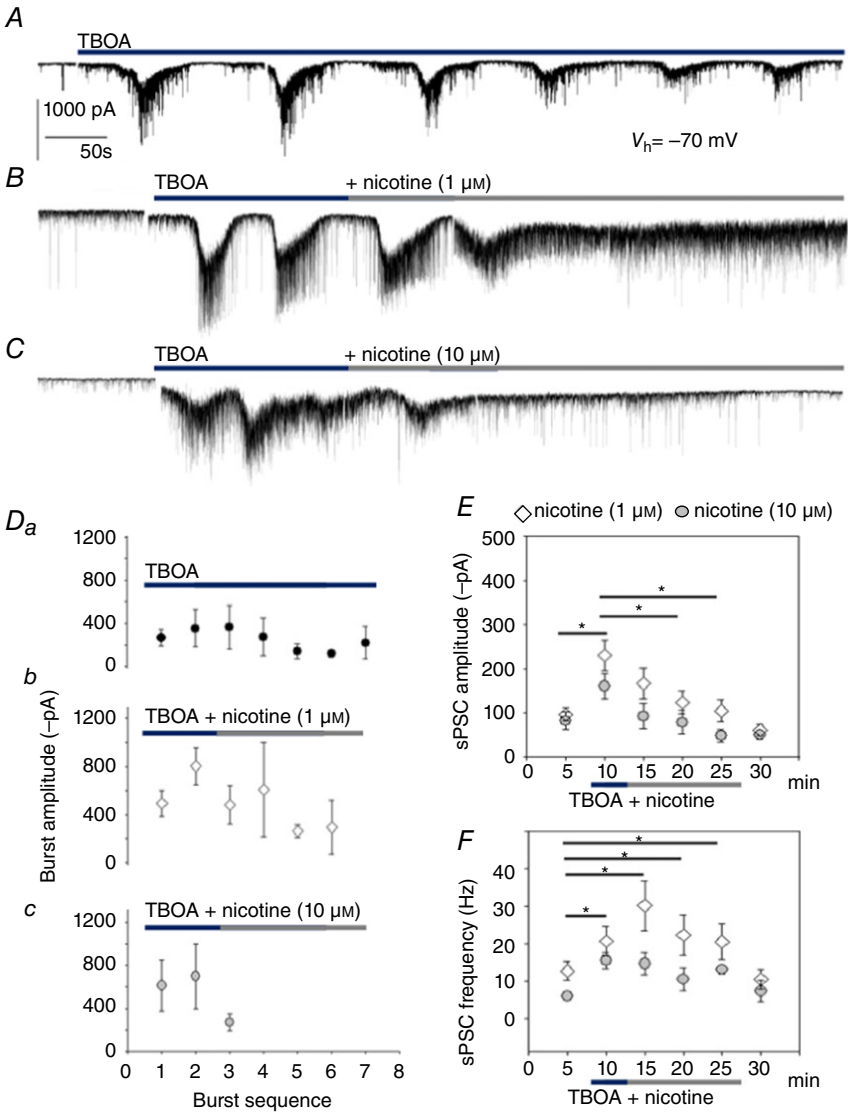

Figure 1. Nicotine depresses bursting activity induced by TBOA
A, record under voltage-clamp configuration ($V_h = -70$ mV) showing bursting activity evoked by 50 μM TBOA. Bursts are characterized by large inward currents with superimposed spikes and interposed spontaneous synaptic events. *B*, subsequent application of 1 μM nicotine decreases burst activity; *C*, higher concentration of nicotine (10 μM) fully blocks bursts. Trace interruptions are due to R_{in} monitoring. *D*, plots of burst amplitude *vs.* burst sequence. In the presence of TBOA (*Da*), on average, cells manifest seven bursts of decreasing amplitude. Co-application of 1 μM nicotine (*Db*) after the first two bursts reduces the burst amplitude. A higher concentration of nicotine (10 μM; *Dc*) fully blocks burst activity. *E*, spontaneous postsynaptic current (sPSC) amplitude is significantly smaller in the presence of nicotine (1 or 10 μM) when compared to TBOA alone. Horizontal bars indicate the data groups tested for statistically significant difference. Nicotine (1 μM): Kruskal–Wallis one-way analysis on ranks test: $P = 0.002$ among groups; Student's *t*-test: $^*P = 0.003$ for control *vs.* TBOA at 10 min, $^*P = 0.026$ TBOA at 10 min. *vs*. TBOA + nicotine at 20 min, $^*P = 0.014$ for TBOA at 10 min. *vs.* TBOA + nicotine at 25 min and $P = 0.003$ for TBOA at 10 min *vs.* wash out; $n = 8$. Nicotine (10 μM): Kruskal–Wallis one-way analysis on ranks test: $P = 0.046$ among groups; Student's *t*-test: $^*P = 0.053$ for control *vs.* TBOA at 10 min, $^*P = 0.029$ TBOA at 10 min. *vs*. TBOA + nicotine at 20 min, $^*P = 0.029$ for TBOA at 10 min. *vs*. TBOA + nicotine at 25 min and $P = 0.029$ for TBOA at 10 min *vs.* wash out; $n = 5$. *F*, sPSC frequency is not influenced by nicotine (1 or 10 μM). Horizontal bars indicate the data groups tested for statistically significant difference. Nicotine (1 μM): Kruskal–Wallis one way analysis on ranks test: $P = 0.011$ among groups; Student's *t*-test: $^*P = 0.028$ for control *vs.* TBOA at 10 min, $^*P = 0.004$ control *vs*. TBOA + nicotine at 15 min and $P = 0.003$ for TBOA + nicotine at 15 min *vs.* wash out, $^*P = 0.015$ for control *vs*. TBOA + nicotine at 20 min and $^*P = 0.009$ for control *vs.* TBOA + nicotine at 25 min; $n = 8$. Nicotine (10 μM): Kruskal–Wallis one-way analysis on ranks test: $P = 0.002$ among groups; Student's *t*-test: $^*P = 0.003$ for control *vs.* TBOA at 10 min, $^*P = 0.024$ control *vs*. TBOA + nicotine at 15 min and $^*P = 0.003$ for control *vs.* TBOA + nicotine at 25 min; $n = 5$.

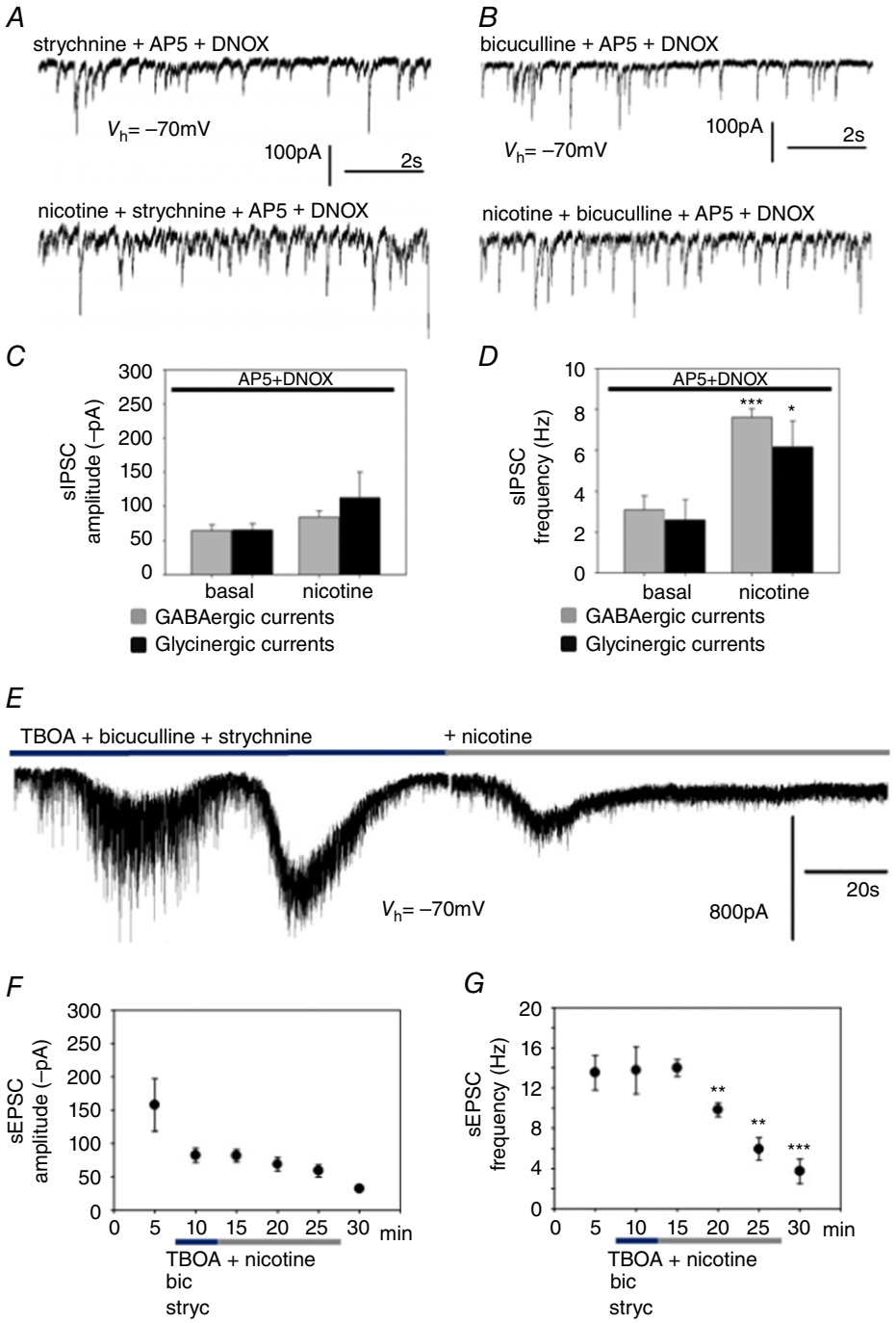

Figure 2. Nicotine effects on inhibitory and excitatory synaptic currents
Voltage clamp traces ($V_h = -70$ mV) showing example of GABAergic (*A*) and glycinergic (*B*) currents under basal (strychnine or bicuculline, respectively plus AP5 + DNQX) or nicotine treatment conditions without application of TBOA. *C*, analysis of synaptic event amplitude shows no effect by 10 μM nicotine on GABAergic ($n = 5$) or glycinergic ($n = 5$) inhibitory currents (sIPSC). *D*, frequency of spontaneous inhibitory post synaptic currents (sIPSC) is significantly augmented by nicotine. Student's *t*-test: $^{***}P \leq 0.001$ for GABAergic currents, $n = 5$; $^{*}P = 0.042$ for glycinergic currents, $n = 5$. *E*, 10 μM nicotine fully blocks burst activity induced by TBOA in the continuous presence of bicuculline (10 μM) and strychnine (0.4 μM). Gap in the trace is for R_{in} monitoring. *F*, amplitude of excitatory synaptic currents (sEPSC) is not changed during TBOA + nicotine application when compared with TBOA alone. Kruskal–Wallis one-way analysis on ranks test: $P = 0.010$ among groups; $n = 4$. *G*, nicotine (10 μM) significantly decreases sEPSC occurrence. Kruskal–Wallis one-way analysis on ranks test: $P \leq 0.001$ among groups; Student's *t*-test: $^{**}P = 0.009$ for TBOA + nicotine at 15 min *vs.* TBOA + nicotine at 20 min; $^{**}P = 0.002$ for TBOA + nicotine at 15 min *vs.* TBOA + nicotine at 25 min; $^{***}P \leq 0.001$ TBOA + nicotine at 15 min *vs.* washout; $n = 4$.

Table 1. HM input resistance (mean ± SEM)

	Input resistance (MΩ)
Control	132 ± 29
TBOA	105 ± 16
TBOA + nicotine	113 ± 17
TBOA + bicuculline + strychnine	109 ± 20
TBOA + bicuculline + strychnine + nicotine	102 ± 24
AP5 + DNQX	157 ± 24
AP5 + DNQX + nicotine	165 ± 35
P (one-way ANOVA)	$P = 0.341$

TBOA data were recorded during the interburst periods, whereas the TBOA + nicotine values were recorded after burst suppression.

We also measured HM input resistance following such pharmacological treatments because changes in multi-site-generated synaptic events may simply originate via alteration in HM passive membrane properties. Thus, Table 1 shows that HM R_{in} values were not statistically different among drug treatments in keeping with former reports (Lamanauskas & Nistri, 2006; Sharifullina & Nistri, 2006; Cifra *et al.* 2011*a*).

The inhibitory effects of nicotine on bursting and related synaptic events should not be confused with the ability by nicotine *per se* (5, 10 or 20 μM) to induce fast oscillations in a subpopulation of HMs (Lamanauskas & Nistri, 2006). In the present study, when synaptic inhibition was pharmacologically suppressed, after 5 min of nicotine application (10 μM), rapid rhythmic oscillations emerged in the majority of HMs (60%, $n = 5$) at oscillatory frequency of 10 ± 1 Hz.

Taken together, these results show that, during excitotoxic stress, nicotine depressed bursting through a combinatorial network process that probably included potentiation of synaptic inhibition and depression of glutamate release. It was, however, noteworthy that, even when synaptic inhibition was blocked, nicotine remained an effective burst suppressor.

nAChR antagonists enhanced bursting activity

To explore any role of endogenous ACh and whether the effects of nicotine could be attributed to nAChR block, we next tested DHβE (5 μM) and MLA (5 nM), namely nAChR antagonists against the neuronal α4 and α7 receptor subunits, respectively (Arroyo-Jiménez *et al.* 1999; Jones *et al.* 2001; Simone *et al.* 2005). Neither DHβE nor MLA significantly reduced the peak amplitude and frequency of sPSCs in control solution (Table 2), confirming that under resting conditions there was no detectable cholinergic transmission on HMs (Lamanauskas & Nistri, 2006).

Table 2. Variation in sPSC amplitude and frequency in the presence of DHβE (5 μM) or MLA (5 or 50 nM) ($n = 5$) (mean ± SEM)

	Amplitude (%)	Frequency (%)
DHβE (5 μM)	85 ± 2	95 ± 4
MLA (5 nM)	92 ± 2	83 ± 5
MLA (50 nM)	105 ± 11	82 ± 6

When these antagonists were applied in combination (Fig. 3*A*) or isolation (Fig. 3*B*, *C*) during TBOA-evoked bursting, they did not interfere with burst parameters (amplitude, duration and period; Fig. 3*D*, *E*). Likewise, co-application of nAChR antagonists with TBOA induced a similar increase in synaptic event amplitude (Fig. 3*F*) and frequency (Fig. 3*G*) as in TBOA alone (Sharifullina & Nistri, 2006). Nevertheless, a distinct scenario appeared when nAChR antagonists were tested on HMs (about 50%) that did not initially burst in the presence of TBOA despite the application of this drug for 15 min. Hence, as shown in Fig. 4*A*–*C*, DHβE and MLA in combination or applied separately unmasked bursting in 6/10 HMs. These results suggest a conditional role for endogenous cholinergic transmission as it could not change established bursting, yet it could decrease the bursting probability in a subgroup of HMs.

The next question was whether burst inhibition evoked by nicotine was mediated via nAChRs. As shown in Fig. 1*Dc*, 10 μM nicotine rapidly suppressed bursts that were arrested after the 3rd event. On the other hand, following co-application of nAChR antagonists together with nicotine after the 2nd event (Fig. 5*A*, *B*), bursts continued in a fashion similar to that detected in TBOA alone solution reaching a total number of seven events (Fig. 1*Da*). Note that the total number of events was 6–7 also in the presence of antagonists applied after the 2nd TBOA-induced burst (Fig. 3*D*).

Excitotoxic cell loss

As previously demonstrated by our laboratory, a significant loss of HMs was detected 4 h after TBOA application through a delayed cell death process (Cifra *et al.* 2011*a*). The present study investigated whether nicotine could prevent this outcome. HM numbers were evaluated with the marker SMI 32, which labels the non-phosphorylated form of neurofilament H (Campbell & Morrison, 1989; Cifra *et al.* 2012). Figure 6*A*, *B* shows that extending the slice incubation period to a maximum of 6 h did not change the number of HMs in sham or TBOA-treated conditions. The nucleus of motoneurons that survived did not show signs of apoptosis or necrosis. Taken together, these data suggest that, within a timeframe of 4 h, the toxic effect of

TBOA (approximately 35% HM death) reached a plateau. Further experiments were therefore performed with a 4 h treatment protocol. Figure 6*C*, *D* shows the extent of HM loss after TBOA treatment *versus* control (sham) or nicotine-alone treatment (Student's *t*-test: $P \leq 0.001$ for sham *vs.* TBOA and $P \leq 0.001$ for TBOA *vs.* nicotine; $n = 9$ slices). This significant loss observed after TBOA alone was contrasted by its co-application with nicotine (10 μM) (Student's *t*-test: $P \leq 0.001$ for TBOA *vs.* TBOA + nicotine; $n = 9$).

Nicotine prevented TBOA-induced oxidative stress damage to HMs

We next queried whether nicotine might have prevented neuronal death induced by TBOA by inhibiting oxidative stress (Selkirk *et al.* 2005; Lewerenz *et al.* 2006; Cifra *et al.* 2011*a*). Thus, DHR 123, a cell-permeable fluorescent probe, was used to detect ROS such as peroxide and peroxynitrite (Cifra *et al.* 2011*a*). Using the experimental paradigm described earlier, Figure 7*A* shows staining with Rho 123 and Hoechst 33342 (for nuclear staining) within

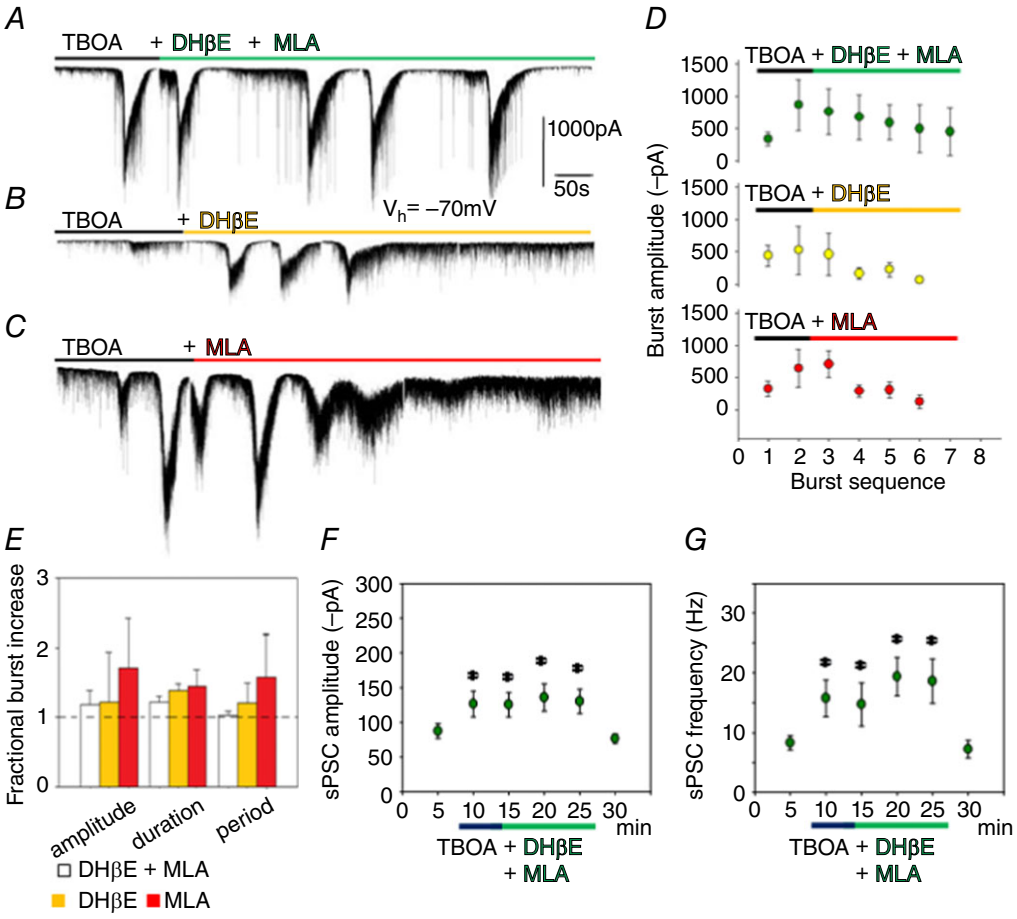

Figure 3. nAChR antagonists facilitate bursting activity
A–C, voltage clamp traces ($V_h = -70$ mV) show bursting activity in the presence of nAChR antagonists DHβE and MLA applied together or in isolation. Traces interrupted for R_{in} monitoring. *D*, plots of average burst amplitude *vs.* burst sequence for the protocols shown in *A–C*. *E*, unchanged burst values (amplitude, duration and period) in the presence of nAChR antagonists. *F*, the increase in sPSC amplitude evoked by TBOA (Sharifullina & Nistri, 2006) persists unchanged even in the presence of antagonists. Kruskal–Wallis one-way analysis on ranks test: $P = 0.042$ among groups; Student's *t*-test: $^*P = 0.022$ for TBOA at 10 min *vs.* wash out, $^*P = 0.015$ for TBOA + DHβE + MLA at 15 min *vs.* wash out, $^*P = 0.011$ for TBOA + DHβE + MLA at 20 min *vs.* wash out, $^*P = 0.022$ for TBOA + DHβE + MLA at 25 min *vs.* wash out; $n = 9$. *G*, the significant increase in sPSC frequency induced by TBOA (Sharifullina & Nistri, 2006) is not altered by nAChR antagonists. Kruskal–Wallis one-way analysis on ranks test: $P = 0.010$ among groups; Student's *t*-test: $^*P = 0.021$ for control *vs.* TBOA at 10 min and $P = 0.042$ for TBOA at 10 min *vs.* wash out, $^*P = 0.047$ for TBOA + DHβE + MLA at 15 min *vs.* wash out, $^*P = 0.010$ for control *vs.* TBOA + DHβE + MLA at 20 min and $P = 0.004$ for TBOA + DHβE + MLA at 20 min *vs.* wash out, $^*P = 0.028$ for control *vs.* TBOA + DHβE + MLA at 25 min and $P = 0.012$ for TBOA + DHβE + MLA at 25 min *vs.* wash out; $n = 9$.

the nucleus hypoglossus following 4 h of incubation in Krebs solution, TBOA (50 μM), TBOA (50 μM) + nicotine (10 μM), or nicotine (10 μM). Figure 7*B* indicates that after 4 h the number of Hoechst-labelled nuclei fell to 70% after TBOA, whereas it remained similar to control when TBOA + nicotine were applied. This observation is, therefore, consistent with the degree of HM losses depicted in Fig. 6. Figure 7*C* summarizes average data for ROS fluorescence: thus, the ratio of rhodamine-positive motoneurons to Hoechst-positive cell nuclei was significantly larger in the presence of TBOA *vs.* sham or nicotine treatment. Co-application of nicotine prevented TBOA-induced cell loss and ROS generation as shown in Fig. 7*A*–*C*.

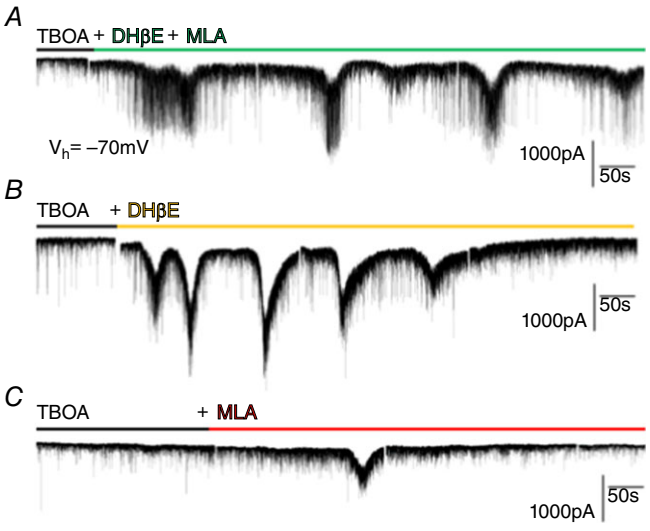

Figure 4. nAChR antagonists trigger bursting activity in non-burster cells
Voltage clamp traces (V_h = −70 mV) indicating examples of antagonists facilitating emergence of bursting in non-burster cells. Gaps in the traces are due to R_{in} monitoring.

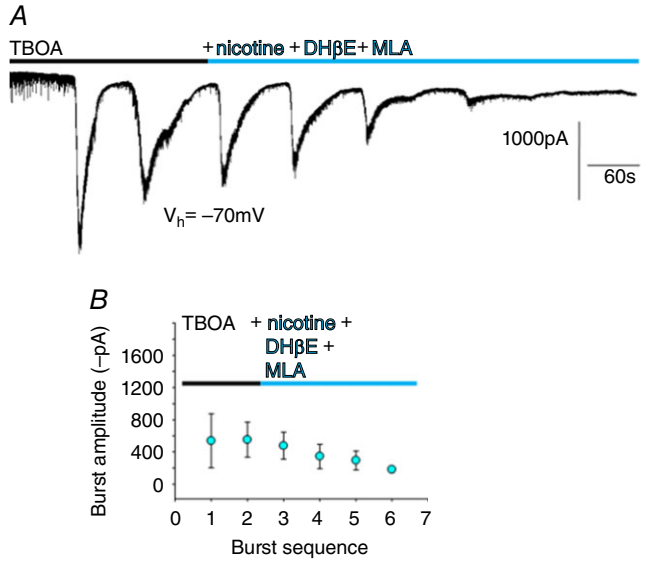

Figure 5. Lack of nicotine-mediated inhibition of bursting by co-application of nAChR antagonists
A, voltage clamp recording (V_h = −70 mV) showing that bursting activity is not blocked by a co-application of nicotine (10 μM), DHβE (5 μM) and MLA (5 nM). *B*, plots of burst amplitude *versus* burst sequence (n = 5). Data are obtained in the presence of bicuculline and strychnine.

nAChR activation stimulated metabolic activity in HMs

To explore the link between ROS generation and perturbed mitochondrial energy metabolism, we examined the metabolic activity of samples after 4 h of treatment using a standard test based on the reduction of MTT to formazan, a non-invasive index of mitochondrial activity (Mosmann, 1983; Mazzone *et al.* 2010; Mazzone & Nistri, 2011; Goiato *et al.* 2015). Formazan formation (Fig. 7*D*) was decreased to 73 ± 4% after TBOA when compared with sham. Co-application of TBOA + nicotine (10 μM) increased MTT reduction to 126 ± 16%, a value similar to the effect produced by nicotine alone (120 ± 14%; n = 4). The data thus indicated that nicotine improved energy metabolism even in conditions of excitotoxic stress applied to brainstem tissue.

Application of TBOA induced UPR

As excitotoxicity is associated with an increase in ROS and mitochondrial dysfunction, this phenomenon is thought to eventually lead to protein misfolding and neurodegeneration (Forder & Tymianski, 2009; Mehta *et al.* 2013). Indeed, under these conditions, protein misfolding induces the UPR, namely a reactive cell process activated in the endoplasmic reticulum (ER) by three major sensors, ATF6 (α and β), IRE1 (α and β) and PERK (Rutkowski & Kaufman, 2004; Doyle *et al.* 2011). ER stress has been reported as an early pathological event in both sALS and fALS (Doyle *et al.* 2011; Hetz *et al.* 2013; Matus *et al.* 2013). We wondered whether TBOA-induced excitotoxicity was followed by activation of UPR. For this, we investigated mRNA expression level of 84 genes correlated with ER stress (Kuny *et al.* 2012) as listed in Supporting Information Fig. S1 and Table S1. We report a discrete increase in the expression of certain genes after 4 h in the presence of TBOA compared with sham or nicotine (Fig. 8). In particular, we observed a significant upregulation of genes involved in ER stress mechanisms (Fig. 8 and Table 3 for statistics) such as apoptosis [Mapk8 (JNK1), Mapk9 (JNK2); Davis, 2000; Shoji *et al.* 2000], cholesterol metabolism regulation (Insig2, Mbtps1, Mbtps2; Kleinfelter *et al.* 2015; Ren *et al.* 2015), control of protein folding quality (Edem1, Rpn1; Qin *et al.* 2012; Wang *et al.* 2015), ER degradation (ERAD; Htra4, Nploc4, Syvn1; Clausen *et al.*

2002; Ballar *et al.* 2011; Nakajima *et al.* 2015), protein folding (Hspa4, Uggt1; Zhou *et al.* 2014; Wang *et al.* 2015), transcription [Atf6, Ern2 (IRE1β); Rutkowski & Kaufman, 2004; Oikawa *et al.* 2012] and translation (Eif2ak2, Ppp1r15b; Kloft *et al.* 2012; Niso-Santano *et al.* 2013). A systematic description of the activity of the single genes studied in the current protocol is provided at: http://www.sabiosciences.com/rt_pcr_product/HTML/PARN-089Z.html#function. These results validated the notion that TBOA-evoked activation of the UPR system was manifested as increased activity of a group of genes related to ER stress, including ATF6 and IRE1β (Rutkowski & Kaufman, 2004; Doyle *et al.* 2011), and that such an effect was inhibited by nicotine.

Previous experiments have indicated the interaction of nicotine with the allosteric protein modulator lynx1 (Miwa *et al.* 1999; Henderson & Lester, 2015) as an important process to provide neuroprotection. Our

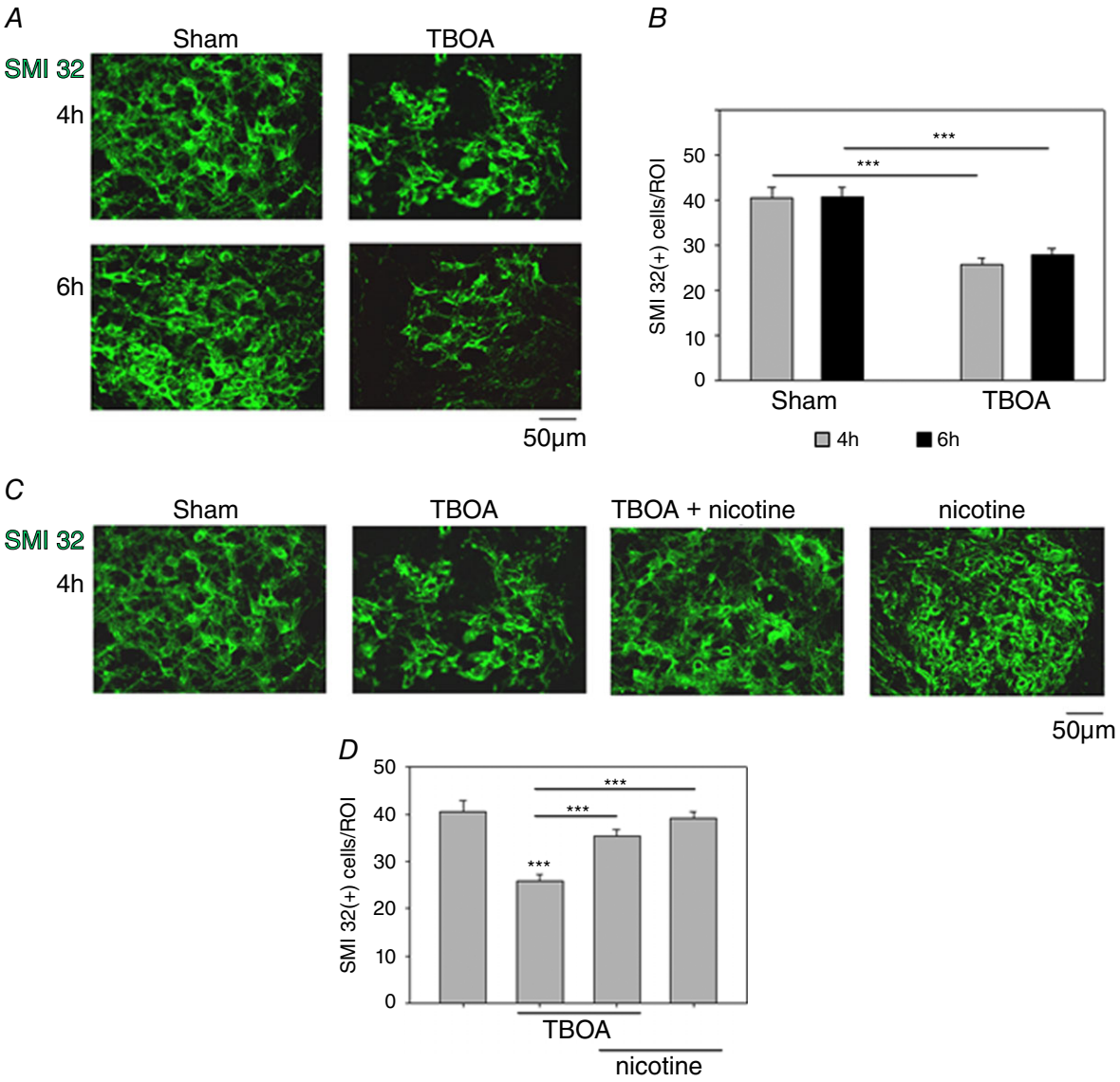

Figure 6. Motoneuron survival following TBOA-induced excitotoxicity
A, example of HMs after 4 h (top row) or 6 h (bottom row) incubation in Krebs solution (sham, left column) or TBOA solution (right column). *B*, bar chart indicating similar loss of HMs after 4 or 6 h of treatment with TBOA. Student's *t*-test: $^{***}P \leq 0.001$ for sham *vs.* TBOA 4 h, $^{***}P \leq 0.001$ for sham *vs.* TBOA 6 h; $n = 9$. *C*, example of HMs labelled with the motoneuron marker SMI 32 after 4 h in Krebs solution (sham), or treated with TBOA, TBOA + nicotine (10 μM), or nicotine (10 μM) alone. *D*, bar chart showing significant loss of motoneurons after TBOA treatment (compared with sham or nicotine data), an effect fully prevented by nicotine. Kruskal–Wallis one-way analysis on ranks test: $P \leq 0.001$ among groups; Student's *t*-test: $^{***}P \leq 0.001$ for sham *vs.* TBOA, $^{***}P \leq 0.001$ for TBOA *vs.* TBOA + nicotine, $^{***}P \leq 0.001$ for TBOA *vs.* nicotine; $n = 9$.

preliminary experiments, however, confirmed that lynx1 is not expressed in the brainstem at neonatal age (Thomsen *et al.* 2014; see Fig. 9). Although the precise role of lynx1 remains incompletely understood (Henderson & Lester, 2015), our data point to additional mechanisms underlying the neuroprotective effect of nicotine.

Nicotine enhanced mechanisms for protein folding and quality control

To handle and correct early UPR-mediated protein misfolding, cells can activate a series of intracellular mechanisms among which UGGT is a key contributor to recognize glycoproteins such as antibodies, cytokines or hormones with minor folding defects (Izumi *et al.* 2012). UGGT can then repair misfolded proteins, making them recognizable by calreticulin for recycling, refolding or degradation (Wang *et al.* 2015). To investigate the extent of protein dysfunction evoked by TBOA and the role of nicotine neuroprotection, we analysed UGGT levels in our model of excitotoxicity. After 4 h of TBOA exposure, a small, yet significant rise in the expression of UGGT was found in brainstem tissue *vs.* control (Fig. 10*A*, *B*). Co-application of nicotine (10 μM) with TBOA restored UGGT levels and, when applied alone, did not induce any significant change (Fig. 10*A*, *B*; $n = 4$).

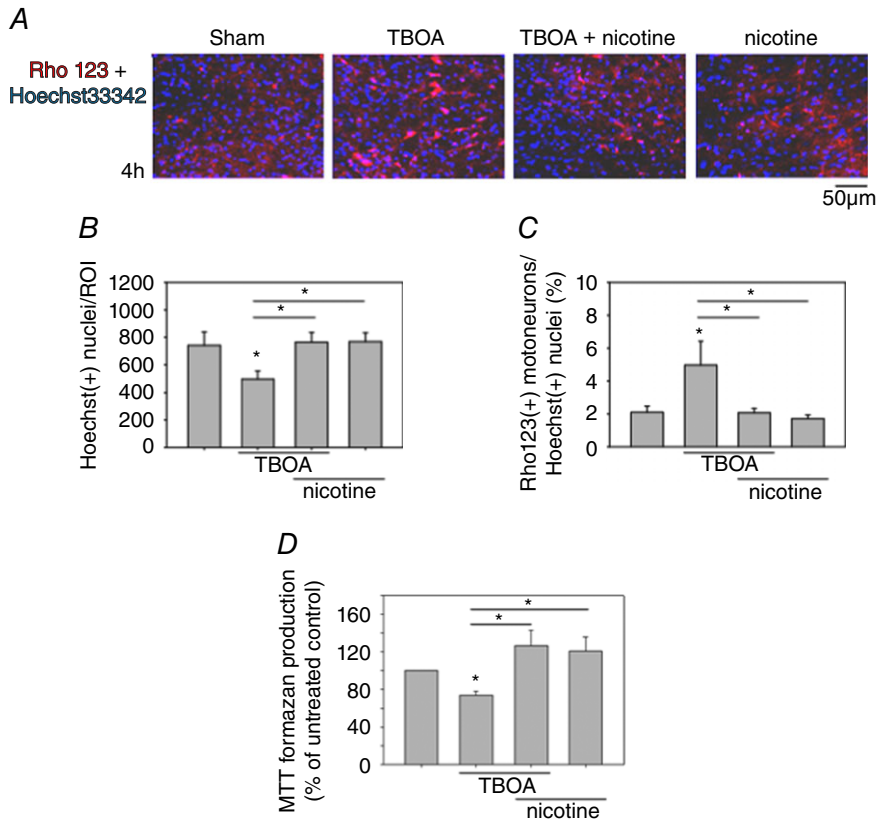

Figure 7. HMs show sign of oxidative stress and deficit in energy metabolism after 4 h application of TBOA
A, example of rhodamine 123 (Rho 123) and Hoechst 33342 staining of slices containing the hypoglossal nucleus incubated for 4 h in Krebs solution (sham), TBOA, TBOA + nicotine (10 μM), or nicotine alone. Rho 123 is used to monitor oxidative stress, whereas Hoechst 33342 is used to label cell nuclei for total cell counting in each slice. *B*, graph showing a significant cell loss after TBOA treatment and protection by nicotine. Kruskal–Wallis one-way analysis on ranks test: $P = 0.025$ among groups; Student's *t*-test: $^*P = 0.040$ for sham *vs.* TBOA, $^*P = 0.018$ for TBOA *vs.* TBOA + nicotine, $^*P = 0.013$ for TBOA *vs.* nicotine; $n = 5$. *C*, bar chart showing higher ratio of rhodamine-positive motoneurons over Hoechst-positive cells after TBOA, an effect prevented by nicotine. Kruskal–Wallis one-way analysis on ranks test: $P = 0.038$ among groups; Mann–Whitney rank sum test: $^*P = 0.057$ for sham *vs.* TBOA, $^*P = 0.057$ for TBOA *vs.* TBOA + nicotine, $^*P = 0.056$ for TBOA *vs.* nicotine; $n = 5$. *D*, bar chart quantifying the percentage of formazan production by brainstem slices. Those treated with TBOA significantly decrease their metabolic activity compared with sham or nicotine: this effect is prevented by nicotine co-application. Kruskal–Wallis one-way analysis on ranks test: $P = 0.030$ among groups; Mann–Whitney rank sum test: $^*P = 0.029$ for sham *vs.* TBOA, $^*P = 0.029$ for TBOA *vs.* TBOA + nicotine, $^*P = 0.057$ for TBOA *vs.* nicotine; $n = 4$.

To further investigate the cellular expression of UGGT, immunohistochemical experiments were performed as illustrated in Fig. 10*C*, *D*. Thus, when examining motoneurons in the ROI exemplified in Fig. 10*C*, the intensity of the UGGT signal was generally very low in sham HMs as quantified in the right-hand side plot for the number of positive cells, which mostly generated a fluorescence signal below 20 AU (Fig. 10*D*, top). After exposure to TBOA (4 h; Fig. 10*C*, *D* middle), surviving cells expressed their UGGT signal mainly above 20 AU. When TBOA and nicotine were co-applied, the UGGT signal was expressed primarily at low intensity (Fig. 10*C*, *D*) in analogy with the data observed when nicotine *per se* was the only slice treatment. Figure 10*E* summarizes average UGGT intensity for single HMs identified in nine slices run in parallel with the protocol delineated above. Thus, TBOA significantly enhanced the UGGT signal, an effect prevented by nicotine. The phenomenon is further illustrated in Fig. 10*F* in which the UGGT fluorescence intensity is plotted against its detection probability. Hence, the plot is largely shifted to the right after TBOA application, demonstrating the higher probability of observing cells with strong fluorescence signal, while nicotine (that *per se* had minimal effect) applied together with TBOA generated a plot virtually indistinguishable from sham.

Discussion

The present study indicates a novel, strong neuroprotection by nicotine via activation of nAChRs that contrasted not only excitotoxic bursts but also prevented cell loss by attenuating the intracellular stress response developing after prolonged exposure to the glutamate uptake blocker TBOA. The experimental use of nicotine was a pharmacological tool to stimulate nAChRs with a metabolically stable agonist. Thus, while these results should not be construed in support for a neuroprotecting role of smoking, they do propose that nAChRs modulate the excitatory stress response of brainstem motoneurons. Pharmacological activation of nAChRs might therefore be considered a strategy to be further studied for neuroprotection using models of motoneuron disease *in vitro* and *in vivo*.

A model of motoneuron excitotoxicity

ALS is a neurodegenerative disease characterized by progressive loss of motoneurons and non-neuronal cells (Myszczynska & Ferraiuolo, 2016; Puentes *et al.* 2016) possibly triggered by raised concentrations of extracellular glutamate up to toxic levels due to impaired cell uptake perhaps caused by environmental chemicals (Rothstein *et al.* 1992, 1995). The hypoglossal nucleus, where motoneurons represent about 90% of the neuronal population (Viana *et al.* 1990; Cifra *et al.* 2011*a*), is strongly affected by this process (Comley *et al.* 2015) because of properties such as expression of GluR2-lacking AMPA receptors (Laslo *et al.* 2001), the large amount of intracellular free Ca^{2+} (Ladewig *et al.* 2003), and relatively low levels of glutamate transporters (Rothstein *et al.* 1992) and Ca^{2+} binding proteins (Medina *et al.* 1996), all factors contributing to HM vulnerability. The *in vitro* model developed by our laboratory is based on pharmacological block of glutamate transporters to tilt the delicate balance between excitation and inhibition and to study HMs for a few hours before tissue deterioration (Sharifullina & Nistri, 2006; Cifra *et al.* 2011*a*). While ALS progresses slowly, in our model motoneuron dysfunction is therefore produced rapidly, yet in a patchwork fashion typical of the clinical conditions: thus, our data may be used to investigate the earliest phenomena that later synergize to gradually determine the clinical onset of the disease.

The present report employed neonatal rat tissue because it is difficult to perform patch-clamp recording from

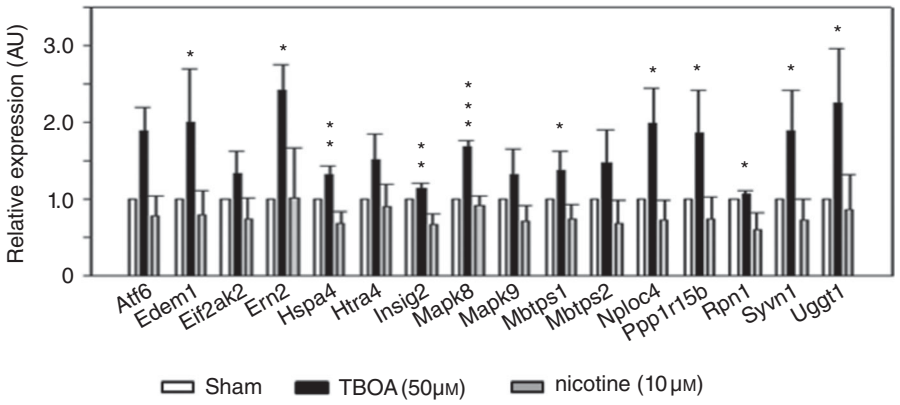

Figure 8. Evaluation of gene profile changes due to UPR stress induced by TBOA
TBOA treatment significantly increases gene expression involved in the UPR stress response. Details of statistical analysis for each gene product considered are provided in Table 3. P values for TBOA *vs.* nicotine: $*P \leq 0.050$, $**P \leq 0.010$, $***P \leq 0.001$; $n = 3$.

Table 3. Statistical analysis of gene products significantly changed after TBOA or nicotine application

	P values			
		Mann–Whitney rank sum test		Student's *t*-test
Gene	Kruskal–Wallis test (among groups)	Sham *vs.* TBOA	Sham *vs.* nicotine	TBOA *vs.* nicotine
Atf6	0.050	0.100	0.700	0.110
Edem1	0.050	0.100	0.700	0.051
Eif2ak2	0.050	0.100	0.700	0.065
Ern2	0.050	0.100	0.700	0.029
Hspa4l	0.004	0.100	0.100	0.004
Htra4	0.050	0.100	0.100	0.074
Insig2	0.004	0.100	0.100	0.007
Mapk8	0.050	0.100	0.700	0.001
Mapk9	0.004	0.100	0.100	0.058
Mbtps1	0.004	0.100	0.100	0.029
Mbtps2	0.050	0.100	0.700	0.063
Nploc4	0.004	0.100	0.100	0.015
Ppp1r15b	0.004	0.100	0.100	0.036
Rpn1	0.004	0.100	0.100	0.020
Syvn1	0.004	0.100	0.100	0.026
Uggt1	0.050	0.100	0.700	0.047

HMs of adult rodents (Jaiswal & Keller, 2009). Our data are consistent with a number of ALS pathogenesis studies done with brainstem slices or cultures from embryonic or neonatal tissue (Singer *et al.* 1998; Ladewig *et al.* 2003; Jaiswal & Keller, 2009; Huang & Gibb, 2014). Notwithstanding these experimental limitations, the model reproduces the principal glutamate hypothesis whereby motoneurons are damaged by hyper-excitability (Vucic & Kiernan, 2010). In line with this notion, recent investigations have indicated that HMs of hSOD1 mice expressing the common genetic mutation G93A already, at neonatal age, show altered dendritic development consistent with changes in membrane excitability (Kanjhan *et al.* 2016).

Our previous studies have indicated that TBOA-induced bursts were not facilitated by the CsCl-based internal solution which was used to minimize leaks currents, and very similar bursting characteristics have been detected when recording with KCl-filled pipettes (Sharifullina & Nistri, 2006; Cifra *et al.* 2011*a*).

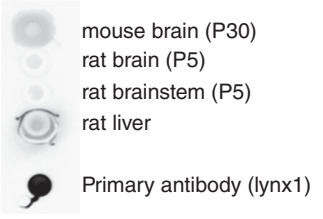

Figure 9. LYNX1 is not detectable in neonatal brainstem tissue
Dot blot experiments showing the presence or the absence of the LYNX1 protein in different samples from mouse and rat tissues at different postnatal ages. Note lack of LYNX1 in P5 rat brain samples.

TBOA-evoked bursts of hypoglossal motoneurons and their block by nicotine

While in the hypoglossal nucleus rhythmicity (often, but not exclusively, related to respiratory patterns) is readily evoked by a series of physiological or pathological conditions (Cifra *et al.* 2009), the rhythm induced by TBOA displays properties that makes it different from bursts elicited, for instance, by NMDA receptor activation (Sharifullina *et al.* 2008). In fact, NMDA-mediated bursts possess distinctive voltage and Mg^{2+} sensitivity, amplitude and frequency (Sharifullina *et al.* 2008): these characteristics do not, however, exclude participation of NMDA receptors to the global network discharges that, via various receptor mechanisms, all contribute to TBOA-evoked events (Cifra *et al.* 2009, 2011*b*). In addition, neonatal rat spinal motoneurons exhibit intrinsic rhythmic oscillations that are typically used to generate fictive locomotion (as reviewed by Kiehn, 2016) and are apparently similar to those observed in the adult spinal cord (Manuel *et al.* 2012). The latter data indicate that NMDA-dependent discharges of neonatal motoneurons comprise persistent inward and outward currents that are not age-dependent.

Application of TBOA, which blocks excitatory amino acid transporters (Shimamoto *et al.* 1998; Sharifullina & Nistri, 2006), allows gradual increase in the extracellular level of glutamate and mimicry of early-stage

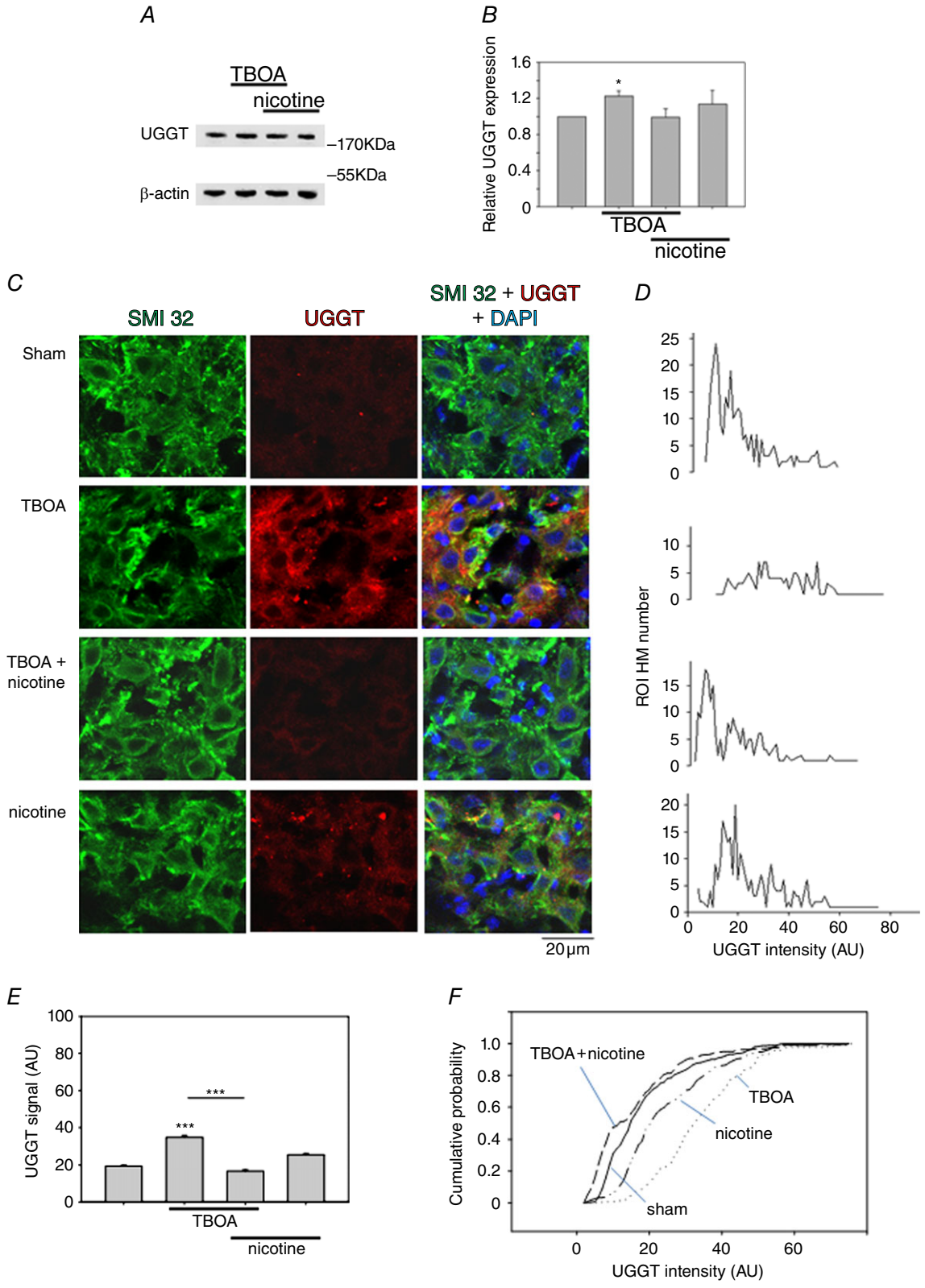

Figure 10. UGGT expression levels in HMs
A, example of Western immunoblotting showing the expression of UGGT in brainstems incubated in Krebs solution, or treated with TBOA, TBOA + nicotine (10 μM), or nicotine. *B*, bar chart quantifying UGGT levels in brainstem samples treated as before, demonstrating increment in UGGT expression after TBOA (Mann–Whitney rank sum test: $^*P = 0.029$ for sham *vs.* TBOA; $n = 4$ brainstems for each group). *C*, example of HMs labelled with the

motoneuron marker SMI 32 (left column) and UGGT (middle column) after 4 h of incubation in Krebs (sham), TBOA, TBOA + nicotine (10 μM), or nicotine solution. Merged images are shown in the right column, where nuclei are visualized with DAPI. *D*, plots showing UGGT fluorescence intensity signal *vs.* HM number observed after different treatments (UGGT-positive HMs: 293, sham; 139, TBOA; 215, TBOA + nicotine; 269, nicotine; $n = 9$ slices for each group). *E*, bar chart quantifying the UGGT signal increase after 4 h of TBOA treatment, an effect prevented by nicotine (Kruskal–Wallis one-way analysis on ranks test: $P \leq 0.001$ among groups; Mann–Whitney rank sum test: $^{***}P \leq 0.001$ for sham *vs.* TBOA; $P \leq 0.001$ for sham *vs.* TBOA + nicotine, $P \leq 0.001$ for sham *vs.* nicotine; $^{***}P \leq 0.001$ for TBOA *vs.* TBOA + nicotine; $P \leq 0.001$ for TBOA *vs.* nicotine; $P \leq 0.001$ TBOA + nicotine *vs.* nicotine; $n = 9$ slices for each group). *F*, plot of cumulative probability distribution of UGGT intensity signal that is shifted to the right by TBOA and returned to sham values in the presence of nicotine (same data as in *E*).

excitotoxicity. Thus, strong network bursting is expressed by nearly half of HMs together with raised intracellular Ca^{2+} followed by delayed neuronal death within a few hours (Sharifullina *et al.* 2005; Sharifullina & Nistri, 2006; Cifra *et al.* 2011*a*). Why some neurons manifest resistance remains unknown.

A neuroprotective action by nAChRs has been proposed against neuroinflammatory processes, glutamate cytotoxicity and, by implication, neurodegenerative diseases such as Alzheimer's disease, Parkinson's disease and ALS (Dajas-Bailador *et al.* 2000; Albuquerque *et al.* 2009; Kawamata *et al.* 2011; Gao *et al.* 2014; Egea *et al.* 2015). To the best of our knowledge, it had not been described before for the hypoglossal nucleus perhaps because cholinergic nerve terminals, from the laterodorsal and pedinculopontine tegmental nuclei, are not abundant and are distributed in an apparently scattered fashion (Rukhadze & Kubin, 2007). A recent study has suggested the presence of motor axon collaterals that may connect motoneurons to their neighbours to increase cholinergic output (Kanjhan *et al.* 2015). Nevertheless, because spontaneous cholinergic events have not been observed even in the presence of anticholinesterases (Quitadamo *et al.* 2005), their contribution to the TBOA-evoked bursts appears limited.

Previous experiments have shown complex effects by nicotine on synaptic transmission of the network impinging upon HMs (Quitadamo *et al.* 2005; Lamanauskas & Nistri, 2006) as validated in the present study with the combined application of nAChR antagonists DHβE and MLA. Despite a degree of receptor desensitization probably produced by nicotine, sustained nAChR activation and modulation of synaptic transmission can occur (Lamanauskas & Nistri, 2006). Previous studies have indicated that nicotine can generate nAChR responses from neuroblastoma cells even after several hours of continuous application (Sokolova *et al.* 2005).We therefore used nicotine as a stable agonist to arrest bursting activity produced by TBOA, and to depress the concomitant increase in sEPSC frequency. These effects could be interpreted as either nicotine-mediated inhibition of network glutamatergic transmission, or enhancement of synaptic inhibition mediated by GABA and glycine (Donato & Nistri, 2000) as confirmed in the present report. Nonetheless, burst arrest by nicotine was observed even when synaptic inhibition was pharmacologically suppressed, suggesting that depression of excitation was an important mode of nicotine action.

nAChR antagonists facilitated excitotoxic bursts induced by TBOA

The dissociation of the HM population into bursters and non-bursters is a phenomenon not yet fully understood as morphological and electrophysiological observations could not identify the underlying cause(s) (Sharifullina & Nistri, 2006). The present study attempted to answer some outstanding issues regarding this question, namely if network cholinergic transmission was fully operative during bursting, and if it had any impact on this process. Thus, we examined the effect of nAChR antagonists on TBOA bursting. In particular, DHβE is a competitive nAChR antagonist preferential for α4 subunit-expressing receptors (Chavez-Noriega *et al.* 1997), whereas MLA is a potent antagonist for α7-containing nAChRs (Palma *et al.* 1996). When DHβE and/or MLA were superfused after inducing bursting activity, there was no significant bursting increment, suggesting that an inhibitory role by endogenous ACh on bursters was minimal. Nevertheless, on non-burster cells the same nAChR antagonists did unmask bursts when applied either in isolation or together. These results confirm the pivotal role of the endogenous cholinergic tone (through $\alpha4\beta2$ and $\alpha7$ nAChRs) to circumscribe bursting during excitotoxic stress. This phenomenon is distinct from cholinergic modulation of motoneuronal excitability (Quitadamo *et al.* 2005; Shao *et al.* 2008). The experiments with nAChR antagonists also allowed us to confirm that the depressant action by nicotine was actually mediated through activation of nAChRs as when agonist and antagonists were co-applied, nicotine lost its ability to suppress bursts.

Nicotine protected hypoglossal motoneurons

Previous studies have reported delayed HM damage by TBOA (Sharifullina & Nistri, 2006; Cifra *et al.* 2011*a*), although the precise mechanism remains unclear. The present study extended the observation time to 6 h

and detected no further HM loss between 4 and 6 h. Thus, a significant decrease in motoneuron numbers (by about 35%) was taken as an established readout of excitotoxicity at 4 h. No sub-region of the hypoglossal nucleus appeared to show selective vulnerability. Similar data were obtained by simply counting Hoechst 33342-positive nuclei. Nicotine *per se* exerted no toxic action on HMs, yet it prevented the HM loss caused by TBOA. This result prompted us to investigate the targets involved in nicotine neuroprotection as well as the implications for surviving HMs. MTT analysis of brainstem tissue reported that mitochondrial activity decreased by approximately 30% after TBOA, in line with the view that even remaining cells probably suffered a degree of metabolic dysfunction. This phenomenon was fully inhibited by nicotine. One possible cause for deficient energy metabolism might have been intracellular buildup of ROS with negative impact on cell survival (Gu *et al.* 2010; Nani *et al.* 2010). In fact, after TBOA application, a significant increase in the number of HMs positive for a ROS fluorescence indicator was detected and fully prevented by nicotine. This finding enabled us to functionally link neuroprotection to prevention of ROS generation and mitochondrial distress.

Cellular site of action of nicotine

nAChRs are widespread along the neuronal plasma membrane, including the cell body and presynaptic terminals (Gotti & Clementi, 2004). Recent studies have, however, revealed that nAChR distribution is not limited to the plasma membrane but it also comprises localization to the outer mitochondrial membrane (Gergalova *et al.* 2012; Lykhmus *et al.* 2014). The main role of mitochondrial nAChRs is attenuation of cytochrome c release, prevention of apoptosis and protection of mitochondria from stress factors (Lykhmus *et al.* 2014). These receptors do not work as classical ion channels, but control different pathways dependent on PI_3K/Akt, CaKMII and Src (Gergalova *et al.* 2012, 2014; Lykhmus *et al.* 2014). Nicotine is expected to act on intracellular receptors because this alkaloid rapidly permeates cell membranes (Albuquerque *et al.* 2009; Henderson & Lester, 2015). When nicotine is chronically applied a population of highly sensitive nAChRs (upregulation) emerges within a few hours (Bencherif *et al.* 1995; Kuryatov *et al.* 2005; Henderson & Lester, 2015) involving various receptor subtypes (Wang *et al.* 1998; Walsh *et al.* 2008). The upregulation induced by nicotine does not apparently require channel activation (Kuryatov *et al.* 2005), or gene transcription (with some exceptions; see Henderson & Lester, 2015) because nAChR mRNA levels are reportedly unchanged after chronic nicotine application, outlining a seemingly post-transcriptional mechanism (Bencherif *et al.* 1995). Overall, the nicotine-enhanced nAChR function is probably the result of a rather complex process (Henderson & Lester, 2015) that comprises, amongst others, accelerated nAChR maturation (Sallette *et al.* 2005) and their increased trafficking to lipid raft membrane regions (Kuryatov *et al.* 2005; Richards *et al.* 2011; Srinivasan *et al.* 2011).

Proposed mechanism of action of nicotine

Protein misfolding associated with hyperactivation of NMDA and Ca^{2+}-permeable (GluR2 subunit lacking) AMPA receptors (Tateno *et al.* 2004; Gu *et al.* 2010; Thellung *et al.* 2013) induces the UPR stress response (Doyle *et al.* 2011). As recently reported by Srinivasan *et al.* (2016), nicotine upregulates genes connected to the UPR process triggered via the ER stress response. Thus, our results demonstrated that TBOA significantly increased the expression of genes related to the ER stress response (Kuny *et al.* 2012) and that HMs might react to it via UGGT, one key protein implicated in the ER quality control system of glycoprotein folding (Wang *et al.* 2015). We posit that excitotoxicity triggered UGGT upregulation and that this reaction was insufficient to arrest the pathological decline in a substantial number of HMs: because nicotine inhibited the deleterious intracellular events activated by TBOA, UGGT hyperactivity had then become unnecessary.

Implications for the pathophysiology of ALS

Our model for the early stage of ALS is based on TBOA application to reproduce EAAT2 impairment and a gradual glutamate increase as observed in the cerebrospinal fluid of ALS patients (Rothstein *et al.* 1992; Fray *et al.* 1998). Experimental block of glutamate uptake increased intracellular free oxygen radicals, mimicking the main features of ALS with subsequent degradation of nuclear and mitochondrial DNA and protein misfolding (Kaur *et al.* 2016). The present results candidate nAChRs as a novel target for the control of network hyperactivation and mitigation of the resulting stress conditions due to impaired glutamate reuptake. Future *in vivo* studies are necessary to explore the use of nAChR agonists as a possible strategy to delay diseases progression in a preclinical model of ALS.

References

de Aguilar J-LG, Echaniz-Laguna A, Fergani A, René F, Meininger V, Loeffler J-P & Dupuis L (2007). Amyotrophic lateral sclerosis: all roads lead to Rome. *J Neurochem* **101**, 1153–1160.

Albuquerque EX, Pereira EFR, Alkondon M & Rogers SW (2009). Mammalian nicotinic acetylcholine receptors: from structure to function. *Physiol Rev* **89**, 73–120.

Arroyo-Jiménez M del M, Bourgeois J-P, Marubio LM, Sourd A-ML, Ottersen OP, Rinvik E, Fairén A & Changeux J-P (1999). Ultrastructural localization of the α4-subunit of the neuronal acetylcholine nicotinic receptor in the rat substantia nigra. *J Neurosci* **19**, 6475–6487.

Ballar P, Pabuccuoglu A & Kose FA (2011). Different p97/VCP complexes function in retrotranslocation step of mammalian Er-associated degradation (ERAD). *Int J Biochem Cell Biol* **43**, 613–621.

Bellingham MC & Berger AJ (1996). Presynaptic depression of excitatory synaptic inputs to rat hypoglossal motoneurons by muscarinic M2 receptors. *J Neurophysiol* **76**, 3758–3770.

Bencherif M, Fowler K, Lukas RJ & Lippiello PM (1995). Mechanisms of up-regulation of neuronal nicotinic acetylcholine receptors in clonal cell lines and primary cultures of fetal rat brain. *J Pharmacol Exp Ther* **275**, 987–994.

Bohnen NI & Frey KA (2007). Imaging of cholinergic and monoaminergic neurochemical changes in neurodegenerative disorders. *Mol Imaging Biol* **9**, 243–257.

Boylan K (2015). Familial amyotrophic lateral sclerosis. *Neurol Clin* **33**, 807–830.

Campbell MJ & Morrison JH (1989). Monoclonal antibody to neurofilament protein (SMI-32) labels a subpopulation of pyramidal neurons in the human and monkey neocortex. *J Comp Neurol* **282**, 191–205.

Chamberlin NL, Bocchiaro CM, Greene RW & Feldman JL (2002). Nicotinic excitation of rat hypoglossal motoneurons. *Neuroscience* **115**, 861–870.

Changeux J-P (2010). Nicotine addiction and nicotinic receptors: lessons from genetically modified mice. *Nat Rev Neurosci* **11**, 389–401.

Chavez-Noriega LE, Crona JH, Washburn MS, Urrutia A, Elliott KJ & Johnson EC (1997). Pharmacological characterization of recombinant human neuronal nicotinic acetylcholine receptors hα2β2, hα2β4, hα3β2, hα3β4, hα4β2, hα4β4 and hα7 expressed in *Xenopus* oocytes. *J Pharmacol Exp Ther* **280**, 346–356.

Cifra A, Nani F, Sharifullina E & Nistri A (2009). A repertoire of rhythmic bursting produced by hypoglossal motoneurons in physiological and pathological conditions. *Philos Trans R Soc B Biol Sci* **364**, 2493–2500.

Cifra A, Nani F & Nistri A (2011*a*). Riluzole is a potent drug to protect neonatal rat hypoglossal motoneurons *in vitro* from excitotoxicity due to glutamate uptake block. *Eur J Neurosci* **33**, 899–913.

Cifra A, Nani F & Nistri A (2011*b*). Respiratory motoneurons and pathological conditions: lessons from hypoglossal motoneurons challenged by excitotoxic or oxidative stress. *Respir Physiol Neurobiol* **179**, 89–96.

Cifra A, Mazzone GL, Nani F, Nistri A, Mladinic M (2012). Postnatal developmental profile of neurons and glia in motor nuclei of the brainstem and spinal cord, and its comparison with organotypic slice cultures. *Dev Neurobiol* **72**, 1140–1160.

Clausen T, Southan C & Ehrmann M (2002). The HtrA family of proteases: implications for protein composition and cell fate. *Mol Cell* **10**, 443–455.

Cleveland DW & Rothstein JD (2001). From Charcot to Lou Gehrig: deciphering selective motor neuron death in ALS. *Nat Rev Neurosci* **2**, 806–819.

Comley L, Allodi I, Nichterwitz S, Nizzardo M, Simone C, Corti S & Hedlund E (2015). Motor neurons with differential vulnerability to degeneration show distinct protein signatures in health and ALS. *Neuroscience* **291**, 216–229.

Dajas-Bailador FA, Lima PA & Wonnacott S (2000). The α7 nicotinic acetylcholine receptor subtype mediates nicotine protection against NMDA excitotoxicity in primary hippocampal cultures through a Ca^{2+} dependent mechanism. *Neuropharmacology* **39**, 2799–2807.

Dani JA & De Biasi M (2001). Cellular mechanisms of nicotine addiction. *Pharmacol Biochem Behav* **70**, 439–446.

Davis RJ (2000). Signal transduction by the JNK group of MAP kinases. *Cell* **103**, 239–252.

Dehkordi O, Millis RM, Dennis GC, Coleman BR, Johnson SM, Changizi L & Ovid Trouth C (2005). Alpha-7 and alpha-4 nicotinic receptor subunit immunoreactivity in genioglossus muscle motoneurons. *Respir Physiol Neurobiol* **145**, 153–161.

Dineley KT, Pandya AA & Yakel JL (2015). Nicotinic ACh receptors as therapeutic targets in CNS disorders. *Trends Pharmacol Sci* **36**, 96–108.

Dominguez del Toro E, Juiz JM, Peng X, Lindstrom J & Criado M (1994). Immunocytochemical localization of the alpha 7 subunit of the nicotinic acetylcholine receptor in the rat central nervous system. *J Comp Neurol* **349**, 325–342.

Donato R & Nistri A (2000). Relative contribution by GABA or glycine to Cl^--mediated synaptic transmission on rat hypoglossal motoneurons *in vitro*. *J Neurophysiol* **84**, 2715–2724.

Doyle KM, Kennedy D, Gorman AM, Gupta S, Healy SJM & Samali A (2011). Unfolded proteins and endoplasmic reticulum stress in neurodegenerative disorders. *J Cell Mol Med* **15**, 2025–2039.

Egea J, Buendia I, Parada E, Navarro E, León R & Lopez MG (2015). Anti-inflammatory role of microglial alpha7 nAChRs and its role in neuroprotection. *Biochem Pharmacol* **97**, 463–472.

Forder JP & Tymianski M (2009). Postsynaptic mechanisms of excitotoxicity: Involvement of postsynaptic density proteins, radicals, and oxidant molecules. *Neuroscience* **158**, 293–300.

Fray AE, Ince PG, Banner SJ, Milton ID, Usher PA, Cookson MR & Shaw PJ (1998). The expression of the glial glutamate transporter protein EAAT2 in motor neuron disease: an immunohistochemical study. *Eur J Neurosci* **10**, 2481–2489.

Gao J, Adam B-L & Terry Jr AV (2014). Evaluation of nicotine and cotinine analogs as potential neuroprotective agents for Alzheimer's disease. *Bioorg Med Chem Lett* **24**, 1472–1478.

Gergalova G, Lykhmus O, Kalashnyk O, Koval L, Chernyshov V, Kryukova E, Tsetlin V, Komisarenko S & Skok M (2012). Mitochondria express α7 nicotinic acetylcholine receptors to regulate Ca^{2+} accumulation and cytochrome c release: study on isolated mitochondria. *PloS One* **7**, e31361.

Gergalova G, Lykhmus O, Komisarenko S & Skok M (2014). α7 nicotinic acetylcholine receptors control cytochrome c release from isolated mitochondria through kinase-mediated pathways. *Int J Biochem Cell Biol* **49**, 26–31.

Goiato MC, Freitas E, dos Santos D, de Medeiros R & Sonego M (2015). Acrylic resin cytotoxicity for denture base – Literature review. *Adv Clin Exp Med* **24**, 679–686.

Gotti C & Clementi F (2004). Neuronal nicotinic receptors: from structure to pathology. *Prog Neurobiol* **74**, 363–396.

Gu Z, Nakamura T & Lipton SA (2010). Redox reactions induced by nitrosative stress mediate protein misfolding and mitochondrial dysfunction in neurodegenerative diseases. *Mol Neurobiol* **41**, 55–72.

Hafström O, Milerad J, Sandberg KL & Sundell HW (2005). Cardiorespiratory effects of nicotine exposure during development. *Respir Physiol Neurobiol* **149**, 325–341.

Henderson BJ & Lester HA (2015). Inside-out neuropharmacology of nicotinic drugs. *Neuropharmacology* **96**, 178–193.

Hetz C, Chevet E & Harding HP (2013). Targeting the unfolded protein response in disease. *Nat Rev Drug Discov* **12**, 703–719.

Huang Z & Gibb AJ (2014). Mg^{2+} block properties of triheteromeric GluN1-GluN2B-GluN2D NMDA receptors on neonatal rat substantia nigra pars compacta dopaminergic neurones: Mg^{2+} block properties of triheteromeric GluN1-GluN2B-GluN2D NMDA receptors. *J Physiol* **592**, 2059–2078.

Izumi M, Makimura Y, Dedola S, Seko A, Kanamori A, Sakono M, Ito Y & Kajihara Y (2012). Chemical synthesis of intentionally misfolded homogeneous glycoprotein: a unique approach for the study of glycoprotein quality control. *J Am Chem Soc* **134**, 7238–7241.

Jaiswal MK & Keller BU (2009). Cu/Zn superoxide dismutase typical for familial amyotrophic lateral sclerosis increases the vulnerability of mitochondria and perturbs Ca^{2+} homeostasis in SOD1G93A mice. *Mol Pharmacol* **75**, 478–489.

Jaiswal SJ, Buls Wollman L, Harrison CM, Pilarski JQ & Fregosi RF (2016). Developmental nicotine exposure enhances inhibitory synaptic transmission in motor neurons and interneurons critical for normal breathing. *Dev Neurobiol* **76**, 337–354.

Jones IW, Bolam JP & Wonnacott S (2001). Presynaptic localisation of the nicotinic acetylcholine receptor $\beta 2$ subunit immunoreactivity in rat nigrostriatal dopaminergic neurones. *J Comp Neurol* **439**, 235–247.

Kanjhan R, Fogarty MJ, Noakes PG & Bellingham MC (2015). Developmental changes in the morphology of mouse hypoglossal motor neurons. *Brain Struct Funct* 10.1007/s00429-015-1130-8.

Kanjhan R, Noakes PG & Bellingham MC (2016). Emerging roles of filopodia and dendritic spines in motoneuron plasticity during development and disease. *Neuronal Plast* 10.1155/2016/3423267.

Kaur SJ, McKeown SR & Rashid S (2016). Mutant SOD1 mediated pathogenesis of amyotrophic lateral sclerosis. *Gene* **577**, 109–118.

Kawamata J, Suzuki S & Shimohama S (2011). Enhancement of nicotinic receptors alleviates cytotoxicity in neurological disease models. *Ther Adv Chronic Dis* **2**, 197–208.

Kiehn O (2016). Decoding the organization of spinal circuits that control locomotion. *Nat Rev Neurosci.* **17**, 224–238.

Kleinfelter LM, Jangra RK, Jae LT, Herbert AS, Mittler E, Stiles KM, Wirchnianski AS, Kielian M, Brummelkamp TR, Dye JM & Chandran K (2015). Haploid genetic screen reveals a profound and direct dependence on cholesterol for hantavirus membrane fusion. *mBio* **6**, e00801.

Kloft N, Neukirch C, Hoven G von, Bobkiewicz W, Weis S, Boller K & Husmann M (2012). A subunit of eukaryotic translation initiation factor 2α-phosphatase (CreP/PPP1R15B) regulates membrane traffic. *J Biol Chem* **287**, 35299–35317.

Kuny S, Gaillard F & Sauvé Y (2012). Differential gene expression in eyecup and retina of a mouse model of Stargardt-like macular dystrophy (STGD3). *Investig Opthalmology Vis Sci* **53**, 664.

Kuryatov A, Luo J, Cooper J & Lindstrom J (2005). Nicotine acts as a pharmacological chaperone to up-regulate human $\alpha 4\beta 2$ acetylcholine receptors. *Mol Pharmacol* **68**, 1839–1851.

Ladewig T, Kloppenburg P, Lalley PM, Zipfel WR, Webb WW & Keller BU (2003). Spatial profiles of store-dependent calcium release in motoneurones of the nucleus hypoglossus from newborn mouse. *J Physiol* **547**, 775–787.

Lamanauskas N & Nistri A (2006). Persistent rhythmic oscillations induced by nicotine on neonatal rat hypoglossal motoneurons *in vitro*. *Eur J Neurosci* **24**, 2543–2556.

Laslo P, Lipski J, Nicholson LF, Miles GB & Funk GD (2001). GluR2 AMPA receptor subunit expression in motoneurons at low and high risk for degeneration in amyotrophic lateral sclerosis. *Exp Neurol* **169**, 461–471.

Laudenbach V, Medja F, Zoli M, Rossi FM, Evrard P, Changeux J-P & Gressens P (2002). Selective activation of central subtypes of the nicotinic acetylcholine receptor has opposite effects on neonatal excitotoxic brain injuries. *FASEB J* **16**, 423–425.

Lewerenz J, Klein M & Methner A (2006). Cooperative action of glutamate transporters and cystine/glutamate antiporter system X_c^- protects from oxidative glutamate toxicity. *J Neurochem* **98**, 916–925.

von Lewinski F & Keller BU (2005). Ca^{2+}, mitochondria and selective motoneuron vulnerability: implications for ALS. *Trends Neurosci* **28**, 494–500.

Lykhmus O, Gergalova G, Koval L, Zhmak M, Komisarenko S & Skok M (2014). Mitochondria express several nicotinic acetylcholine receptor subtypes to control various pathways of apoptosis induction. *Int J Biochem Cell Biol* **53**, 246–252.

Manuel M, Li Y, ElBasiouny SM, Murray K, Griener A, Heckman CJ & Bennett DJ (2012). NMDA induces persistent inward and outward currents that cause rhythmic bursting in adult rodent motoneurons. *J Neurophysiol* **108**, 2991–2998.

Marchetti C, Pagnotta S, Donato R & Nistri A (2002). Inhibition of spinal or hypoglossal motoneurons of the newborn rat by glycine or GABA. *Eur J Neurosci* **15**, 975–983.

Matus S, Lopez E, Valenzuela V, Nassif M & Hetz C (2013). Functional contribution of the transcription factor ATF4 to the pathogenesis of amyotrophic lateral sclerosis. *PLoS ONE* **8**, e66672.

Mazzone GL, Margaryan G, Kuzhandaivel A, Nasrabady SE, Mladinic M & Nistri A (2010). Kainate-induced delayed onset of excitotoxicity with functional loss unrelated to the extent of neuronal damage in the *in vitro* spinal cord. *Neuroscience* **168**, 451–462.

Mazzone GL & Nistri A (2011). Delayed neuroprotection by riluzole against excitotoxic damage evoked by kainate on rat organotypic spinal cord cultures. *Neuroscience* **190**, 318–327.

McKay BE, Placzek AN & Dani JA (2007). Regulation of synaptic transmission and plasticity by neuronal nicotinic acetylcholine receptors. *Biochem Pharmacol* **74**, 1120–1133.

Medina L, Figueredo-Cardenas G, Rothstein JD & Reiner A (1996). Differential abundance of glutamate transporter subtypes in amyotrophic lateral sclerosis (ALS)-vulnerable versus ALS-resistant brain stem motor cell groups. *Exp Neurol* **142**, 287–295.

Mehta A, Prabhakar M, Kumar P, Deshmukh R & Sharma PL (2013). Excitotoxicity: Bridge to various triggers in neurodegenerative disorders. *Eur J Pharmacol* **698**, 6–18.

Miwa JM, Ibañez-Tallon I, Crabtree GW, Sánchez R, Sali A, Role LW & Heintz N (1999). lynx1, an endogenous toxin-like modulator of nicotinic acetylcholine receptors in the mammalian CNS. *Neuron* **23**, 105–114.

Mladinic M, Bianchetti E, Dekanic A, Mazzone GL & Nistri A (2014). ATF3 is a novel nuclear marker for migrating ependymal stem cells in the rat spinal cord. *Stem Cell Res* **12**, 815–827.

Mosmann T (1983). Rapid colorimetric assay for cellular growth and survival: application to proliferation and cytotoxicity assays. *J Immunol Methods* **65**, 55–63.

Myszczynska M & Ferraiuolo L (2016). New *in vitro* models to study amyotrophic lateral sclerosis. *Brain Pathol* **26**, 258–265.

Nagao M, Misawa H, Kato S & Hirai S (1998). Loss of cholinergic synapses on the spinal motor neurons of amyotrophic lateral sclerosis. *J Neuropathol Exp Neurol* **57**, 329–333.

Nakajima F, Aratani S, Fujita H, Yagishita N, Ichinose S, Makita K, Setoguchi Y & Nakajima T (2015). Synoviolin inhibitor LS-102 reduces endoplasmic reticulum stress-induced collagen secretion in an *in vitro* model of stress-related interstitial pneumonia. *Int J Mol Med* **35**, 110–116.

Nakamizo T, Kawamata J, Yamashita H, Kanki R, Kihara T, Sawada H, Akaike A & Shimohama S (2005). Stimulation of nicotinic acetylcholine receptors protects motor neurons. *Biochem Biophys Res Comm* **330**, 1285–1289.

Nani F, Cifra A & Nistri A (2010). Transient oxidative stress evokes early changes in the functional properties of neonatal rat hypoglossal motoneurons *in vitro*. *Eur J Neurosci* **31**, 951–966.

Ngo ST & Steyn FJ (2015). The interplay between metabolic homeostasis and neurodegeneration: insights into the neurometabolic nature of amyotrophic lateral sclerosis. *Cell Regen* **4**, 5.

Niso-Santano M, Shen S, Adjemian S, Malik SA, Mariño G, Lachkar S, Senovilla L, Kepp O, Galluzzi L, Maiuri MC & Kroemer G (2013). Direct interaction between STAT3 and EIF2AK2 controls fatty acid-induced autophagy. *Autophagy* **9**, 415–417.

Nistri A, Ostroumov K, Sharifullina E & Taccola G (2006).Tuning and playing a motor rhythm: how metabotropic glutamate receptors orchestrate generation of motor patterns in the mammalian central nervous system. *J Physiol* **572**, 323–334.

Oikawa D, Kitamura A, Kinjo M & Iwawaki T (2012). Direct association of unfolded proteins with mammalian ER stress sensor, IRE1β;. *PLoS ONE* **7**, e51290.

Pagnotta SE, Lape R, Quitadamo C & Nistri A (2005). Pre- and postsynaptic modulation of glycinergic and gabaergic transmission by muscarinic receptors on rat hypoglossal motoneurons *in vitro*. *Neuroscience* **130**, 783–795.

Palma E, Bertrand S, Binzoni T & Bertrand D (1996). Neuronal nicotinic alpha 7 receptor expressed in *Xenopus* oocytes presents five putative binding sites for methyllycaconitine. *J Physiol* **491**, 151–161.

Pilarski JQ, Wakefield HE, Fuglevand AJ, Levine RB & Fregosi RF (2012). Increased nicotinic receptor desensitization in hypoglossal motor neurons following chronic developmental nicotine exposure. *J Neurophysiol* **107**, 257–264.

Poppe L, Rué L, Robberecht W & Van Den Bosch L (2014). Translating biological findings into new treatment strategies for amyotrophic lateral sclerosis (ALS). *Exp Neurol* **262**, Part B, 138–151.

Puentes F, Malaspina A, van Noort JM & Amor S (2016). Non-neuronal cells in ALS: role of glial, immune cells and blood-CNS barriers. *Brain Pathol* **26**, 248–257.

Qin S-Y, Hu D, Matsumoto K, Takeda K, Matsumoto N, Yamaguchi Y & Yamamoto K (2012). Malectin forms a complex with ribophorin I for enhanced association with misfolded glycoproteins. *J Biol Chem* **287**, 38080–38089.

Quitadamo C, Fabbretti E, Lamanauskas N & Nistri A (2005). Activation and desensitization of neuronal nicotinic receptors modulate glutamatergic transmission on neonatal rat hypoglossal motoneurons. *Eur J Neurosci* **22**, 2723–2734.

Ren R, Zhou X, He Y, Ke M, Wu J, Liu X, Yan C, Wu Y, Gong X, Lei X, Yan SF, Radhakrishnan A & Yan N (2015). Crystal structure of a mycobacterial Insig homolog provides insight into how these sensors monitor sterol levels. *Science* **349**, 187–191.

Richards CI, Srinivasan R, Xiao C, Mackey EDW, Miwa JM & Lester HA (2011). Trafficking of $\alpha 4^*$ nicotinic receptors revealed by superecliptic phluorin. *J Biol Chem* **286**, 31241–31249.

Riljak V, Benes J, Pokorný J & Myslivecek J (2011). Neuroprotective effect of nicotine against kainic acid excitotoxicity is associated with alpha-bungarotoxin insensitive receptors subtype of nAChRs. *Neuro Endocrinol Lett* **32**, 816–820.

Robinson DM, Peebles KC, Kwok H, Adams BM, Clarke L-L, Woollard GA & Funk GD (2002). Prenatal nicotine exposure increases apnoea and reduces nicotinic potentiation of hypoglossal inspiratory output in mice. *J Physiol* **538**, 957–973.

Rothstein JD, Martin LJ & Kuncl RW (1992). Decreased glutamate transport by the brain and spinal cord in amyotrophic lateral sclerosis. *N Engl J Med* **326**, 1464–1468.

Rothstein JD, Van Kammen M, Levey AI, Martin LJ & Kuncl RW (1995). Selective loss of glial glutamate transporter GLT-1 in amyotrophic lateral sclerosis. *Ann Neurol* **38**, 73–84.

Rukhadze I & Kubin L (2007). Mesopontine cholinergic projections to the hypoglossal motor nucleus. *Neurosci Lett* **413**, 121–125.

Rutkowski DT & Kaufman RJ (2004). A trip to the ER: coping with stress. *Trends Cell Biol* **14**, 20–28.

Sasaki S, Komori T & Iwata M (2000). Excitatory amino acid transporter 1 and 2 immunoreactivity in the spinal cord in amyotrophic lateral sclerosis. *Acta Neuropathol (Berl)* **100**, 138–144.

Sallette J, Pons S, Devillers-Thiery A, Soudant M, Prado de Carvalho L, Changeux J-P & Corringer PJ (2005). Nicotine upregulates its own receptors through enhanced intracellular maturation. *Neuron* **46**, 595–607.

Selkirk JV, Nottebaum LM, Vana AM, Verge GM, Mackay KB, Stiefel TH, Naeve GS, Pomeroy JE, Petroski RE, Moyer J, Dunlop J & Foster AC (2005). Role of the GLT-1 subtype of glutamate transporter in glutamate homeostasis: the GLT-1-preferring inhibitor WAY-855 produces marginal neurotoxicity in the rat hippocampus. *Eur J Neurosci* **21**, 3217–3228.

Shao XM, Tan W, Xiu J, Puskar N, Fonck C, Lester HA & Feldman JL (2008). Alpha4* nicotinic receptors in preBotzinger complex mediate cholinergic/nicotinic modulation of respiratory rhythm. *J Neurosci* **28**, 519–528.

Sharifullina E & Nistri A (2006). Glutamate uptake block triggers deadly rhythmic bursting of neonatal rat hypoglossal motoneurons. *J Physiol* **572**, 407–423.

Sharifullina E, Ostroumov K & Nistri A (2005). Metabotropic glutamate receptor activity induces a novel oscillatory pattern in neonatal rat hypoglossal motoneurones. *J Physiol* **563**, 139–159.

Sharifullina E, Ostroumov K, Grandolfo M & Nistri A (2008). *N*-methyl-D-aspartate triggers neonatal rat hypoglossal motoneurons *in vitro* to express rhythmic bursting with unusual Mg^{2+} sensitivity. *Neuroscience* **154**, 804–820.

Sharma G & Vijayaraghavan S (2001). Nicotinic cholinergic signaling in hippocampal astrocytes involves calcium-induced calcium release from intracellular stores. *Proc Natl Acad Sci USA* **98**, 4148–4153.

Sharma G & Vijayaraghavan S (2002). Nicotinic receptor signaling in nonexcitable cells. *J Neurobiol* **53**, 524–534.

Shaw PJ (2005). Molecular and cellular pathways of neurodegeneration in motor neurone disease. *J Neurol Neurosurg Psychiatry* **76**, 1046–1057.

Shimamoto K, Lebrun B, Yasuda-Kamatani Y, Sakaitani M, Shigeri Y, Yumoto N & Nakajima T (1998). DL-Threo-β-benzyloxyaspartate, a potent blocker of excitatory amino acid transporters. *Mol Pharmacol* **53**, 195–201.

Shoji M, Iwakami N, Takeuchi S, Waragai M, Suzuki M, Kanazawa I, Lippa CF, Ono S & Okazawa H (2000). JNK activation is associated with intracellular β-amyloid accumulation. *Mol Brain Res* **85**, 221–233.

Simone RD, Ajmone-Cat MA, Carnevale D & Minghetti L (2005). Activation of α7 nicotinic acetylcholine receptor by nicotine selectively up-regulates cyclooxygenase-2 and prostaglandin E2 in rat microglial cultures. *J Neuroinflammation* **2**, 4.

Singer JH, Talley EM, Bayliss DA & Berger AJ (1998). Development of glycinergic synaptic transmission to rat brain stem motoneurons. *J Neurophysiol* **80**, 2608–2620.

Sokolova E, Matteoni C & Nistri A (2005). Desensitization of neuronal nicotinic receptors of human neuroblastoma SH-SY5Y cells during short or long exposure to nicotine. *Br J Pharmacol* **146**, 1087–1095.

Spreux-Varoquaux O, Bensimon G, Lacomblez L, Salachas F, Pradat PF, Le Forestier N, Marouan A, Dib M & Meininger V (2002). Glutamate levels in cerebrospinal fluid in amyotrophic lateral sclerosis: a reappraisal using a new HPLC method with coulometric detection in a large cohort of patients. *J Neurol Sci* **193**, 73–78.

Srinivasan R, Pantoja R, Moss FJ, Mackey EDW, Son CD, Miwa J & Lester HA (2011). Nicotine up-regulates $\alpha4\beta2$ nicotinic receptors and ER exit sites via stoichiometry-dependent chaperoning. *J Gen Physiol* **137**, 59–79.

Srinivasan R, Henley BM, Henderson BJ, Indersmitten T, Cohen BN, Kim CH, McKinney S, Deshpande P, Xiao C & Lester HA (2016). Smoking-relevant nicotine concentration attenuates the unfolded protein response in dopaminergic neurons. *J Neurosci* **36**, 65–79.

Tateno M, Sadakata H, Tanaka M, Itohara S, Shin R-M, Miura M, Masuda M, Aosaki T, Urushitani M, Misawa H & Takahashi R (2004). Calcium-permeable AMPA receptors promote misfolding of mutant SOD1 protein and development of amyotrophic lateral sclerosis in a transgenic mouse model. *Hum Mol Genet* **13**, 2183–2196.

Thellung S, Gatta E, Pellistri F, Corsaro A, Villa V, Vassalli M, Robello M & Florio T (2013). Excitotoxicity through NMDA receptors mediates cerebellar granule neuron apoptosis induced by prion protein 90-231 fragment. *Neurotox Res* **23**, 301–314.

Thomsen MS, Cinar B, Jensen MM, Lyukmanova EN, Shulepko MA, Tsetlin V, Klein AB & Mikkelsen JD (2014). Expression of the Ly-6 family proteins Lynx1 and Ly6H in the rat brain is compartmentalized, cell-type specific, and developmentally regulated. *Brain Struct Funct* **219**, 1923–1934.

Van Den Bosch L, Van Damme P, Bogaert E & Robberecht W (2006). The role of excitotoxicity in the pathogenesis of amyotrophic lateral sclerosis. *Biochim Biophys Acta* **1762**, 1068–1082.

Viana F, Gibbs L & Berger AJ (1990). Double- and triple-labeling of functionally characterized central neurons projecting to peripheral targets studied *in vitro*. *Neuroscience* **38**, 829–841.

Vucic S & Kiernan MC (2010). Upregulation of persistent sodium conductances in familial ALS. *J Neurol Neurosurg Psychiatry* **81**, 222–227.

Walsh H, Govind AP, Mastro R, Hoda JC, Bertrand D, Vallejo Y & Green WN (2008). Up-regulation of nicotinic receptors by nicotine varies with receptor subtype. *J Biol Chem* **283**, 6022–6032.

Wang F, Nelson ME, Kuryatov A, Olale F, Cooper J, Keyser K & Lindstrom J (1998). Chronic nicotine treatment up-regulates human $\alpha3\beta2$ but not $\alpha3\beta4$ acetylcholine receptors stably transfected in human embryonic kidney cells. *J Biol Chem* **273**, 28721–28732.

Wang Q, Groenendyk J & Michalak M (2015). Glycoprotein quality control and endoplasmic reticulum stress. *Molecules* **20**, 13689–13704.

Wevers A (2011). Localisation of pre- and postsynaptic cholinergic markers in the human brain. *Behav Brain Res* **221**, 341–355.

Zhou FM, Wilson CJ & Dani JA (2002). Cholinergic interneuron characteristics and nicotinic properties in the striatum. *J Neurobiol* **53**, 590–605.

Zhou W-L, Gao X-B & Picciotto MR (2015). Acetylcholine acts through nicotinic receptors to enhance the firing rate of a subset of hypocretin neurons in the mouse hypothalamus through distinct presynaptic and postsynaptic mechanisms. *eNeuro* **2**, e0052.

Zhou Y, Xu L, Song X, Ding L, Chen J, Wang C, Gan Y, Zhu X, Yu Y & Liang Q (2014). The potential role of heat shock proteins in acute spinal cord injury. *Eur Spine J* **23**, 1480–1490.

Additional information

Competing interests

The authors declare no competing interests.

Author contributions

Conception and design of the work, SC, MT, AN; acquisition, analysis and interpretation of data for the work, SC, MT; drafting the work or revising it critically for important intellectual content, SC, MT, AN. All authors have approved the final version of the manuscript and agree to be accountable for all aspects of the work in ensuring that questions related to the accuracy or integrity of any part of the work are appropriately investigated and resolved. All persons designated as authors qualify for authorship, and all those who qualify for authorship are listed.

Funding

This work was supported by an intramural SISSA grant.

Acknowledgements

We thank Drs Malgorzata Serzysko and Sandra Vilotti for help with the real-time PCR experiments and Drs Jessica Franzot and Micaela Grandolfo for their support with Western blot and histological data.

Supporting information

The following supporting information is available in the online version of this article.

Table S1. Full list of the 84 gene products investigated and their function.
Fig. S1. Detailed list of changes in gene product expression after exposure to TBOA, or TBOA plus nicotine (*vs.* control conditions).

Neuroscience Letters 639 (2017) 43–48

Contents lists available at ScienceDirect

Neuroscience Letters

journal homepage: www.elsevier.com/locate/neulet

Research article

Nicotinic receptors modulate the onset of reactive oxygen species production and mitochondrial dysfunction evoked by glutamate uptake block in the rat hypoglossal nucleus

Maria Tortora, Silvia Corsini*, Andrea Nistri

Department of Neuroscience, International School for Advanced Studies (SISSA), Trieste, Italy

HIGHLIGHTS

- Glutamate uptake block evokes hypoglossal motoneuron damage due to excitotoxicity.
- Reactive oxygen species are the earliest excitotoxic players for oxidative damage.
- Mitochondrial energy deficit is manifested later.
- Intrinsic cholinergic transmission is inadequate to arrest these events.
- Nicotinic receptor activation by nicotine provides strong neuroprotection.

ARTICLE INFO

Article history:
Received 14 October 2016
Received in revised form
21 November 2016
Accepted 12 December 2016
Available online 19 December 2016

Keywords:
Excitotoxicity
TBOA
ROS
Brainstem
Nicotine
Motoneuron

ABSTRACT

In several neurodegenerative diseases, glutamate-mediated excitotoxicity is considered to be a major process to initiate cell degeneration. Indeed, subsequent to excessive glutamate receptor stimulation, reactive oxygen species (ROS) generation and mitochondrial dysfunction are regarded as two major gateways leading to neuron death. These processes are mimicked in an *in vitro* model of rat brainstem slice when excitotoxicity is induced by DL-*threo*-β-benzyloxyaspartate (TBOA), a specific glutamate-uptake blocker that increases extracellular glutamate. Our recent study has demonstrated that brainstem hypoglossal motoneurons, which are very vulnerable to this damage, were neuroprotected from excitotoxicity with nicotine application through the activation of nicotinic acetylcholine receptors (nAChRs) and subsequent inhibition of ROS and mitochondrial dysfunction. The present study examined if endogenous cholinergic activity exerted any protective effect in this pathophysiological model and how ROS production (estimated with rhodamine fluorescence) and mitochondrial dysfunction (measured as methyltetrazolium reduction) were time-related during the early phase of excitotoxicity (0–4 h). nAChR antagonists did not modify TBOA-evoked ROS production (that was nearly doubled over control) or mitochondrial impairment (25% decline), suggesting that intrinsic nAChR activity was insufficient to contrast excitotoxicity and needed further stimulation with nicotine to become effective. ROS production always preceded mitochondrial dysfunction by about 2 h. Nicotine prevented both ROS production and mitochondrial metabolic depression with a delayed action that alluded to a complex chain of events targeting these two lesional processes. The present data indicate a relatively wide time frame during which strong nAChR activation can arrest a runaway neurotoxic process leading to cell death.

1. Introduction

In physiological conditions astrocytes and neurons tightly regulate the extracellular concentration of glutamate by membrane transporters [1] whose disruption causes excitotoxicity reported to occur in neurodegenerative diseases [2]. A significant example of increased extracellular glutamate related to neurodegeneration onset is amyotrophic lateral sclerosis (ALS) since the discovery of high levels of glutamate in the cerebrospinal fluid of ALS patients

Abbreviations: ACh, acetylcholine; ALS, amyotrophic lateral sclerosis; DHβE, dihydro-beta-erythroidine; DHR 123, dihydrorhodamine; EAATs, excitatory amino acid transporters; HMs, hypoglossal motoneurons; MLA, methyllycaconitine; MTT, mitochondrial toxicity test; nAChR, nicotinic acetylcholine receptor; Rho 123, rhodamine 123; ROS, reactive oxygen species; TBOA, DL-*threo*-beta-benzyloxyaspartate.

* Corresponding author at: SISSA, via Bonomea 265, 34136 Trieste, Italy.
E-mail address: scorsini@sissa.it (S. Corsini).

http://dx.doi.org/10.1016/j.neulet.2016.12.021
0304-3940/

[3–5]. Glutamate-excitotoxicity may evoke oxidative stress [6–8], due to accumulation of reactive oxygen species (ROS), and subsequent cell death [9]. In this scenario, an important role is also played by the mitochondrial respiratory chain whose collapse produces energy dysfunction including imbalanced Ca^{2+} homeostasis [10,11]. Since experimental block of excitatory aminoacid transporters (EAATs) reflects the pathological condition often present in ALS [12,13], we devised a model to mimic the early presymptomatic stage by pharmacological inhibition of glutamate uptake with DL-*threo*-beta-benzyloxyaspartate (TBOA). Thus, we used hypoglossal motoneurons (HMs) as an *in vitro* test system because these cells are very vulnerable to the ALS bulbar type [14].

It is well documented that nicotine can provide neuroprotection in certain neurodegenerative diseases [15]. Cholinergic transmission, mediated by nicotinic acetylcholine receptors (nAChRs), is widely distributed through the brain to regulate different processes contributing to synaptic transmission as well as to neuronal protection and cognitive performance efficiency [16,17]. In the brainstem cholinergic projections from pontine nuclei to the hypoglossal nucleus activate mainly α7 and α4β2 nAChRs that may confer neuroprotection after excitotoxic insult [18,19] even in neonatal animal models [15]. We have recently discovered that, in the nucleus hypoglossus, nicotine could prevent TBOA-induced motoneuron loss via inhibition of complex effects that include pathological bursting, ROS generation and mitochondrial dysfunction [20]. In this chain of events, while bursting emerges rapidly and induces irreversible increase in intracellular free Ca^{2+} within 30 min [21], the time course of excitotoxicity-evoked ROS production and mitochondrial damage remains unknown, a result potentially useful to develop future neuroprotective strategies. This issue was investigated in the present report. Furthermore, a role of endogenous acetylcholine (ACh) activity on downstream ROS production and mitochondrial energy metabolism has not been determined during the early phase of excitotoxicity. Thus, the present study explored these questions by applying dihydro-beta-erythroidine (DHβE) and methyllycaconitine (MLA; antagonists against the neuronal α4 and α7 receptor subunits, respectively) during the time frame of 4 h that ensures optimal viability of the brainstem slice preparation in physiological conditions [22].

2. Material and methods

2.1. Ethical approval

The Scuola Internazionale Superiore di Studi Avanzati (SISSA) ethics committee (prot. 3599, 28 May 2012) approved all experiments and treatment protocols carried out in accordance with the European Union rules for animal experimentation. The number of animals used for the present experiments and their suffering were minimized. Experiments were performed with an *in vitro* model of brainstem slices removed from neonatal Wistar rats (postnatal days 2–5; P2-P5) under i.p. urethane anesthesia (10% solution, 0.1 mL injection).

2.2. Slice preparation

Brainstems were cut in ice-cold, oxygenated (95% O2/5% CO2) Krebs solution, containing (in mM): 130 NaCl; 3 KCl; NaH2PO4, 1 CaCl2, 1.5 NaH2PO4, 5 MgCl2, 25 NaHCO3, and 18.5 glucose (pH 7.4; 300–320 mos ml l^{-1}) inside a Vibratome chamber (Leica 1000S, Wetzlar, Germany) [20,23]. Slices (250–450 μm thick) containing the hypoglossal nucleus were independently treated with TBOA (50 μM), TBOA + DHβE (5 μM) + MLA (5 nM), TBOA + nicotine, or nicotine (10 μM) for 0.5, 2, or 4 h at room temperature under continuous oxygenation. These concentrations were selected on the basis of our former neuroprotection experiments [20,21]. As control, untreated slices were processed as described below immediately after cutting procedures (t = 0 h) or after 0.5, 2, or 4 h of incubation in Krebs solution (sham). Measurements of ROS and mitochondrial metabolism were performed at 0.5, 2 and 4 h, i.e. from the earliest time of electrophysiological dysfunction [21] to the maximum slice damage time [20]. Quantification of HM loss after exposure to TBOA for 4 h was performed as described in our former studies [20,23] using an analogous region of interest (ROI).

2.3. Intracellular measurements of ROS generation

To investigate the generation of intracellular free oxygen species, dihydrorhodamine 123 (DHR 123; Molecular Probes, Invitrogen, Carlsbad, CA, USA) was used as a membrane permeable dye that, by oxidation, yields the fluorescence probe rhodamine 123 (Rho 123) [22]. After rapid rinsing in Krebs solution, slices (250 μm thick) were treated with DHR123 (5 μM) and the nuclear dye Hoechst 33342 (10 mg/mL stock from Molecular Probes; dilution 1:1000) for 20 min at room temperature. Hoechst 33342 was used for counterstaining as it emits blue fluorescence once bound to double-stranded DNA. Finally, slices were washed and transferred into a Petri dish (containing Krebs solution) to be examined with a TCS SP2 Leica confocal microscope (20X objective and 2X magnification). For fluorescence imaging of rhodamine 123 (Rho 123, the oxidized form of DHR 123) staining, slices were visualized by excitation at 514 nm and emission at 530–610 nm, while Hoechst 33342 was excited by ultraviolet light (blue fluorescence emission at 460–490 nm). For each slice side and for both hypoglossal nuclei, a 40 μm z- stack (corresponding to one HM plane) was acquired (5 μm step size) to reconstruct an average fluorescence signal that was independently processed by the experimenter (blind to the treatment) with ImageJ software (version 1.44p, W. Rasband, National Institutes of Health, Bethesda, MD, USA). Rho 123 fluorescence was not evaluated for TBOA + nicotine at 0.5 h, and nicotine at 0.5 and 2 h.

2.4. MTT mitochondrial toxicity test

Mitochondrial toxicity test (MTT) is a standard colorimetric assay for assessing cell viability. As described by Mosmann [24] and reported earlier in our laboratory [20], NADPH-dependent cellular oxido-reductase enzymes may be considered a direct index of cell viability and mitochondrial energy metabolism. These enzymes are capable of reducing the tetrazolium dye MTT 3-(4,5-dimethylthiazol-2-yl)-2,5-diphenyltetrazolium bromide to its insoluble formazan, which has purple color whose intensity can be quantified. Under continuous oxygenation in Krebs solution, two slices (450 μm thick) were incubated as described above. For this experiment, nicotine (10 μM) or rotenone (1 μM) treatments lasted 4 h. Rotenone was used as a control for its capacity to interfere with the electron transport respiratory chain in mitochondria by inhibiting the transfer of electrons from complex I to ubiquinone [25]. After treatment, at the above indicated time points, slices were incubated with MTT (0.5 mg/mL; Sigma-Aldrich, Saint Louis, MO, USA) for 2 h at room temperature under oxygenation. MTT was firstly dissolved (5 mg/mL) in phosphate buffer (pH 7.4) and then diluted to 0.5 mg/mL in Krebs solution. Later, slices were treated with 0.5 mL hydrochloric acid plus 0.04 M isopropanol and shaken in a roller drum overnight at room temperature. Lysates were then centrifuged at 10,000*g* for 5 min and their absorbance values (wave length = 550 nm) were evaluated with a Bio-Rad microplate reader (model 550, Bio-Rad Laboratories, Poole, UK). Values were normalized with respect to the lysate protein content assayed with the bicinchoninic acid method (Sigma).

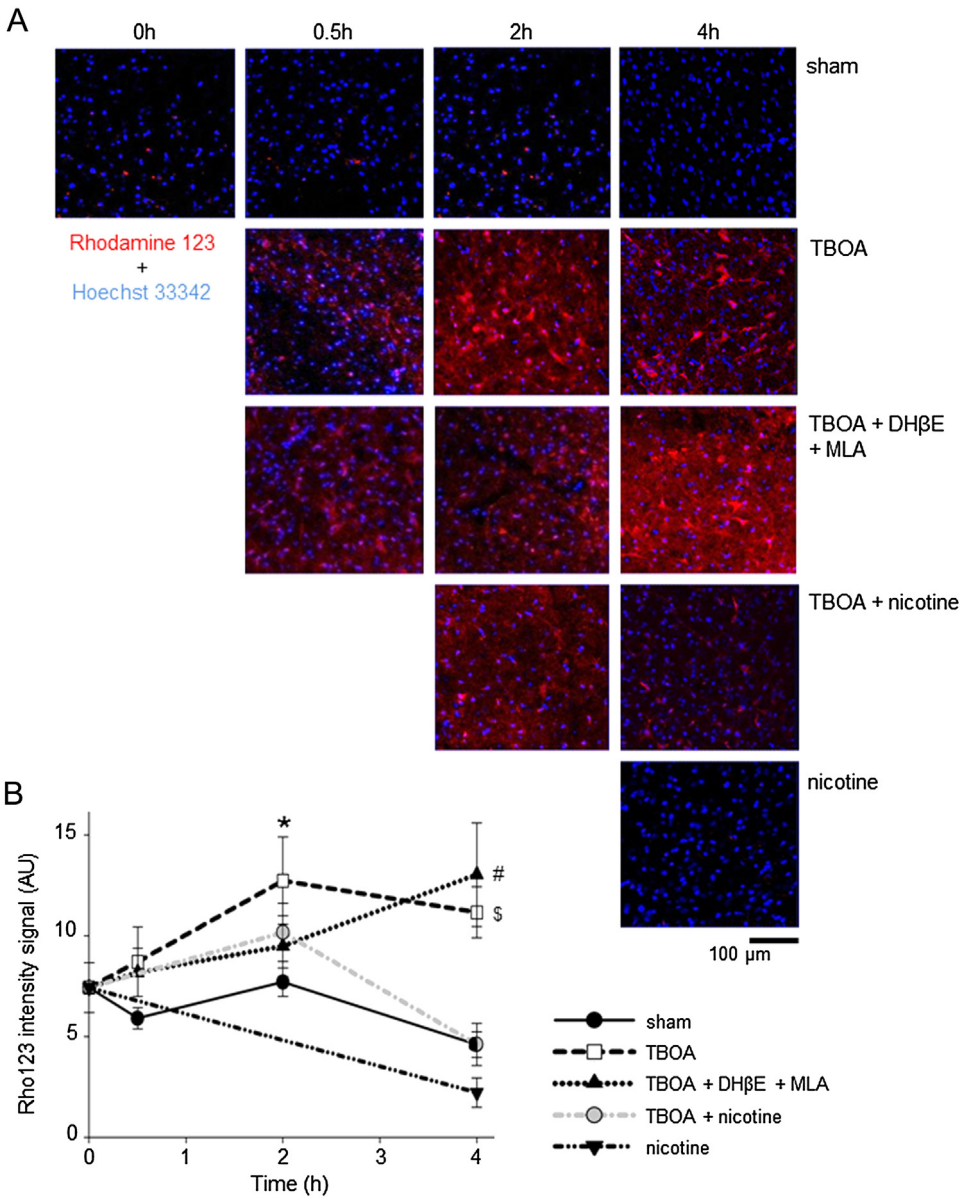

Fig 1. Time course of ROS expression in the nucleus hypoglossus. (A) Histological examples of the nucleus hypoglossus stained with Rho 123 (red pseudocolor), as ROS indicator, and Hoechst 33342 (blue pseudocolor), as counterstaining, at 0, 0.5, 2, or 4 h in sham preparation or treated with TBOA (50 µM), TBOA + DHβE (5 µM) + MLA (5 nM), TBOA + nicotine (10 µM), or nicotine alone. (B) Plot quantifies the Rho 123 intensity signal (AU). In sham condition ROS expression significantly changes (One Way ANOVA: $P = 0.015$; n = 5, 0 h; 8, 0.5 h; 8, 2 h; 10, 4 h); $P = 0.02$ between 2 and 4 h values (Student's *t*-test). No difference among any treatment is observed at 0.5 h. Values for TBOA treated slices are significantly different from sham ones at 2 h (*; Student's *t*-test: $P = 0.052$; n = 9) and 4 h ($; Student's *t*-test: $P \leq 0.001$; n = 9). When TBOA is applied together with DHβE + MLA, there is a similar increase in ROS value (#; Student's *t*-test: $P \leq 0.001$; n = 9). Co-applied TBOA and nicotine (n = 4) or nicotine alone (n = 4) yields ROS signal not different from sham. (For interpretation of the references to colour in this figure legend, the reader is referred to the web version of this article.)

2.5. Drugs

The following drugs were used: DHβE (Tocris, Bristol, UK), MLA (Sigma-Aldrich), nicotine (Sigma-Aldrich), rotenone (Sigma-Aldrich), and TBOA (Tocris).

2.6. Statistical analysis

Results were expressed as means ± standard error of the mean; *n* refers to the number of slices for each independent experiment. We first assessed the normality and equality normality distribution of the data and applied parametric and non-parametric tests for further evaluation. For statistical analysis, Student's t-test was applied to compare differences between two parametric groups, whereas the Mann-Whitney test was applied to compare two non-parametric groups. To compare multiple groups of parametric and non-parametric data we used the One Way ANOVA and the Kruskal-Wallis test, respectively. Differences with $P \leq 0.05$ were accepted as statistically significant.

3. Results

While our former data indicated that endogenous ACh played a role in regulating the rapid onset of excitotoxic bursting evoked by TBOA [20], it remained to be clarified if this effect was translated into at least partial neuroprotection via activation of nAChRs. Previous studies have shown that the HM number remains stable for up to 4 h in control condition [20]. Thus, prolonged exposure to TBOA induces a significant cell loss, which in the present study

was quantified as 37 ± 2 HMs vs. 46 ± 3 in control solution ($P < 0.05$, n = 13) using a similar ROI as reported earlier [20,23].

The pathway to HM death involves two major gateways, namely intracellular ROS accumulation and mitochondrial dysfunction. It was, therefore, of interest to explore if endogenous ACh was targeting these processes, their time relation and whether the effect of endogenous ACh was comparable with the one by nicotine. For this purpose, we used nAChR antagonists applied to the nucleus hypoglossus and performed confocal analysis of intracellular ROS level. Fig. 1A shows the ROS signal in sham condition and at 0, 0.5, 2 or 4 h after treatment with TBOA, TBOA + DHβE + MLA, TBOA + nicotine, or nicotine. A comparatively low level of basal oxidative stress was detected in this nucleus even at t = 0 (7.4 ± 1.2 AU; Fig. 1B): this condition possibly reflected the experimental manipulation procedures as it declined 4 h later under resting conditions (filled circles, continuous line in Fig. 1 B). In particular, the main difference was observed between 2 and 4 h (Student's *t*-test: $P = 0.02$; n = 8, at 2 h and 10, at 4 h). Application of TBOA elicited a large ($P = 0.052$; n = 9) rise in ROS at 2 h as exemplified in Fig. 1A and quantified in Fig. 1B (open squares, dashed line). This increment remained sustained even at 4 h ($P \leq 0.001$, n = 9). As shown in Fig. 1A, B, when TBOA was co-applied with the nAChR antagonists DHβE and MLA, the Rho 123 intensity signal was similar to the one observed with TBOA alone at 4 h (when it was significantly higher than sham; $P \leq 0.001$; n = 9; see filled triangles, dotted line). Nicotine per se did not alter the ROS signal at 4 h vs. sham (Fig. 1A, B; inverted filled triangle). Nevertheless, co-application of TBOA and nicotine inhibited the rise in ROS intensity as shown in Fig. 1A, B ($P = 0.009$, n = 4; grey circles, dotted/dashed line).

We next examined mitochondrial activity by measuring the reduction of MTT to formazan [24] using the same protocols employed for the experiments depicted in Fig. 1. The graph for sham condition (Fig. 2, filled circles, continuous line) shows that, over 4 h, there was no significant change in mitochondrial energy metabolism. After TBOA application there was a delayed (4 h), significant ($P = 0.04$; n = 4) fall in MTT production (open squares, dashed line) without earlier (2 h) change. This response pattern was essentially the same 4 h after co-applying TBOA with the nAChR antagonists ($P = 0.03$; n = 5; filled triangles and dotted line in Fig. 2). Nicotine application (Fig. 2, inverted triangle) significantly ($P \leq 0.001$; n = 5) enhanced MTT reduction at 4 h (30.8 ± 0.14 AU), an effect that was approximately 50% higher than sham values (19.6 ± 0.13; n = 5). When nicotine was co-applied with TBOA (Fig. 2, grey circles), the delayed rise in formazan production was still observed (P = 0.008, n = 9), indicating strong contrast to the mitochondrial activity depression evoked by TBOA. As a further control of the MTT method efficiency, we also tested the effect of the powerful mitochondrial poison rotenone [25] that after 4 h application induced a strong decrease in MTT reduction (Fig. 2, open circle; $P \leq 0.01$, n = 6).

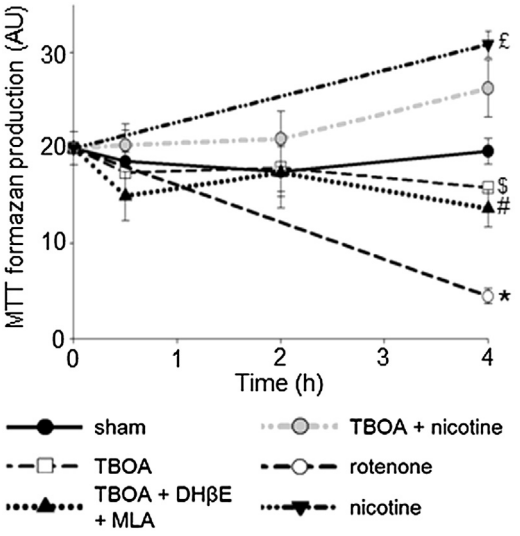

Fig. 2. Quantification of mitochondrial metabolism following excitotoxic stress. Plot quantifying formazan production (AU) at 0, 0.5, 2, or 4 h in sham condition (filled circles) or after treatment with TBOA (open squares), TBOA + DHβE + MLA (filled triangles), TBOA + nicotine (grey circles), rotenone (open circle), or nicotine alone (reverse triangle). In sham condition mitochondrial metabolism remains unchanged over the 4 h time lapse (n = 6 samples at 0 h, 9 at 0.5 h, 5 at 2 h, and 5 at 4 h). Among treatments no changes are observed either at 0.5 h (n = 8 samples for TBOA, 9 for TBOA + DHβE + MLA, and 4 for TBOA + nicotine) or at 2 h (n = 5 samples for TBOA, 5 for TBOA + DHβE + MLA, and 8 for TBOA + nicotine). After 4 h treatment a significant reduction in formazan production is detected in presence of TBOA ($; Student's *t*-test: $P = 0.045$ vs. sham; $P = 0.008$ vs. TBOA + nicotine; and $P \leq 0.001$ vs. nicotine; n = 4) or TBOA + DHβE + MLA (#; Student's *t*-test: $P = 0.03$ vs. sham; $P = 0.004$ vs. TBOA + nicotine; and $P \leq 0.001$ vs. nicotine; n = 5). Nicotine alone significantly enhances mitochondrial metabolism compared to sham at 4 h (£; Student's *t*-test: $P \leq 0.001$; n = 5). Rotenone significantly decreases formazan production at 4 h against all other values (*; Student's *t*-test: $P \leq 0.01$; n = 6).

4. Discussion

The novel finding of the present report is the identification of oxidative damage of HMs as one early consequence of TBOA-mediated excitotoxicity, while the dysfunction of mitochondrial energy metabolism occurred later. In view of the observed time course of these processes, the nicotine neuroprotective effect could be exerted over a few hours.

4.1. An in vitro model of motoneuronal excitotoxicity

Our current *in vitro* model, based on glutamate uptake block, allowed us to monitor the development of oxidative stress and mitochondrial function in the hypoglossal nucleus challenged by excitotoxicity. Thus, future experiments to inhibit each one of these two processes might be differentially studied for their impact on cell death.

Evaluation of intracellular ROS generation following various insults is routinely performed using fluorescent probes that react with a host of ROS [26,27]. This approach is, therefore, helpful to identify how widespread in a cell population ROS production is, while the identification of ROS compounds requires distinct biochemical assays. While DCFH-DA and DHR are often used as fluorescent probes that are transformed into active compounds after cell membrane permeation, we employed the latter because of ease of comparison with our former studies [23,28] and lower propensity to generate additional ROS via their chemical reaction [29].

In control condition the Rho-mediated ROS signal slowly declined suggesting metabolic stabilization in line with the cell viability (4 h) previously reported [20,23]. The maximum level of oxidative stress induced by TBOA was already reached at 2 h, whereas the significant impairment in mitochondrial metabolism was experimentally observed after 4 h. In analogy with previous observations [20], the impairment of mitochondrial function evoked by TBOA was significant, yet much less intense than the toxic effect by rotenone, in accordance with the discrete nature of HM damage in this model.

One interesting result of the present study is that after 0.5 h of glutamate uptake block (despite earlier onset of intense network bursting [20–22]), there was no detectable increase in ROS generation or deficit in mitochondrial metabolism. These findings validate the notion that, in our model, excitotoxicity was caused by a slowly developing cell death process [21].

4.2. nAChRs and motoneuronal excitotoxicity

Pharmacological block of nAChRs enabled us to estimate the role of endogenous ACh in the neurotoxicity model. Hence, co-application of nAChR antagonists and TBOA did not change the increase in ROS level or the reduction in formazan production at 4 h. The issue of endogenous ACh action remains complex because blocking nAChRs does not suppress bursting, yet it facilitates onset of bursting in 60% of silent motoneurons [20]. Because the distribution of cholinergic fibres is scattered in the nucleus hypoglossus [30], the effectiveness of cholinergic modulation is likely to depend on the extent and distribution of afferent pathways impinging on motoneurons. This view is consistent with the frequent presynaptic location of ACh receptors [31].

Boosting cholinergic activity with nicotine application consistently antagonized the excitotoxicity evoked by TBOA. Indeed, after 4 h, it fully protected cells from oxidative stress and metabolic impairment. On the basis of recently published results [20], our data confirm that nicotine per se was not toxic and it actually improved the parameters measured at 4 h with respect to sham.

4.3. Nicotine antioxidant properties

Because of their limited antioxidant mechanisms [26,27], neurons are vulnerable to toxicity from ROS that damage lipids, proteins and nucleic acids [32]. Mitochondria play a Janus-like role in ROS metabolism. On the one hand, they express a range of antioxidant proteins to contrast ROS increase, such as superoxide dismutase (SOD), glutathione peroxidase, glutathione reductase and thioredoxin [33]. On the other, the mitochondrial respiratory chain is a major producer of intracellular ROS and becomes an important origin of the ROS damaging effects [34]. Within this context, nicotine is reported to possess antioxidant properties through radical scavenging that might confer neuroprotective effects [35]. This process is likely to originate from nicotine facilitating NADH binding to complex I, inducing a decrease in superoxide anion generation [36]. While our data are compatible with this phenomenon, they also show that inhibition by nicotine of TBOA-evoked ROS occurred earlier than mitochondrial dysfunction. It is feasible, therefore, that ROS were abundantly produced even when the mitochondrial energy metabolism was not yet severely decreased.

While $\alpha7$ and $\alpha4\beta2$ nAChRs involved in synaptic transmission are located on the plasma membrane [37,38], they have also been discovered on mitochondrial membranes [39,40]. In particular, $\alpha7$ nAChRs prevent cytochrome c release and consequently apoptosis [40] by activating intramitochondrial kinases [41]. Likewise, activation of mitochondrial $\alpha4\beta2$ nAChRs inhibits Ca^{2+}-calmodulin-dependent kinase II (CAMKII) and Src-kinases involved in cytochrome c release [39]. These findings indicate that nicotine might have induced neuroprotection not only by activating and modulating synaptic transmission, but also via a discrete site of intracellular action on mitochondria in view of the high membrane permeability of this alkaloid [42,43] .

5. Conclusions

It is generally assumed that ALS is the result of defective cellular mechanisms which include oxidative stress, mitochondrial dysfunction, and excitotoxicity [44]. Overstimulation of ionotropic glutamate receptors is highly implicated in this process of neuronal death [45] via a cascade of cell damaging processes [2,46]. Because ROS inhibits glutamate uptake [47] and glutamate induces ROS generation [48], a mutually-reinforcing process of cell damage is likely to be produced with later decline in mitochondrial activity. Endogenous cholinergic transmission is insufficient to arrest this vicious circle unless strong stimulation of nAChRs with nicotine is produced to exert a robust neuroprotective effect.

Conflict of interest

none

Contributors

MT, SC, AN design the experiments; MT, SC performed research; MT, SC, AN wrote manuscript.

Acknowledgement

This work was supported by an intramural SISSA grant.

References

[1] B. Billups, D. Rossi, T. Oshima, O. Warr, M. Takahashi, M. Sarantis, M. Szatkowski, D. Attwell, Physiological and pathological operation of glutamate transporters, Prog. Brain Res. 116 (1998) 45–57.
[2] H. Prentice, J.P. Modi, J.-Y. Wu, Mechanisms of neuronal protection against excitotoxicity endoplasmic reticulum stress, and mitochondrial dysfunction in stroke and neurodegenerative diseases, Oxid. Med. Cell. Longev. 2015 (2015) 964518.
[3] J.D. Rothstein, G. Tsai, R.W. Kuncl, L. Clawson, D.R. Cornblath, D.B. Drachman, A. Pestronk, B.L. Stauch, J.T. Coyle, Abnormal excitatory amino acid metabolism in amyotrophic lateral sclerosis, Ann. Neurol. 28 (1990) 18–25.
[4] J.D. Rothstein, R. Kuncl, V. Chaudhry, L. Clawson, D.R. Cornblath, J.T. Coyle, D.B. Drachman, Excitatory amino acids in amyotrophic lateral sclerosis: an update, Ann. Neurol. 30 (1991) 224–225.
[5] O. Spreux-Varoquaux, G. Bensimon, L. Lacomblez, F. Salachas, P.F. Pradat, N. Le Forestier, A. Marouan, M. Dib, V. Meininger, Glutamate levels in cerebrospinal fluid in amyotrophic lateral sclerosis: a reappraisal using a new HPLC method with coulometric detection in a large cohort of patients, J. Neurol. Sci. 193 (2002) 73–78.
[6] J.T. Coyle, P. Puttfarcken, Oxidative stress, glutamate, and neurodegenerative disorders, Science 262 (1993) 689–695.
[7] I.I. Kruman, W.A. Pedersen, J.E. Springer, M.P. Mattson, ALS-linked Cu/Zn-SOD mutation increases vulnerability of motor neurons to excitotoxicity by a mechanism involving increased oxidative stress and perturbed calcium homeostasis, Exp. Neurol. 160 (1999) 28–39.
[8] J.D. Rothstein, Current hypotheses for the underlying biology of amyotrophic lateral sclerosis, Ann. Neurol. 65 (2009) S3–9.
[9] J.D. Jacintho, P. Kovacic, Neurotransmission and neurotoxicity by nitric oxide, catecholamines, and glutamate: unifying themes of reactive oxygen species and electron transfer, Curr. Med. Chem. 10 (2003) 2693–2703.
[10] E. Bogaert, C. d'Ydewalle, L. Van Den Bosch, Amyotrophic lateral sclerosis and excitotoxicity: from pathological mechanism to therapeutic target, CNS Neurol, Disord. Drug Targets 9 (2010) 297–304.
[11] A. Atlante, P. Calissano, A. Bobba, S. Giannattasio, E. Marra, S. Passarella, Glutamate neurotoxicity, oxidative stress and mitochondria, FEBS Lett. 497 (2001) 1–5.
[12] J.D. Rothstein, M. Van Kammen, A.I. Levey, L.J. Martin, R.W. Kuncl, Selective loss of glial glutamate transporter GLT-1 in amyotrophic lateral sclerosis, Ann. Neurol. 38 (1995) 73–84.
[13] S. Sasaki, T. Komori, M. Iwata, Excitatory amino acid transporter 1 and 2 immunoreactivity in the spinal cord in amyotrophic lateral sclerosis, Acta Neuropathol. (Berl.). 100 (2000) 138–144.
[14] S.G. Carriedo, H.Z. Yin, J.H. Weiss, Motor neurons are selectively vulnerable to AMPA/kainate receptor-mediated injury in vitro, J.Neurosci 16 (1996) 4069–4079.
[15] K.T. Dineley, A.A. Pandya, J.L. Yakel, Nicotinic ACh receptors as therapeutic targets in CNS disorders, Trends Pharmacol. Sci. 36 (2015) 96–108.
[16] S.F. Colombo, F. Mazzo, F. Pistillo, C. Gotti, Biogenesis, trafficking and up-regulation of nicotinic ACh receptors, Biochem. Pharmacol. 86 (2013) 1063–1073.
[17] C. Gotti, F. Clementi, Neuronal nicotinic receptors: from structure to pathology, Prog. Neurobiol. 74 (2004) 363–396.
[18] V. Laudenbach, F. Medja, M. Zoli, F.M. Rossi, P. Evrard, J.-P. Changeux, P. Gressens, Selective activation of central subtypes of the nicotinic acetylcholine receptor has opposite effects on neonatal excitotoxic brain injuries, FASEB 16 (2002) 423–425.
[19] T. Nakamizo, J. Kawamata, H. Yamashita, R. Kanki, T. Kihara, H. Sawada, A. Akaike, S. Shimohama, Stimulation of nicotinic acetylcholine receptors protects motor neurons, Biochem. Biophys. Res. Commun. 330 (2005) 1285–1289.
[20] S. Corsini, M. Tortora, A. Nistri, Nicotinic receptor activation contrasts pathophysiological bursting and neurodegeneration evoked by glutamate

uptake block on rat hypoglossal motoneurons, J. Physiol. (2016), epub ahead of print.
[21] E. Sharifullina, A. Nistri, Glutamate uptake block triggers deadly rhythmic bursting of neonatal rat hypoglossal motoneurons, J. Physiol. 572 (2006) 407–423.
[22] F. Nani, A. Cifra, A. Nistri, Transient oxidative stress evokes early changes in the functional properties of neonatal rat hypoglossal motoneurons in vitro, Eur. J. Neurosci. 31 (2010) 951–966.
[23] A. Cifra, F. Nani, A. Nistri, Riluzole is a potent drug to protect neonatal rat hypoglossal motoneurons in vitro from excitotoxicity due to glutamate uptake block, Eur. J. Neurosci. 33 (2011) 899–913.
[24] T. Mosmann, Rapid colorimetric assay for cellular growth and survival: application to proliferation and cytotoxicity assays, J. Immunol. Method 65 (1983) 55–63.
[25] N. Li, K. Ragheb, G. Lawler, J. Sturgis, B. Rajwa, J.A. Melendez, J.P. Robinson, Mitochondrial complex I inhibitor rotenone induces apoptosis through enhancing mitochondrial reactive oxygen species production, J. Biol. Chem. 278 (2003) 8516–8525.
[26] S. Leutner, A. Eckert, W.E. Müller, ROS generation, lipid peroxidation and antioxidant enzyme activities in the aging brain, J. Neural Transm. 108 (2001) 955–967.
[27] L.L. Dugan, S.L. Sensi, L.M. Canzoniero, S.D. Handran, S.M. Rothman, T.S. Lin, M.P. Goldberg, D.W. Choi, Mitochondrial production of reactive oxygen species in cortical neurons following exposure to N-methyl-D-aspartate, J. Neurosci 15 (1995) 6377–6388.
[28] A. Cifra, F. Nani, E. Sharifullina, A. Nistri, A repertoire of rhythmic bursting produced by hypoglossal motoneurons in physiological and pathological conditions, Philos. Trans. R. Soc. Lond. B Biol. Sci. 364 (2009) 2493–2500.
[29] B. Kalyanaraman, V. Darley-Usmar, K.J.A. Davies, P.A. Dennery, H.J. Forman, M.B. Grisham, G.E. Mann, K. Moore, L.J. Roberts, H. Ischiropoulos, Measuring reactive oxygen and nitrogen species with fluorescent probes: challenges and limitations, Free Radic. Biol. Med. 52 (2012) 1–6.
[30] P.B. Clarke, Nicotinic receptors in mammalian brain: localization and relation to cholinergic innervation, Prog. Brain Res. 98 (1993) 77–83.
[31] S. Wonnacott, Presynaptic nicotinic ACh receptors, Trends Neurosci. 20 (1997) 92–98.
[32] M. Erat, M. Ciftci, K. Gumustekin, M. Gul, Effects of nicotine and vitamin E on glutathione reductase activity in some rat tissues in vivo and in vitro, Eur. J. Pharmacol. 554 (2007) 92–97.
[33] M.A. Perez-Pinzon, R.A. Stetler, G. Fiskum, Novel mitochondrial targets for neuroprotection, J. Cereb. Blood Flow Metab. 32 (2012) 1362–1376.
[34] T. Suhm, M. Ott, Mitochondrial translation and cellular stress response, Cell Tissue Res. (2016).
[35] B. Ferger, C. Spratt, C.D. Earl, P. Teismann, W.H. Oertel, K. Kuschinsky, Effects of nicotine on hydroxyl free radical formation in vitro and on MPTP-induced neurotoxicity in vivo, Naunyn. Schmiedebergs Arch. Pharmacol. 358 (1998) 351–359.
[36] A. Cormier, C. Morin, R. Zini, J.P. Tillement, G. Lagrue, In vitro effects of nicotine on mitochondrial respiration and superoxide anion generation, Brain Res. 900 (2001) 72–79.
[37] C.R. Breese, C. Adams, J. Logel, C. Drebing, Y. Rollins, M. Barnhart, B. Sullivan, B.K. Demasters, R. Freedman, S. Leonard, Comparison of the regional expression of nicotinic acetylcholine receptor α7 mRNA and [^{125}Iα–bungarotoxin binding in human postmortem brain, J. Comp. Neurol. 387 (1997) 385–398.
[38] J. Lindstrom, Nicotinic acetylcholine receptors in health and disease, Mol. Neurobiol. 15 (1997) 193–222.
[39] O. Lykhmus, G. Gergalova, L. Koval, M. Zhmak, S. Komisarenko, M. Skok, Mitochondria express several nicotinic acetylcholine receptor subtypes to control various pathways of apoptosis induction, Int. J. Biochem. Cell Biol. 53 (2014) 246–252.
[40] G. Gergalova, O. Lykhmus, S. Komisarenko, M. Skok, α7 nicotinic acetylcholine receptors control cytochrome c release from isolated mitochondria through kinase-mediated pathways, Int. J. Biochem. Cell Biol. 49 (2014) 26–31.
[41] F. Dajas-Bailador, S. Wonnacott, Nicotinic acetylcholine receptors and the regulation of neuronal signalling, Trends Pharmacol. Sci. 25 (2004) 317–324.
[42] F.A. Dajas-Bailador, P.A. Lima, S. Wonnacott, The α7 nicotinic acetylcholine receptor subtype mediates nicotine protection against NMDA excitotoxicity in primary hippocampal cultures through a Ca^{2+} dependent mechanism, Neuropharmacology 39 (2000) 2799–2807.
[43] J. Hukkanen, P. Jacob, N.L. Benowitz, Metabolism and disposition kinetics of nicotine, Pharmacol. Rev. 57 (2005) 79–115.
[44] D.W. Cleveland, J.D. Rothstein, From Charcot to Lou Gehrig: deciphering selective motor neuron death in ALS, Nat. Rev. Neurosci. 2 (2001) 806–819.
[45] M. Tymianski, M.P. Charlton, P.L. Carlen, C.H. Tator, Source specificity of early calcium neurotoxicity in cultured embryonic spinal neurons, J. Neurosci. 13 (1993) 2085–2104.
[46] P.J. Shaw, P.G. Ince, Glutamate, excitotoxicity and amyotrophic lateral sclerosis, J. Neurol. 244 (Suppl 2) (1997) S3–14.
[47] A. Volterra, D. Trotti, S. Floridi, G. Racagni, Reactive oxygen species inhibit high-affinity glutamate uptake: molecular mechanism and neuropathological implications, Ann. N. Y. Acad. Sci. 738 (1994) 153–162.
[48] S.D. Rao, H.Z. Yin, J.H. Weiss, Disruption of glial glutamate transport by reactive oxygen species produced in motor neurons, J. Neurosci. 23 (2003) 2627–2633.

Nicotine protects rat hypoglossal motoneurons from excitotoxic death via downregulation of connexin 36

Authors: Silvia Corsini, Maria Tortora, Rossana Rauti, Andrea Nistri

Department of Neuroscience, International School for Advanced Studies (SISSA), Trieste, Italy

Corresponding author: Andrea Nistri, SISSA, via Bonomea 265, 34136 Trieste, Italy; tel: +39 040 3787 718; e-mail: nistri@sissa.it

Running title: nicotine neuroprotection

Abstract

Motoneuron disease including amyotrophic lateral sclerosis may be due, at an early stage, to deficit in the extracellular clearance of the excitatory transmitter glutamate. A model of glutamate-mediated excitotoxic cell death based on pharmacological inhibition of its uptake was used to investigate how activation of neuronal nicotinic receptors by nicotine might protect motoneurons. Hypoglossal motoneurons (HMs) in neonatal rat brainstem slices were exposed to the glutamate uptake blocker DL-threo-β-benzyloxyaspartate (TBOA) that evoked large Ca^{2+} transients time-locked among nearby HMs, whose number fell by about 30% 4 h later. Since nicotine or the gap junction blocker carbenoxolone suppressed bursting, we studied connexin 36 (Cx36) which constitutes gap junctions in neurons and found it largely expressed by HMs. Cx36 was downregulated when nicotine or carbenoxolone was coapplied with TBOA. Expression of Cx36 was preferentially observed in cytosolic rather than membrane fractions after nicotine and TBOA, suggesting protein redistribution with no change in synthesis. Nicotine raised the expression of heat shock protein70 (Hsp70), a protective factor that binds the apoptotic inducing factor (AIF) whose nuclear translocation is a cause of cell death. TBOA increased intracellular AIF, an effect blocked by nicotine. These results indicate that activation of neuronal nicotinic receptors is an early tool for protecting motoneurons from excitotoxicity and that this process is carried out via the combined decrease in Cx36 activity, overexpression of Hsp70 and fall in AIF translocation. Thus, retarding or inhibiting HM death may be experimentally achieved by targeting one of these processes leading to motoneuron death.

Introduction

The neurodegenerative disease amyotrophic lateral sclerosis (ALS) is characterized by motoneuron death in the brainstem and spinal cord. While the etiopathology remains unclear, it is likely due to a complex interplay among pathogenic factors such as glutamate-mediated excitotoxicity, oxidative stress with reactive oxygen species (ROS) generation, and mitochondrial dysfunction (1). The brainstem nucleus hypoglossus is often affected early, thus leading to dysarthria and dysphagia (2). Hypoglossal motoneurons (HMs) are very vulnerable because of their high basal intracellular free Ca^{2+} (3), expression of Ca^{2+} permeable AMPA receptors (4), and comparatively low levels of glutamate transporters (5). In ALS these properties are exacerbated by impaired glutamate transport (as observed in post-mortem tissues; 5,6) and increased level of glutamate in cerebrospinal fluid (7): therefore, excitotoxicity is an important candidate for causing the disease. Nonetheless, motoneuron death has usually a patchy distribution and a slow progression (8) associated with muscle weakness and fasciculations (9), indicating that an unresolved interaction among discrete intracellular death mechanisms is probably taking place.

In the past few years, a simple *in vitro* model of excitotoxic stress applied to rat HMs has been developed by our laboratory (10–12). It consists of mimicking the pathological process of motoneuron hyperexcitability and excitotoxicity in the nucleus hypoglossus through pharmacological inhibition of glutamate uptake with DL-threo-β-benzyloxyaspartate (TBOA). Salient characteristics of this model are generation of electrical bursting among HMs interconnected via gap junctions (12) and slow onset of cell

death (11) via production of ROS and subsequent mitochondrial energy deficit in a subset of motoneurons (13). One essential property of HMs is their ability to generate "group bursting" dependent on the membrane expression of gap junctions (14,15) made by connexins, of which connexin 36 (Cx36) is highly represented in the nervous system (16,17). Gap junctions may also be due to pannexins, particularly pannexin 1 (Panx1) which share, with connexins, similar topology, permeability and gating (17,18). In case of cell stress, expression of connexins and pannexins may increase the probability of damage diffusion and cell death (16).

We recently observed that nicotine (selective agonist on nicotinic acetylcholine receptor, nAChR) prevents cell death, hyperexcitability, mitochondrial dysfunction, oxidative and ER stress (13). Because in cultured endothelial cells nicotine downregulates connexins (19,20), we wondered if a similar process could account for neuroprotection of HMs. To this aim, we studied how nicotine could modulate Ca^{2+} transients, Cx36 and Panx1, and compared it with the effects of the gap junction blocker carbenoxolone (21). In analogy with previous reports (22,23), we used expression of heat shock protein 70 (Hsp70) and apoptosis-inducing factor (AIF) as indices of cell protection or death, respectively.

Results

Network distribution of Ca^{2+} signals induced by TBOA

TBOA (50 μM) induces bursting activity in about 50% of HMs (12,13) with large inward currents translated into strong intracellular Ca^{2+} transients (24). The present study

investigated $[Ca^{2+}]_i$ changes in the hypoglossal nucleus (Fig. 1A, B; movie 1-3) to monitor in detail mechanisms of excitation spread. To this purpose, we performed continuous imaging (10 min) of $[Ca^{2+}]_i$ transients as shown in Fig. 1B and movies 1-3, in which about thirty HMs for each slice were recorded during application of TBOA. Fig. 1A shows representative examples (taken from five HMs) recorded in the presence of TBOA alone (top records; movie 1), or co-applied with nicotine (10 μM) + TBOA (Fig. 1A middle; movie 2), or with carbenoxolone (200 μM) + TBOA (Fig. 1A bottom; movie 3). TBOA induced transients in about 50% of HMs (50 ± 8%, n = 5 slices), a value reduced to 36 ± 14% (n = 5 slices) in presence of nicotine, and to 14 ± 7% when carbenoxolone was coapplied (Mann-Whitney test: P = 0.016 for TBOA vs. carbenoxolone + TBOA, n = 5 slices). On average, nicotine or carbenoxolone significantly decreased the number of transients evoked by TBOA (Fig. 1C) as they fell from 4.4 ± 0.4 (n = 69 HMs) to 2.8 ± 0.2 (Mann-Whitney test: P = 0.006, n = 40 HMs) in presence of nicotine, or to 2.3 ± 0.3 (Mann-Whitney test: P = 0.002, n = 18 HMs) with carbenoxolone coapplication. However, neither nicotine nor carbenoxolone changed the basal level of $[Ca^{2+}]_i$ at 10 min. Fig. 1D shows a plot of the number of transients against cumulative probability. Thus, the plot for nicotine or carbenoxolone co-application is significantly shifted to the left (Kolmogorov-Smirnov test: $P \leq 0.001$ for TBOA, solid line vs. nicotine + TBOA, dotted line; and $P \leq 0.001$ for TBOA vs. carbenoxolone + TBOA, dashed line), demonstrating increased probability to observe fewer events than in the presence of TBOA alone.

Because of the scattered onset of $[Ca^{2+}]_i$ transients (movie 1-3), we studied whether topographical distance between two motoneurons was predictive of the closely-spaced

activity. Thus, Fig. 2 compares the inter-neuronal distance with the latency between the first calcium transient of each cell pair (Fig. 2A). The top plot (Fig. 2B), which refers to TBOA-treated cells only, shows how the latency between transients was closely related to their distance and that the vast majority of latency values were below 100 s. Conversely, when nicotine or carbenoxolone was co-applied with TBOA (Fig. 2C, D), the plots were made up by a cloud of widely scattered points and the latency values were larger than 200 s even for closely located HMs. These data demonstrated the asynchronous occurrence of $[Ca^{2+}]_i$ changes when nicotine or carbenoxolone were co-applied.

Nicotine or carbenoxolone modulates Cx36 expression.

Because HM bursting is supported by a variety of mechanisms including gap junctions (14,15,24,25), the above results raised the hypothesis that nicotine (like carbenoxolone) might impair intercellular communication via Cx36 and Panx1. Because mitochondrial dysfunction and motoneuron death are observed after 4 h treatment with TBOA (13), we evaluated Cx36 expression (Fig. 3A-C; red) in relation to immunoreactivity of single HMs (identified with SMI 32 immunostaining; green). DAPI was used for nuclear staining (blue). In accordance with previous studies (26,27), Cx36 immunoreactivity was distributed through the soma of HMs as shown in Fig. 3A (middle column) and quantified in Fig. 3C: the Cx36 signal was not significantly altered by TBOA alone in the cells that remained after the excitotoxic stimulation, while the motoneuronal number after TBOA (Fig. 3D) fell by approximately 30%. When nicotine was co-applied with TBOA, the Cx36 immunoreactivity was significantly decreased (Fig. 3A, C) and the average number of motoneurons was similar to sham (Fig. 3D). An analogous result was observed when

carbenoxolone was co-applied with TBOA (Fig. 3A, C, D). Nicotine per se did not change the average Cx36 signal (Fig. 3A, C) or motoneuron survival (Fig. 3D; 13).

To further investigate the amount of expressed Cx36 under various experimental conditions, Western blot experiments were performed as depicted in Fig. 4 using brainstem tissue blocks in order to collect a sufficient amount of protein. Evaluation of Cx36 total lysate (approximately 36 kDa) samples confirmed unchanged protein quantity after 4 h treatment with TBOA (0.99 ± 0.07, n = 9 brainstems) or nicotine (0.94 ± 0.07, n = 6 brainstems; Fig. 4A). In support of the immunohistochemical data (Fig. 3A-C), we observed that, when samples were treated with nicotine + TBOA or carbenoxolone + TBOA, Cx36 expression was significantly reduced to 0.89 ± 0.07 (Mann-Whitney test: $P = 0.038$; n = 9 brainstems) or 0.82 ± 0.08 (Mann-Whitney test: $P \leq 0.001$; n = 5 brainstems), respectively. We further explored the distribution of Cx36 in membrane and cytoplasmic compartments. In the case of nicotine exposure there was a small, yet significant decrease in Cx36 membrane expression (Fig. 4B; Mann-Whitney test: $P = 0.008$ for sham vs. nicotine; n = 5 brainstems) concomitant with a corresponding increase in the cytoplasmic fraction (Fig. 4C; Mann-Whitney test: $P = 0.008$ for sham vs. nicotine; n = 5 brainstems). The fall in membrane expression of Cx36 was intensified when nicotine was co-applied with TBOA (Fig. 4B; Mann-Whitney test: $P = 0.016$ for sham vs. nicotine + TBOA; n = 5 brainstems) in association with a significant rise in the cytoplasmic expression (Fig. 4C; Mann-Whitney test: $P = 0.008$ for sham vs. nicotine + TBOA; n = 5 brainstems). Interestingly, neither compartmental expression was modified by TBOA alone, perhaps suggesting that the manifestation of the action of this drug required an unchanged Cx36

141 expression. These effects of Cx36 compartmentalization were not due to changes in its
142 synthesis as qPCR experiments showed no alteration in the Cx36 gene product (Fig. 5A;
143 Kruskal-Wallis test: P = 0.21 among groups; n = 6 brainstems).

144 *Hsp70 and AIF contrasting expression in HMs*

145 In case of excitotoxicity, motoneuronal survival may depend on the relative intracellular
146 expression of Hsp70 and AIF with cell-protecting or cell-damaging properties, respectively
147 (22,23). Fig. 5B, C shows that, after TBOA or nicotine treatment, Hsp70 expression was
148 unchanged compared with basal sham conditions. When nicotine and TBOA were co-
149 applied, Hsp70 expression was significantly enhanced (Mann-Whitney test: P = 0.008 for
150 sham vs. nicotine + TBOA; Student's *t*-test: P = 0.053 for nicotine + TBOA vs. nicotine; n
151 = 5 brainstems). Thus, during excitotoxic stimulation, application of nicotine enhanced
152 Hsp70 expression, thus strengthening the neuroprotective processes of motoneurons. In
153 fact, protection of motoneurons from excitotoxicity depends to a large extent on the
154 binding by Hsp70 of AIF, a mitochondrial factor released by metabolically-damaged
155 motoneurons (22,23). When, during excitotoxicity, Hsp70 expression is insufficient to bind
156 AIF, the latter migrates to the cell nucleus and inactivates DNA (28). We, therefore,
157 studied immunohistochemical expression of AIF when TBOA was applied alone or
158 together with nicotine. Fig. 6A shows examples of AIF immunoreactivity increased after
159 TBOA administration with broad distribution within nuclear (delineated by the blue line in
160 Fig. 6B for DAPI staining) and non-nuclear compartments as indicated by the line scan red
161 trace that had higher value throughout (Fig. 6B; note different ordinate scale for the
162 various treatment protocols). Viceversa, the level of AIF was low in the presence of

nicotine with or without TBOA (Fig. 6B), suggesting that nicotine kept the AIF level at sham-like condition. These data are quantified in the bar graph of Fig. 6C in which the average fluorescence signal (AU) of AIF in basal condition was 16.1 ± 3.2 (n = 9 slices) and significantly increased to 60 ± 7.8 ($P \leq 0.001$, n = 19 slices) after TBOA exposure, while it was low when nicotine was co-applied with TBOA ($P = 0.014$, n = 16 slices). It should be noted that nicotine (n = 6 slices) per se left unchanged the AIF immunoreactivity compared with sham.

Unchanged expression of Panx1

We sought to understand whether nicotine or carbenoxolone could change other proteins such as Panx1 reputed to make gap junctions. To this end, immunohistochemical and western blot experiments were performed as illustrated in Fig. 7A-C. Hence, Panx1immunoreactivity was readily detected in HMs as depicted in Fig 7A and remained unchanged following TBOA with or without nicotine protocols (Fig. 7B). Likewise, Panx1 protein expression was very similar among all these treatments, indicating that Panx1 was not involved in nicotine neuroprotection at least within the 4 h experimental timeframe.

Discussion

The principal finding of the present study was the demonstration that, during an excitotoxic stimulus, nicotine perturbed the emergence of coordinated Ca^{2+} transients among HMs, decreased the expression of Cx36 at membrane level, enhanced the expression of Hsp70 while diminishing the one of AIF. These data were critical

components of the HM neuroprotective action by this alkaloid. Since many effects of nicotine were replicated by carbenoxolone, it is likely that inhibition of Cx36 was essential to uncouple motoneurons from their collective bursting behavior that was prodromic to cell distress and death.

Motoneurons wired together, die together

Inhibition of glutamate uptake recruits clusters of motoneurons in group bursting processes that, if continued unabated, will lead to significant neuronal death (12). Since our recent work indicates that nicotine largely suppresses bursting (13), we investigated whether this phenomenon was translated into dissociation of intense discharges (recorded as Ca^{2+} transients) among motoneurons. Indeed, following application of nicotine or the gap junction blocker carbenoxolone, bursting became sparse and, importantly, was followed by a significant protection of HMs from death. This realization implies that the severity of damage was perhaps dependent on the collective activation and recruitment of clusters of HMs into pathological discharges, and led us to study the role of gap junctions (known to exist among HMs; 14,15) mediated by Cx36 in this process.

Connexins and cell death

Cx36 is the most prevalent gap junction protein expressed by neurons (16,17). It electrically couples neighboring cells by allowing transcellular communication and exchange of Ca^{2+}, Na^{+}, K^{+}, and other small (<1-1.5 kDa) hydrophilic molecules (17,29). Many factors regulate the activity of gap junction channels, including changes in voltage, $[Ca^{2+}]_i$, pH (30), connexin phosphorylation, (30,31) and ROS (32). In the past few years

205 many other components of intra-/extracellular signaling have been associated with plasma
206 membrane hemichannels such as facilitation of glutamate release from astrocytes (33) and
207 apoptosis (29). Indeed, gap junction-related apoptosis has been demonstrated by
208 carbenoxolone-mediated prevention (34), and by the spreading of death signals within a
209 cell cluster via gap junctions (34,35). This mode of propagation from injured to uninjured
210 close neighbor cells is classified as bystander killing (the 'kiss of death'; 16,29). An
211 interaction among connexins and mitochondrial AIF in cardiomyocytes has been described
212 with potential effects on mitochondrial respiration and ROS signaling (36). Whether this
213 process could also occur in motoneurons remained unclear.

214 During NMDA receptor-mediated excitotoxicity a strong reduction in neuronal death of
215 cultured cortical neurons is obtained when Cx36 is pharmacologically blocked or
216 genetically ablated, indicating that the expression level of Cx36 critically modulates
217 neuronal death (25,37). Thus, the observation of basal expression of Cx36 by HMs made
218 this protein a likely candidate in the excitotoxic cell death. It was of interest that, following
219 glutamate uptake block and loss of a number of HMs, surviving cells did not show
220 impaired Cx36 expression, alluding to the possibility that these cells had relied on certain
221 intrinsic mechanisms to withstand the injury process.

222 *Nicotine prevents HM excitotoxic death via Cx36 downregulation*

223 In endothelial cell cultures, nicotine, via membrane ACh receptors, down-regulates
224 various connexins through intracellular pathways (19,20) that impact their turnover (20). In
225 excitotoxic stress, we actually detected a fall in Cx36 immunoreactivity of HMs when

nicotine (or carbenoxolone) was applied with TBOA, a result which was accompanied by no significant loss of HMs. Although nicotine can decrease excitatory synaptic transmission on HMs (13,38), the analogy with the effects by carbenoxolone and the downregulated immunopositivity of Cx36 suggested that Cx36 were important targets to restrain excitotoxicity. Because our model did not allow prolonged observation of the timecourse of nicotine effects, it is difficult to reveal the dynamics of Cx36 turnover over an extended time profile in a relatively thick brainstem slice. It was, however, clear that changes in Cx36 synthesis had not taken place in view of the negative qPCR data. Circumstantial evidence was sought with tissue fractionation experiments in which we sought the relative distribution of Cx36 among membrane and cytosolic fractions. Despite the limitation inherent in the use of brainstem tissue blocks containing a heterogeneous cell population, we detected a significant decrease in the Cx36 membrane fraction together with a notable rise in its cytoplasmic fraction. These data implied that the expression and perhaps the function of Cx36 at membrane level were impaired with nicotine application. Our model also indicated that the effect by nicotine had a degree of specificity since Panx1 expression was unchanged by nicotine. We cannot, however, rule out that the long life-cycle of Panx1 (39) had precluded detecting a later alteration following nicotine application.

Nicotine modulated Hsp70 expression as a gateway to cell survival against AIF-mediated death

One further result of interest was the observation that nicotine and TBOA application evoked a significant increase in Hsp70 expression, while nicotine or TBOA alone did not

248 change this protein. Since the intracellular expression of Hsp70 is an important biomarker
249 of the ability of motoneurons to resist to excitotoxicity (22), we surmise that surviving
250 cells had an adequate Hsp70 expression even though these data were obtained from
251 brainstem tissue rather than single HMs. The perturbation triggered by TBOA plus the
252 effects of nicotine probably synergized to raise Hsp70 expression and extend
253 neuroprotection. These observations, therefore, provided an interesting clue to further
254 explore the mechanism of nicotine neuroprotection. Our view was in line with reports of
255 nicotine ability to enhance Hsp70 expression in lung vessels and ovarian tissue culture
256 (40,41), and to block AIF lethal translocation into the nucleus (28). The
257 immunofluorescent data showed that, at HM level, TBOA clearly enhanced the expression
258 of AIF, a factor released by distressed mitochondria, and that this biomarker was
259 distributed throughout the motoneuron including its nucleus. Co-application of TBOA and
260 nicotine normalized the rise in AIF expression and restituted sham like condition,
261 suggesting that the effect of this death factor was inhibited likely as a consequence of the
262 raised Hsp70 expression in the cytoplasm.

263 *A scenario for motoneuron protection by nicotine*

264 Fig. 8 depicts an idealized diagram we propose to account for the complex process of HM
265 death evoked by glutamate uptake block and the intervention levels exerted by nicotine.
266 Excitotoxicity, induced by the impairment of excitatory amino acid transporters with
267 TBOA (42), severely damages motoneurons by excessive glutamate receptor stimulation
268 that induces strong network bursting (11–13,24) among electrically-coupled HMs. This
269 phenomenon elicits excessive Ca^{2+} influx, that depolarizes the neuronal membrane

potential to activate further Ca^{2+} influx (43,44) and intracellular second messengers in a death cell cascade (45,46). The role by mitochondria in Ca^{2+} buffering may lead to mitochondrial membrane depolarization (43,44,47) and perturbation of the respiratory chain (43,44). This process is compounded by ROS-evoked oxidative stress (13,48,49). In this vicious sequence, cell damage is extended via gap junctions (16,25,50) activated by ROS (32).

In conclusion, we propose that a potential device to contrast excitotoxic damage to HMs is activation of nAChRs. The mechanism linking nAChR activation to inhibition of Cx36 activity remains unsolved and requires future investigation. We can posit that, since nicotine is reported to enhance protein kinase C (PKC; 51–53), PKC-mediated connexin phosphorylation is a putative process to reduce gap junction-dependent intercellular communication (54). Finally, our data are not intended to support a neuroprotecting role of smoking, rather to prompt a strategy for further investigation of inhibiting motoneuron disease *in vitro* and *in vivo* with novel tools to stimulate nAChRs.

Materials and methods

Ethical approval

All experiments were performed following the ethical guidelines for the use and the care of laboratory animals of National Institutes of Health. The Scuola Internazionale Superiore di Studi Avanzati (SISSA) ethics committee (prot. 3599, 28 May 2012) approved all treatment protocols which were in agreement with the European Union rules for animal

291 experimentation. We made all the effort to minimize the use and the suffering of the
292 animals, and reduce their number for experimentation.

293 *Slice preparation and drug application protocols*

294 Experiments were carried out on neonatal Wistar rats (postnatal days 1-6; P1-P6), rapidly
295 decapitated under i.p. urethane anaesthesia (10% solution, 0.1 ml injection volume).
296 Brainstems were removed in continuously carbogenated (95% O_2 and 5% CO_2) ice-cold
297 Krebs solution containing (in mM): 130 NaCl, 3 KCl, 1.5 NaH_2PO_4, 1 $CaCl_2$, 5 $MgCl_2$, 25
298 $NaHCO_3$ and 18.5 glucose (pH 7.4; 300-330 mOsm/l). For Ca^{2+} imaging and
299 immunohistochemical experiments, slices (270-450 µm thick) containing the nucleus
300 hypoglossus were immediately cut with a vibrating tissue slicer (Leica VT 1000S, Wetzlar,
301 Germany). Slices (or intact brainstems for molecular biology) were then rapidly transferred
302 to an incubation chamber for 20 min at 32°C and then recovered for 10 min at room
303 temperature. Details of the experimental procedure were previously published (12,55).

304 With the exception of slices for the calcium imaging technique, samples were subsequently
305 incubated for 4 h at room temperature in continuously carbogenated Krebs solution (sham),
306 TBOA (50 µM; Sigma-Aldrich, Saint Louis, MO, USA), TBOA + nicotine (10 µM;
307 Sigma-Aldrich), nicotine, or TBOA + carbenoxolone (200 µM; Sigma-Aldrich) and
308 processed as indicated later. Experiments were run in parallel to minimize the bias.

309 *Intracellular Ca^{2+} imaging $[Ca^{2+}]_i$*

310 In accordance with formerly described protocols (12,56), slices (270 µm thick) were
311 loaded with the fluorescent Ca^{2+} dye Fluo-3, AM (4 µM, Molecular Probes, Invitrogen,

312 Carlsbad, CA, USA) for 1h in continuously carbogenated Krebs solution. After 30 min
313 wash, samples were transferred into the recording chamber of the Nikon Eclipse T1
314 microscope (Nikon, Tokyo, Japan), where the nuclei hypoglossi were identified with a 40x
315 objective (aperture 0.60). Drug concentrations were chosen on the basis of previous reports
316 (12,13) and applied acutely in accordance with the following protocols (10 min): TBOA
317 (50 μM), nicotine (10 μM) + TBOA (50 μM); carbenoxolone (200 μM) + TBOA (50 μM).
318 Ca^{2+} fluorescent emission was excited at a fixed wavelength of 488 nm generated by a
319 Nikon intensilight C-HGFI lamp (Nikon) and detected with the digital CMOS camera
320 ORCA-Flash 4.0 (Hamamatsu Photonic, Hamamatsu City, Japan). Images were acquired
321 with the Fiji software (ImageJ, Wayne Rasband, National Institued of Health, USA; 57)
322 with 150 ms exposure time. In each slice, a small region of interest (ROI) was placed over
323 about 30 randomly distributed motoneurons easily recognizable for their somatic diameter
324 (> 20 μm). Traces extrapolated with Igor Pro software (version 6.37, Wavemetrics, Lake
325 Oswego, OR, USA) were analyzed with the software Clampfit 10.0 (Molecular Devices
326 Corporation, Sunnyvale, CA, USA). Ca^{2+} transients were analyzed if events had a duration
327 < 20 s and a rise phase faster than the decay. Transients were expressed as $\Delta F/F_0$, the
328 amplitude fractional increase, where ΔF is the fluorescence rise over baseline, and F_0 the
329 baseline fluorescence level; $[Ca^{2+}]_i$ elevations were considered significant when they
330 exceeded 5 times the noise standard deviation (58,59).

331 *Immunohistochemistry*

332 At the end of 4 h experiments, slices were fixed in PBS containing 4% paraformaldehyde
333 for 4 h at 4°C, treated for cryoprotection in 30% sucrose for 72 h at 4°C, and finally frozen

for at least 12 h in an embedding mounting medium. Embedded slices were then cut with a cryostat in 30 µm tissue sections. Samples were blocked (in a PBS-based solution containing: 10% normal goat serum, 50% BSA and 3% Triton X-100) for 2 h at room temperature and incubated overnight at 4°C with the primary antibodies anti-SMI 32 (mouse monoclonal, 1:200 dilution; cat. #: 801701; BioLegend, San Diego, CA, USA; for validation see 51), anti-Cx36 (rabbit polyclonal, 1:300 dilution; cat. #: ACC-209; Alomone, Jerusalem, Israel; 27), anti-Pannexin 1 (Panx1; rabbit polyclonal, 1:300 dilution; cat. #: ACC-234; Alomone; 60), or anti-AIF (rabbit polyclonal, 1:200 dilution; cat. #: AB16501; Millipore, Billerica, MA, USA;61). AlexaFluor 488 and 594 (1:500 dilution; Life Technologies, Carlsbad, CA, USA) were used as secondary antibodies and applied for 2h at room temperature. Antibodies were diluted in an antibody PBS-based solution containing: 2% normal goat serum, 10% BSA and 1% Triton X-100. After secondary antibody incubation, slices were rinsed and stained with the DNA dye DAPI diluted in PBS (1:1 000; Sigma-Aldrich), for 20 min at room temperature. To reduce fading, slices were mounted with fluorescence mounting medium (Dako, Glostrup, Denmark) and images acquired by either a Zeiss Axioskop2 microscope (20x; Oberkochen, Germany) or a confocal Nikon microscope (40x in oil) with 1 µm z sectioning. Images were analyzed with the Volocity software (PerkinElmer, Waltham, MA, USA).

Western blot

Analysis of quantitative and qualitative protein expression was performed with a standard Western blot technique on whole brainstem treated as described above in accordance with the previously published protocol (62). Total lysates, cytoplasmic and membrane fractions

were analyzed. Total lysates were obtained by homogenizing samples in CHAPS buffer solution (0.5% CHAPS, 50 mM Tris pH 7.5, 1 mM EDTA, 150 mM NaCl, 10% glycerol plus protease inhibitors mixture and reducing agents; Complete, Roche Applied Science, Basel, Switzerland; and Sigma-Aldrich). A hypotonic lysis buffer (10 mM HEPES pH 7.9 with 1.5 mM $MgCl_2$ and 10 mM KCl plus protease inhibitors mixture and reducing agents) was used to process samples for membrane and cytoplasmic extraction, which were then centrifuged for 5 min at 4000 rpm at 4°C and the supernatant transferred to ultracentrifuge tubes for centrifugation (1 h) at 100 000g. Cytoplasmic proteins were considered those in the supernant, whereas the pellet was formed by membrane proteins which were re-suspended in the extraction buffer (20 mM HEPES pH 7.9, with 1.5 mM $MgCl_2$, 0.2 mM EDTA, 25% glycerol, 1% SDS plus protease inhibitors mixture and reducing agents). Samples were then immunoblotted with rabbit anti-Cx36 (1:200, Alomone), rabbit anti-Panx 1 (1:400, Alomone), mouse anti-Hsp70 (1:5 000, Abcam, Cambridge, UK), mouse anti-β-actin (1:2 000, Sigma-Aldrich), mouse anti-β-tubulin (1:2 000, Sigma-Aldrich), or mouse anti-synaptophysin (1:10 000, Millipore) antibodies. Because both Cx36 and Panx1 encode consensus sites for phosphorylation and glycosilation, it is, thus, common to observe more than one band in the immunoblotting gels (39,63) as reported in the present study as well. The enhanced chemiluminescence light system (ECL, Amersham Bioscience, Piscataway, NJ, USA) was used to detect signals recorded with the digital imaging system Alliance 4.7 (UVItech, Cambridge, UK) and quantified with the software Alliance LD2-77-WL (UVItec).

Real Time-PCR

PCR experiments were performed on total RNA isolated from tissues, treated as described above, using the Triazol reagent (Invitrogen). RNase-free DNase (Ambion, Austin, TX, USA) was used for RNA extraction and cDNA was purified using the RNeasy Mini Kit (QIAGEN, Hilden, Germany), according to the respective manufacturer's instructions. Single strand cDNA samples were obtained using the iScriptcDNA Synthesis Kit (Bio-Rad) from at least 20 ng of purified RNA. The new synthesized cDNA was amplified using the oligonucleotide primer listed in Table 1, the nucleic acid stain iQ SYBER Green Supermix (Bio-Rad) and an iCycler IQ Real time PCR System (Bio-Rad).

Statistics

Results were expressed as means ± standard error of the mean (SEM) and collected from at least three different experiments, where *n* refers to the number of slices or brainstems for each independent experiment, as indicated, and N refers to the number of times an experiment was repeated. Using the standard software SigmaStat 3.5 (Systat Software, Inc., Chicago, IL, USA), the normality test was used to discriminate between parametric and non-parametric data in the statistical analysis. In particular, two parametric groups were processed with the Student's *t*-test, whereas the Mann-Whitney test was used for non-parametric values. Multiple groups were analyzed with the One-way Anova if parametric or with the Kuskal-Wallis One-way Anova on ranks if data were non-parametric. Cumulative probabilities were compared with the Kolmogorov-Smirnov test. Groups of data were accepted as statistically different if $P \leq 0.05$.

Acknowledgements

This work was supported by an intramural SISSA grant. We thank Dr. Nicola Secomandi for help with calcium imaging experimental setting and videos. RR is the recipient of a research fellowship supported by the grant PRIN-MIUR No. 2012MYESZW.

Conflict of Interest: the authors declare no competing financial interests in the work described.

Supplementary information is available at "Cell death and disease" website.

Movie 1. TBOA application onto hypoglossal motoneurons.

Movie 2. Nicotine + TBOA application onto hypoglossal motoneurons.

Movie 3. Carbenoxolone + TBOA application onto hypoglossal motoneurons.

References

1. Orsini M, Oliveira AB, Nascimento OJM, Reis CHM, Leite MAA, de Souza JA, et al. Amyotrophic Lateral Sclerosis: New Perpectives and Update. *Neurol Int* 2015; **7**; doi 10.4081/ni.2015.5885

2. Kühnlein P, Gdynia H-J, Sperfeld A-D, Lindner-Pfleghar B, Ludolph AC, Prosiegel M, et al. Diagnosis and treatment of bulbar symptoms in amyotrophic lateral sclerosis. *Nat Clin Pract Neurol* 2008; **7**:366–374.

417 3. Ladewig T, Kloppenburg P, Lalley PM, Zipfel WR, Webb WW, Keller BU. Spatial
418 profiles of store-dependent calcium release in motoneurones of the nucleus
419 hypoglossus from newborn mouse. *J Physiol* 2003; **547**:775–787.

420 4. Laslo P, Lipski J, Nicholson LF, Miles GB, Funk GD. GluR2 AMPA receptor subunit
421 expression in motoneurons at low and high risk for degeneration in amyotrophic
422 lateral sclerosis. *Exp Neurol* 2001; **169**: 461–471.

423 5. Rothstein JD, Martin LJ, Kuncl RW. Decreased Glutamate Transport by the Brain
424 and Spinal Cord in Amyotrophic Lateral Sclerosis. *N Engl J Med* 1992; **326**: 1464–
425 1468.

426 6. Cleveland DW, Rothstein JD. From Charcot to Lou Gehrig: deciphering selective
427 motor neuron death in ALS. *Nat Rev Neurosci* 2001; **2**: 806–819.

428 7. Spreux-Varoquaux O, Bensimon G, Lacomblez L, Salachas F, Pradat PF, Le Forestier
429 N, et al. Glutamate levels in cerebrospinal fluid in amyotrophic lateral sclerosis: a
430 reappraisal using a new HPLC method with coulometric detection in a large cohort of
431 patients. *J Neurol Sci* 2002; **193**: 73–78.

432 8. Swash M, Ingram D. Preclinical and subclinical events in motor neuron disease. *J*
433 *Neurol Neurosurg Psychiatry* 1988; **51**: 165–168.

434 9. Kiernan MC, Vucic S, Cheah BC, Turner MR, Eisen A, Hardiman O, et al.
435 Amyotrophic lateral sclerosis. *Lancet* 2011; **377**: 942–955.

436 10. Cifra A, Nani F, Nistri A. Respiratory motoneurons and pathological conditions:
437 lessons from hypoglossal motoneurons challenged by excitotoxic or oxidative stress.
438 *Respir Physiol Neurobiol* 2011; **179**: 89–96.

439 11. Cifra A, Nani F, Nistri A. Riluzole is a potent drug to protect neonatal rat hypoglossal
440 motoneurons in vitro from excitotoxicity due to glutamate uptake block. *Eur J*
441 *Neurosci* 2011; **33**: 899–913.

442 12. Sharifullina E, Nistri A. Glutamate uptake block triggers deadly rhythmic bursting of
443 neonatal rat hypoglossal motoneurons. *J Physiol* 2006; **572**: 407–423.

444 13. Corsini S, Tortora M, Nistri A. Nicotinic receptor activation contrasts
445 pathophysiological bursting and neurodegeneration evoked by glutamate uptake block
446 on rat hypoglossal motoneurons. *J Physiol* 2016; doi: 10.1113/JP272591

447 14. Feldman JL, Del Negro CA. Looking for inspiration: new perspectives on respiratory
448 rhythm. *Nat Rev Neurosci* 2006; **7**: 232–242.

449 15. Feldman JL, Del Negro CA, Gray PA. Understanding the rhythm of breathing: so
450 near, yet so far. *Annu Rev Physiol* 2013; **75**: 423–452.

451 16. Moore KB, O'Brien J. Connexins in neurons and glia: targets for intervention in
452 disease and injury. *Neural Regen Res* 2015; **10**: 1013–1017.

453 17. Vinken M. Introduction: connexins, pannexins and their channels as gatekeepers of
454 organ physiology. *Cell Mol Life Sci* 2015; **72**: 2775–2778.

18. Esseltine JL, Laird DW. Next-Generation Connexin and Pannexin Cell Biology. *Trends Cell Biol* 2016; **26**: 944–955.

19. Haussig S, Schubert A, Mohr F-W, Dhein S. Sub-chronic nicotine exposure induces intercellular communication failure and differential down-regulation of connexins in cultured human endothelial cells. *Atherosclerosis* 2008; **196**: 210–218.

20. Tsai C-H, Yeh H-I, Tian T-Y, Lee Y-N, Lu C-S, Ko Y-S. Down-regulating effect of nicotine on connexin43 gap junctions in human umbilical vein endothelial cells is attenuated by statins. *Eur J Cell Biol* 2004; 82: 589–595.

21. Davidson JS, Baumgarten IM. Glycyrrhetinic acid derivatives: a novel class of inhibitors of gap-junctional intercellular communication. Structure-activity relationships. *J Pharmacol Exp Ther* 1988; **246**: 1104–1107.

22. Shabbir A, Bianchetti E, Cargonja R, Petrovic A, Mladinic M, Pilipović K, et al. Role of HSP70 in motoneuron survival after excitotoxic stress in a rat spinal cord injury model in vitro. *Eur J Neurosci* 2015; **42**: 3054–3065.

23. Bianchetti E, Mladinic M, Nistri A. Mechanisms underlying cell death in ischemia-like damage to the rat spinal cord in vitro. *Cell Death Dis* 2013; **4**: e707.

24. Sharifullina E, Ostroumov K, Nistri A. Metabotropic glutamate receptor activity induces a novel oscillatory pattern in neonatal rat hypoglossal motoneurones. *J Physiol* 2005; **563**: 139–159.

474 25. Belousov AB, Fontes JD. Neuronal gap junction coupling as the primary determinant
475 of the extent of glutamate-mediated excitotoxicity. *J Neural Transm* 1996; **121**: 837–
476 846.

477 26. Hilgen G, von Maltzahn J, Willecke K, Weiler R, Dedek K. Subcellular distribution
478 of connexin45 in OFF bipolar cells of the mouse retina. *J Comp Neurol* 2011; **519**:
479 433–450.

480 27. Marina N, Becker DL, Gilbey MP. Immunohistochemical detection of connexin36 in
481 sympathetic preganglionic and somatic motoneurons in the adult rat. *Auton Neurosci*
482 *Basic Clin* 2008; **139**: 15–23.

483 28. Ravagnan L, Gurbuxani S, Susin SA, Maisse C, Daugas E, Zamzami N, et al. Heat-
484 shock protein 70 antagonizes apoptosis-inducing factor. *Nat Cell Biol* 2001; **3**: 839–
485 843.

486 29. Decrock E, Vinken M, De Vuyst E, Krysko DV, D'Herde K, Vanhaecke T, et al.
487 Connexin-related signaling in cell death: to live or let die? *Cell Death Differ* 2009;
488 **16**: 524–536.

489 30. Peracchia C. Chemical gating of gap junction channels: Roles of calcium, pH and
490 calmodulin. *Biochim Biophys Acta BBA - Biomembr* 2004; **1662**: 61–80.

491 31. Lampe PD, Lau AF. The effects of connexin phosphorylation on gap junctional
492 communication. *Int J Biochem Cell Biol* 2004; **36**: 1171–1186.

493 32. Ramachandran S, Xie L-H, John SA, Subramaniam S, Lal R. A Novel Role for
494 Connexin Hemichannel in Oxidative Stress and Smoking-Induced Cell Injury. *PLOS*
495 *ONE* 2007; **2**: e712.

496 33. Ye Z-C, Wyeth MS, Baltan-Tekkok S, Ransom BR. Functional hemichannels in
497 astrocytes: a novel mechanism of glutamate release. *J Neurosci* 2003; **23**: 3588–3596.

498 34. Decrock E, De Vuyst E, Vinken M, Van Moorhem M, Vranckx K, Wang N, et al.
499 Connexin 43 hemichannels contribute to the propagation of apoptotic cell death in a
500 rat C6 glioma cell model. *Cell Death Differ* 2008; **16**: 151–163.

501 35. Kalvelyte A, Imbrasaite A, Bukauskiene A, Verselis VK, Bukauskas FF. Connexins
502 and apoptotic transformation. *Biochem Pharmacol* 2003; **66**: 1661–1672.

503 36. Denuc A, Núñez E, Calvo E, Loureiro M, Miro-Casas E, Guarás A, et al. New
504 protein–protein interactions of mitochondrial connexin 43 in mouse heart. *J Cell Mol*
505 *Med* 2016; **20**: 794–803.

506 37. Vaccari JC de R, Corriveau RA, Belousov AB. Gap Junctions Are Required for
507 NMDA Receptor–Dependent Cell Death in Developing Neurons. *J Neurophysiol*
508 2007; **98**: 2878–2886.

509 38. Quitadamo C, Fabbretti E, Lamanauskas N, Nistri A. Activation and desensitization
510 of neuronal nicotinic receptors modulate glutamatergic transmission on neonatal rat
511 hypoglossal motoneurons. *Eur J Neurosci* 2005; **22**: 2723–2734.

512 39. Penuela S, Bhalla R, Gong X-Q, Cowan KN, Celetti SJ, Cowan BJ, et al. Pannexin 1
513 and pannexin 3 are glycoproteins that exhibit many distinct characteristics from the
514 connexin family of gap junction proteins. *J Cell Sci* 2007; **120**: 3772–3783.

515 40. Canoz O, Gunes T, Deniz K, Akgun H, Balkanli S. Perinatal expression of HSP70
516 and VEGF in neonatal rat lung vessels exposed to nicotine during gestation. *APMIS*
517 2006; **114**: 10–14.

518 41. Hahn GM, Shiu EC, Auger EA. Mammalian stress proteins HSP70 and HSP28
519 coinduced by nicotine and either ethanol or heat. *Mol Cell Biol* 1991; **11**: 6034–6040.

520 42. Shimamoto K, Lebrun B, Yasuda-Kamatani Y, Sakaitani M, Shigeri Y, Yumoto N, et
521 al. dl-threo-β-Benzyloxyaspartate, A Potent Blocker of Excitatory Amino Acid
522 Transporters. *Mol Pharmacol* 1998; **53**: 195–201.

523 43. Gleichmann M, Collis LP, Smith PJS, Mattson MP. Simultaneous Single Neuron
524 Recording of O_2 Consumption, $[Ca^{2+}]_i$ and Mitochondrial Membrane Potential in
525 Glutamate Toxicity. *J Neurochem* 2009; **109**: 644–655.

526 44. Rueda CB, Llorente-Folch I, Traba J, Amigo I, Gonzalez-Sanchez P, Contreras L, et
527 al. Glutamate excitotoxicity and Ca^{2+}-regulation of respiration: Role of the Ca^{2+}
528 activated mitochondrial transporters (CaMCs). *Biochim Biophys Acta BBA - Bioenerg*
529 2016; **1857**: 1158–1166.

530 45. Connolly NMC, Prehn JHM. The metabolic response to excitotoxicity – lessons from
531 single-cell imaging. *J Bioenerg Biomembr* 2014; **47**: 75–88.

532 46. Kritis AA, Stamoula EG, Paniskaki KA, Vavilis TD. Researching glutamate –
533 induced cytotoxicity in different cell lines: a comparative/collective analysis/study.
534 *Front Cell Neurosci* 2015; **9**: 91.

535 47. Calvo M, Sanz-Blasco S, Caballero E, Villalobos C, Núñez L. Susceptibility to
536 excitotoxicity in aged hippocampal cultures and neuroprotection by non-steroidal
537 anti-inflammatory drugs: role of mitochondrial calcium. *J Neurochem* 2015; **132**:
538 403–417.

539 48. Nguyen D, Alavi MV, Kim K-Y, Kang T, Scott RT, Noh YH, et al. A new vicious
540 cycle involving glutamate excitotoxicity, oxidative stress and mitochondrial
541 dynamics. *Cell Death Dis* 2011; **2**: e240.

542 49. Yan M, Zhu W, Zheng X, Li Y, Tang L, Lu B, et al. Effect of glutamate on lysosomal
543 membrane permeabilization in primary cultured cortical neurons. *Mol Med Rep* 2016;
544 **13**: 2499-2505.

545 50. Belousov AB. Novel model for the mechanisms of glutamate-dependent
546 excitotoxicity: Role of neuronal gap junctions. *Brain Res* 2012; **1487**: 123–130.

547 51. Koide M, Nishizawa S, Yamamoto S, Yamaguchi M, Namba H, Terakawa S.
548 Nicotine Exposure, Mimicked Smoking, Directly and Indirectly Enhanced Protein
549 Kinase C Activity in Isolated Canine Basilar Artery, Resulting in Enhancement of
550 Arterial Contraction. *J Cereb Blood Flow Metab* 2005; **25**: 292–301.

551 52. Tuominen RK, McMillian MK, Ye H, Stachowiak MK, Hudson PM, Hong JS.
552 Long-Term Activation of Protein Kinase C by Nicotine in Bovine Adrenal
553 Chromaffin Cells. *J Neurochem* 1992; **58**: 1652–1658.

554 53. Messing RO, Stevens AM, Kiyasu E, Sneade AB. Nicotinic and muscarinic agonists
555 stimulate rapid protein kinase C translocation in PC12 cells. *J Neurosci* 1989; **9**: 507–
556 512.

557 54. Pogoda K, Kameritsch P, Retamal MA, Vega JL. Regulation of gap junction channels
558 and hemichannels by phosphorylation and redox changes: a revision. *BMC Cell Biol*
559 2016; **17** Suppl 1: 11.

560 55. Nani F, Cifra A, Nistri A. Transient oxidative stress evokes early changes in the
561 functional properties of neonatal rat hypoglossal motoneurons in vitro. *Eur J*
562 *Neurosci* 2010; **31**: 951–966.

563 56. Fabbro A, Skorinkin A, Grandolfo M, Nistri A, Giniatullin R. Quantal release of ATP
564 from clusters of PC12 cells. *J Physiol* 2004; **560**: 505–517.

565 57. Schindelin J, Arganda-Carreras I, Frise E, Kaynig V, Longair M, Pietzsch T, et al.
566 Fiji: an open-source platform for biological-image analysis. *Nat Methods* 2012; **9**:
567 676–682.

568 58. Rauti R, Lozano N, León V, Scaini D, Musto M, Rago I, et al. Graphene Oxide
569 Nanosheets Reshape Synaptic Function in Cultured Brain Networks. *ACS Nano* 2016;
570 **10**:4459–4471.

571 59. Bosi S, Rauti R, Laishram J, Turco A, Lonardoni D, Nieus T, et al. From 2D to 3D:
572 novel nanostructured scaffolds to investigate signalling in reconstructed neuronal
573 networks. *Sci Rep* 2015; **5**:9562.

574 60. Beckel JM, Daugherty SL, Tyagi P, Wolf-Johnston AS, Birder LA, Mitchell CH, et
575 al. Pannexin 1 channels mediate the release of ATP into the lumen of the rat urinary
576 bladder. *J Physiol* 2015; **593**: 1857–1871.

577 61. Kanungo AK, Hao Z, Elia AJ, Mak TW, Henderson JT. Inhibition of Apoptosome
578 Activation Protects Injured Motor Neurons from Cell Death. *J Biol Chem* 2008; **283**:
579 22105–22112.

580 62. Mladinic M, Bianchetti E, Dekanic A, Mazzone GL, Nistri A. ATF3 is a novel
581 nuclear marker for migrating ependymal stem cells in the rat spinal cord. *Stem Cell*
582 *Res* 2014; **12**: 815–827.

583 63. Solan JL, Lampe PD. Connexin phosphorylation as a regulatory event linked to gap
584 junction channel assembly. *Biochim Biophys Acta - Biomembr* 2005; **1711**: 154–163.

585 64. Haefliger J-A, Martin D, Favre D, Petremand Y, Mazzolai L, Abderrahmani A, et al.
586 Reduction of connexin36 content by ICER-1 contributes to insulin-secreting cells
587 apoptosis induced by oxidized LDL particles. *PloS One* 2013; **8**: e55198.

588 65. Wang Z, Si L-Y. Hypoxia-inducible factor-1α and vascular endothelial growth factor
589 in the cardioprotective effects of intermittent hypoxia in rats. *Ups J Med Sci* 2013;
590 **118**: 65–74.

66. Yao L, Chen X, Tian Y, Lu H, Zhang P, Shi Q, et al. Selection of housekeeping genes for normalization of RT-PCR in hypoxic neural stem cells of rat in vitro. *Mol Biol Rep* 2011; **39**: 569–576.

596 **Figure legends:**

597 **Figure 1. $[Ca^{2+}]_i$ transients evoked by TBOA.** (A) Example of records of $[Ca^{2+}]_i$ changes
598 simultaneously taken from 5 HMs in the same slice preparation in presence of TBOA (50
599 μM; top), nicotine (10 μM) + TBOA (middle), or carbenoxolone (200 μM) + TBOA
600 (bottom). (B) Example of slice preparation containing HMs. Each ROI indicates a different
601 cell used for analysis. Bar = 50 μm. (C) Box plot of the number of transients evoked during
602 the different treatment listed above; nicotine or carbenoxolone coapplication with TBOA
603 significantly reduces the number of the events (Mann-Whitney test: ** P = 0.006 for
604 TBOA vs. nicotine + TBOA, and ** P = 0.002 for TBOA vs. carbenoxolone + TBOA; n:
605 69, TBOA; 40, nicotine + TBOA; 18, carbenoxolone + TBOA; N = 5). (D) When TBOA is
606 applied alone, the cumulative probability line (solid line) is significantly shifted to the right
607 compared with nicotine + TBOA (dotted line) or carbenoxolone + TBOA (dashed line;
608 Kolmogorov-Smirnov statistic test: $P \leq 0.001$ for TBOA vs. nicotine + TBOA, and $P \leq$
609 0.001 for TBOA vs. carbenoxolone + TBOA).

610

611 **Figure 2. Topographic distribution of Ca^{2+} transients according to inter-cell distance.**
612 (A) Example of latency analysis taken as interval between Ca^{2+} transient onset in two
613 nearby HMs. (B-D) Inter-cell latency scatter plots in presence of TBOA (50 μM; B), or
614 nicotine (10 μM) + TBOA (C), or carbenoxolone (200 μM) + TBOA (D). Each data point
615 represents coupling latency in a pair of cells.

616

Figure 3. Nicotine and carbenoxolone induce significant reduction in Cx36 expression. (A) Example of HMs after 4h incubation in Krebs (sham), TBOA, nicotine + TBOA, nicotine, or carbenoxolone + TBOA. HMs were labeled with SMI 32 (green pseudocolor; left column), as motoneuronal marker, or Cx36 (red pseudocolor; middle column). The right column shows merged images where DAPI (blue pseudocolor) is used to visualize nuclei. (B) Histograms quantify the Cx36 signal decrease after 4h of nicotine + TBOA (Student's *t*-test: *** $P \leq 0.001$ for sham vs. nicotine + TBOA, * $P = 0.038$ for TBOA vs. nicotine + TBOA, and ** $P = 0.005$ for nicotine + TBOA vs. nicotine) or carbenoxolone + TBOA treatments (Student's *t*-test: *** $P \leq 0.001$ for sham vs. carbenoxolone + TBOA, and * $P = 0.012$ for nicotine vs. carbenoxolone + TBOA). Cx36 mean signal (AU): 58 ± 4.9, sham (n = 10, N = 3); 48 ± 7.2, TBOA (n = 15, N = 4); 30 ± 3.4, nicotine + TBOA (n = 14, N = 3); 58 ± 10, nicotine (n = 8, N = 3); 32 ± 2.8, carbenoxolone + TBOA (n = 11, N = 4). (C) Plot indicates significant HM loss after TBOA treatment, an effect fully prevented by nicotine or carbenoxolone co-application (HMs: 40 ± 3, sham; 28 ± 1, TBOA; 48 ± 3, nicotine + TBOA; 40 ± 2, nicotine; 41 ± 2, carbenoxolone + TBOA; Student's *t*-test: # $P = 0.014$ for sham vs. TBOA, $P \leq 0.001$ for TBOA vs. nicotine + TBOA, $P = 0.002$ for TBOA vs. nicotine and $P \leq 0.001$ for TBOA vs. carbenoxolone + TBOA).

Figure 4. Brainstem Cx36 expression decreases due to nicotine or carbenoxolone application. (A) example of Western immunoblotting (top) showing the expression of Cx36 in brainstems incubated for 4h in Krebs, or treated with TBOA, nicotine + TBOA,

639 nicotine, or carbenoxolone + TBOA. Histograms (bottom) quantifying the significantly
640 decreased Cx36 levels after treatment with nicotine + TBOA (Mann-Whitney test: * P =
641 0.038 for sham vs. nicotine + TBOA; n, N = 9) or carbenoxolone + TBOA (Mann-Whitney
642 test: *** $P \leq 0.001$ for sham vs. carbenoxolone + TBOA; n, N = 5). (B, C) example of
643 Western blot (top) showing Cx36 expression in membrane (B) or the cytoplasmic (C)
644 fractions of samples treated as described above. Histograms illustrate how nicotine alone
645 or co-applied induces a significant decrease of Cx36 expression in the membrane pool (B,
646 bottom; Mann-Whitney test: * P = 0.016 for sham vs. nicotine + TBOA and **P = 0.016
647 for sham vs. nicotine; n, N = 5) and an increase in the cytoplasmic one (C, bottom; Mann-
648 Whitney test: ** P = 0.008 for sham vs. nicotine + TBOA and **P = 0.008 for sham vs.
649 nicotine; n, N = 5).

650

651 **Figure 5. Cx36 mRNA levels and Hsp70 expression.** (A) Plot illustrating unchanged
652 values of Cx36 mRNA levels among different treatments. Fractional Cx36 expression
653 (AU): 1 ± 0.0, sham; 0.9 ± 0.2, TBOA; 1 ± 0.3, nicotine + TBOA; 1.3 ± 0.2, nicotine (n, N
654 = 6). (B) Example of Hsp70 immunoblotting. (C) Histogram quantifying the significant
655 increase of Hsp70 expression after nicotine + TBOA treatment (Mann-Whitney test: ** P =
656 0.008 for sham vs. nicotine + TBOA; Student's *t*-test: *P = 0.053 for nicotine vs.nicotine +
657 TBOA; n, N = 5).

658

Figure 6. Expression of AIF in HMs. (A) Confocal images of SMI 32 (left; green), AIF (middle; red), and DAPI (blue; merged image, right) of motoneurons in control condition or after TBOA (50 μM), nicotine (10 μM) + TBOA, or nicotine alone. (B) Line scan analysis for the cells indicated by the bars in (A). Nuclear area is delimited by the strong DAPI distribution. Note different ordinate calibrations. The large rise in AIF with TBOA is prevented by nicotine. (C) Histograms show average AIF intensity signal in cell soma. There is no difference between sham (n = 9, N = 4) and nicotine (n = 6, N = 3) data (Mann-Whitney test: P = 0.14). TBOA treatment (n = 19, N = 7) induces a large increase in AIF expression ($, Mann-Whitney test: $P \leq 0.001$ for sham vs. TBOA, P = 0.014 for TBOA vs. nicotine + TBOA, and $P \leq 0.001$ for TBOA vs. nicotine). Nicotine + TBOA (n = 16, N = 5) elicits a comparatively smaller increase in AIF (#, Mann-Whitney test: P = 0.016 for sham vs. nicotine + TBOA).

Figure 7. Panx1 expression remains unchanged. (A) Example of HMs after 4h incubation in Krebs (sham), TBOA, nicotine + TBOA, or nicotine, labeled with the neuronal marker SMI 32 (left column; green), or Panx1 (middle column; red). Merged images are shown on the right column where DAPI (blue) is used as nuclear marker. (B) Histograms quantifying unchanged levels of Panx1 among the treatments described above. (C) Example of Western immunoblotting (top) showing the unchanged expression of Panx1 in brainstems incubated as described above.

Figure 8. Idealized diagram to account for the toxic effects by TBOA and their antagonism by nicotine on HMs. (A) In the presence of TBOA, glutamate (filled red circled) released from presynaptic terminals acts on AMPA, kainate, and NMDA receptors to depolarize HMs and open voltage dependent Ca^{2+} channels (VDCC). TBOA-mediated Inhibition of glutamate uptake by astrocytes leads to intensification of glutamate effects with build-up of intracellular free Ca^{2+} which acts on mitochondria and favors production of ROS, release of AIF and DNA damage. This process is greatly amplified by the bidirectional (red arrows) operation of gap junctions (Cx36; filled blue cylinders) that spread and recruit HMs into a hyperexcitable state with deleterious consequences on cell survival. (B) In the presence of nicotine the neurotoxic effect of TBOA is largely attenuated. Nicotine exerts multiple effects via nAChRs located on presynaptical terminals (with consequent decrease in glutamate release), HM membrane and even mitochondria. Through these effects nicotine strongly decreases the motoneuron coupling via gap junctions through redistribution of Cx36 subunits, therefore disjoining motoneurons from their collective excitatory behavior. Our hypothesis is that this process is accompanied by activation of PKC that inhibits Cx36 activity, reduction in production of ROS, and facilitation of the effect of Hsp70 to sequester AIF and prevent its nuclear migration. For references see text.

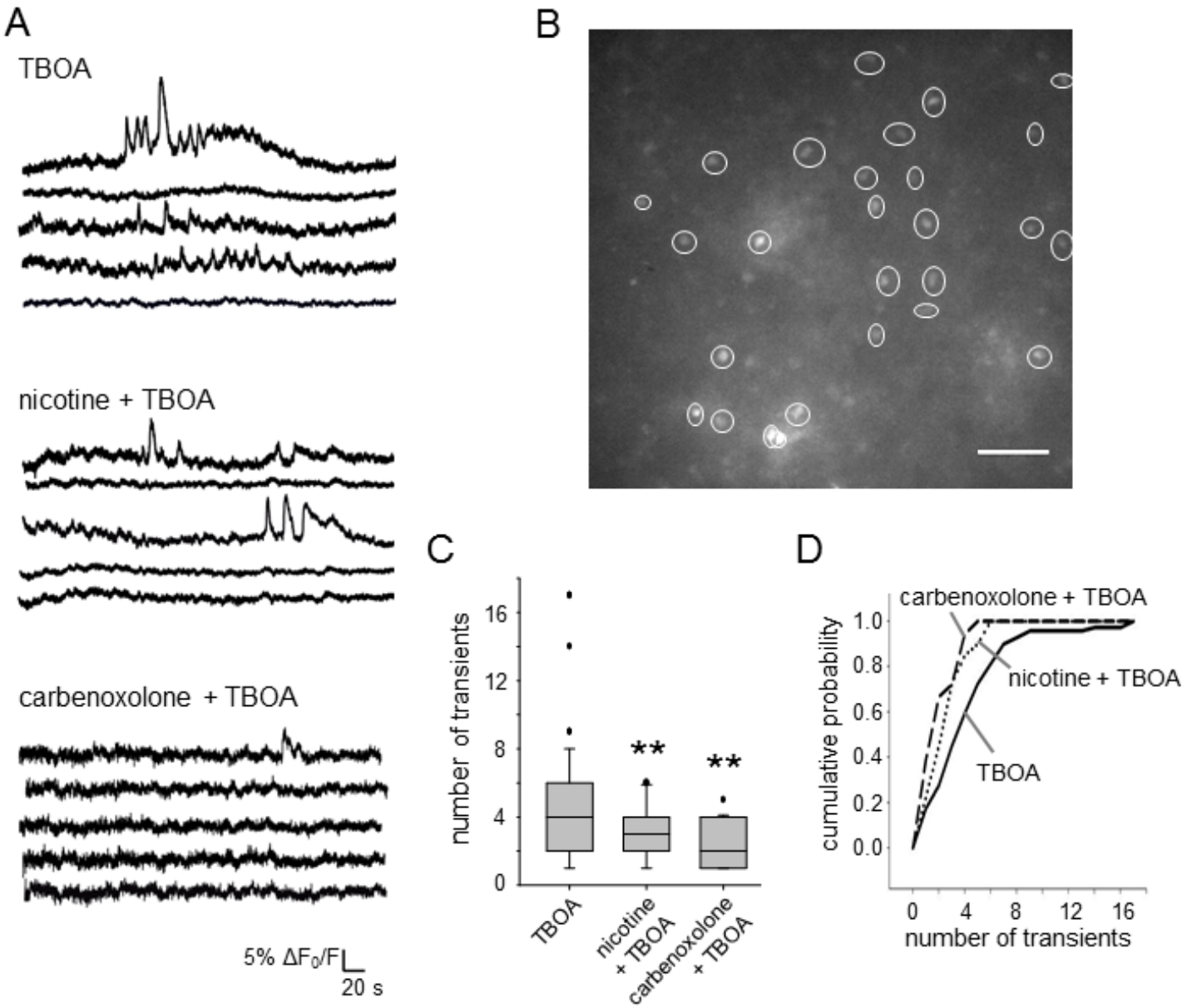
A
TBOA
nicotine + TBOA
carbenoxolone + TBOA
5% ΔF0/F
20 s
B
C
number of transients
16
12
8
4
0
**
**
TBOA
nicotine + TBOA
carbenoxolone + TBOA
D
carbenoxolone + TBOA
nicotine + TBOA
TBOA
cumulative probability
1.0
0.8
0.6
0.4
0.2
0.0
0
4
8
12
16
number of transients

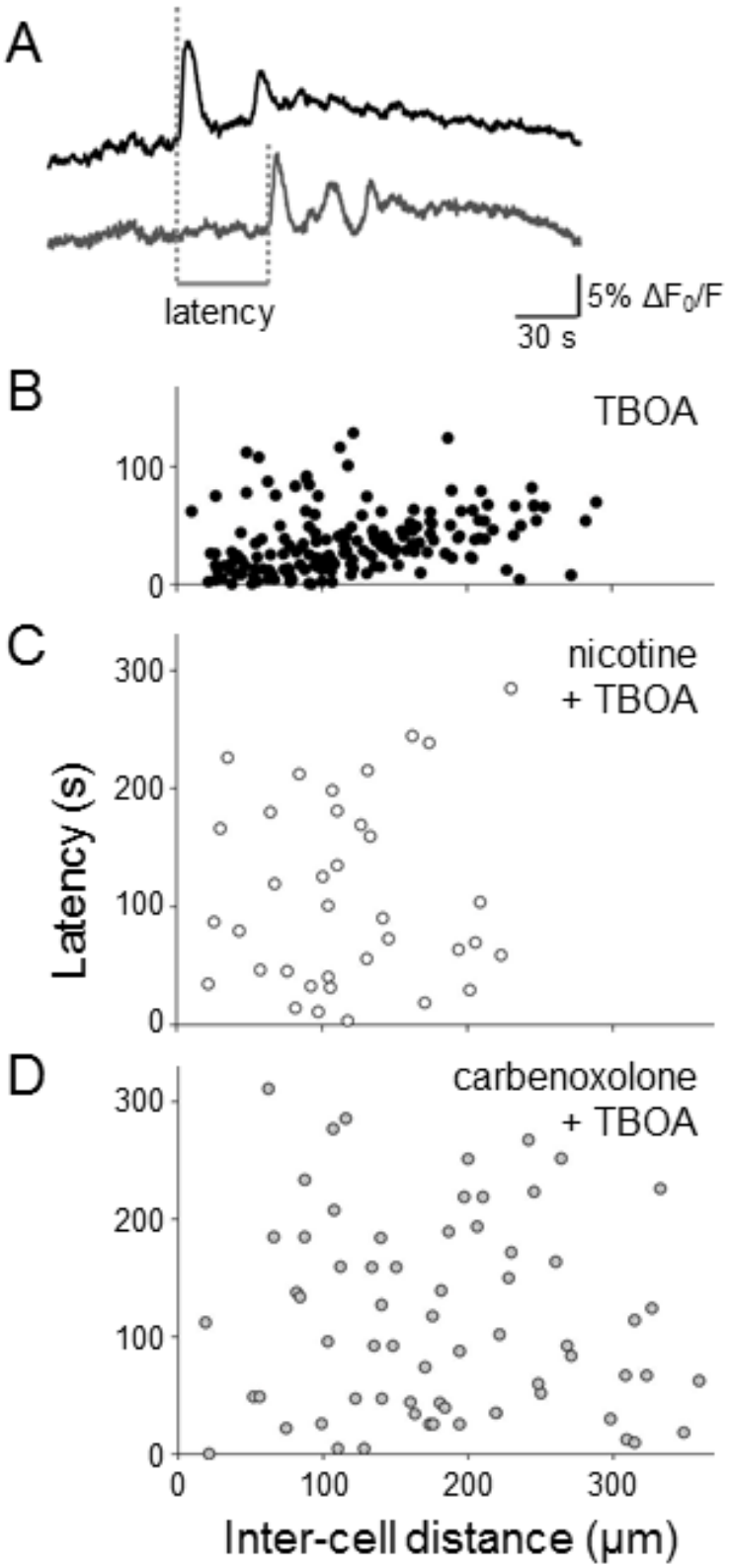
A
latency
5% ΔF0/F
30 s
B
TBOA
100
0
C
nicotine
+ TBOA
300
200
100
0
Latency (s)
D
carbenoxolone
+ TBOA
300
200
100
0
0
100
200
300
Inter-cell distance (μm)

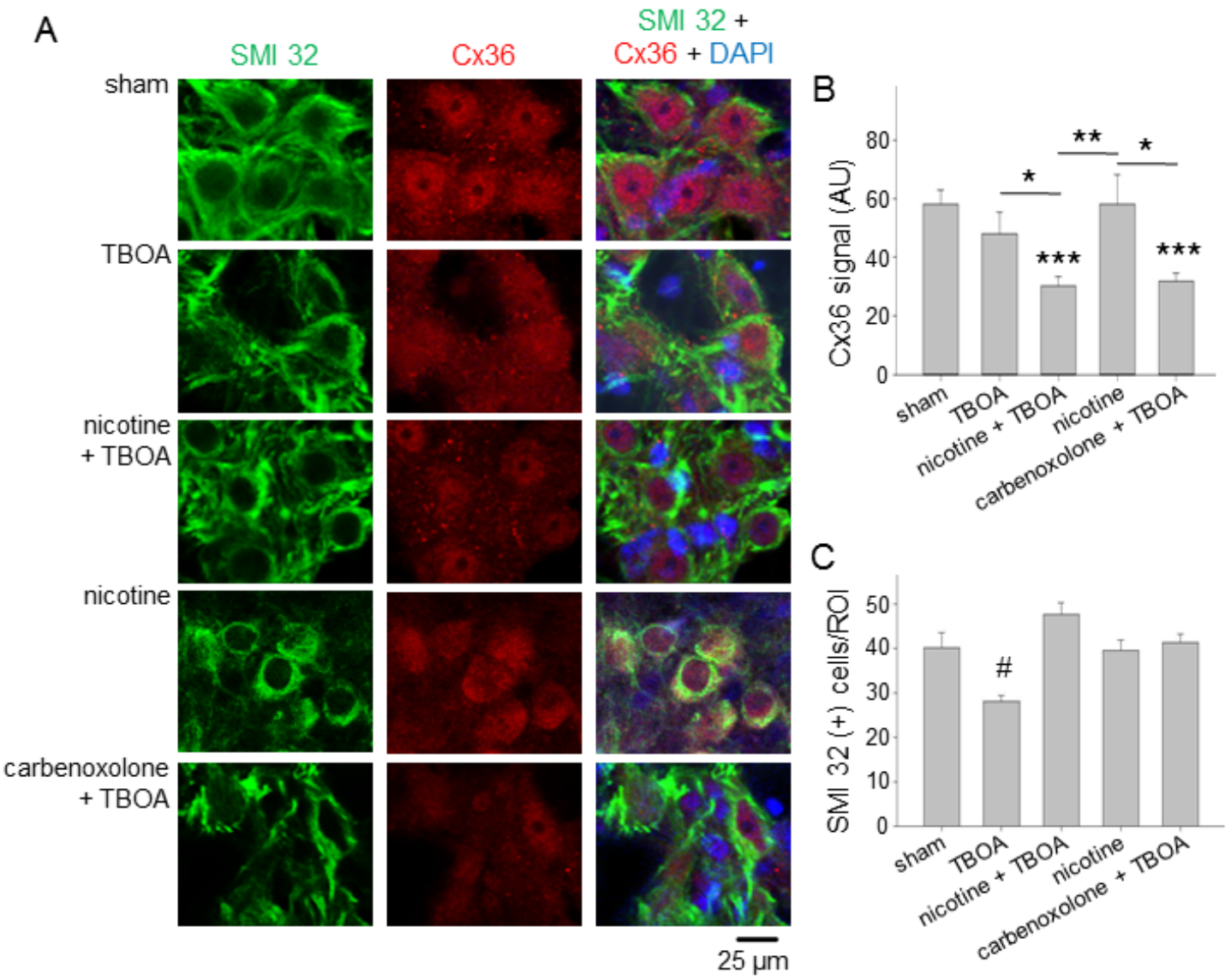
A
SMI 32
Cx36
SMI 32 +
Cx36 + DAPI
sham
TBOA
nicotine
+ TBOA
nicotine
carbenoxolone
+ TBOA
25 µm
B
Cx36 signal (AU)
0
20
40
60
80
*
**
*
***
***
sham
TBOA
nicotine + TBOA
nicotine
carbenoxolone + TBOA
C
SMI 32 (+) cells/ROI
0
10
20
30
40
50
#
sham
TBOA
nicotine + TBOA
nicotine
carbenoxolone + TBOA

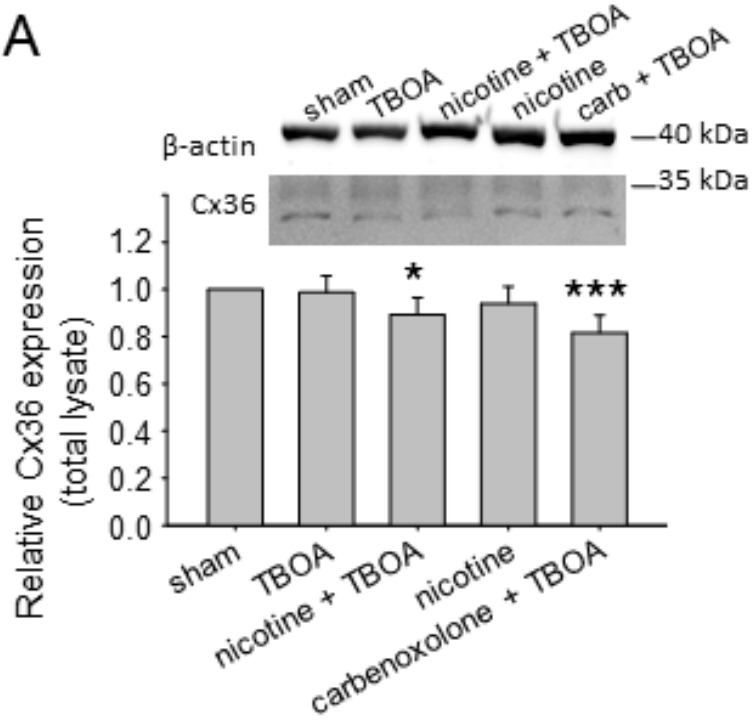
A
sham
TBOA
nicotine + TBOA
nicotine
carb + TBOA
β-actin
—40 kDa
—35 kDa
Cx36
Relative Cx36 expression
(total lysate)
1.2
1.0
0.8
0.6
0.4
0.2
0.0
*
***
sham
TBOA
nicotine + TBOA
nicotine
carbenoxolone + TBOA

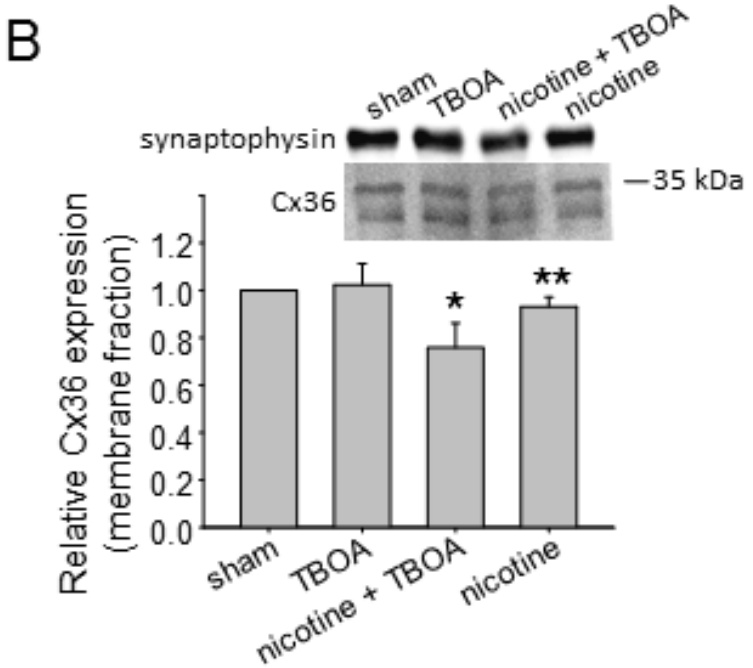
B
sham
TBOA
nicotine + TBOA
nicotine
synaptophysin
—35 kDa
Cx36
Relative Cx36 expression
(membrane fraction)
1.2
1.0
0.8
0.6
0.4
0.2
0.0
*
**
sham
TBOA
nicotine + TBOA
nicotine

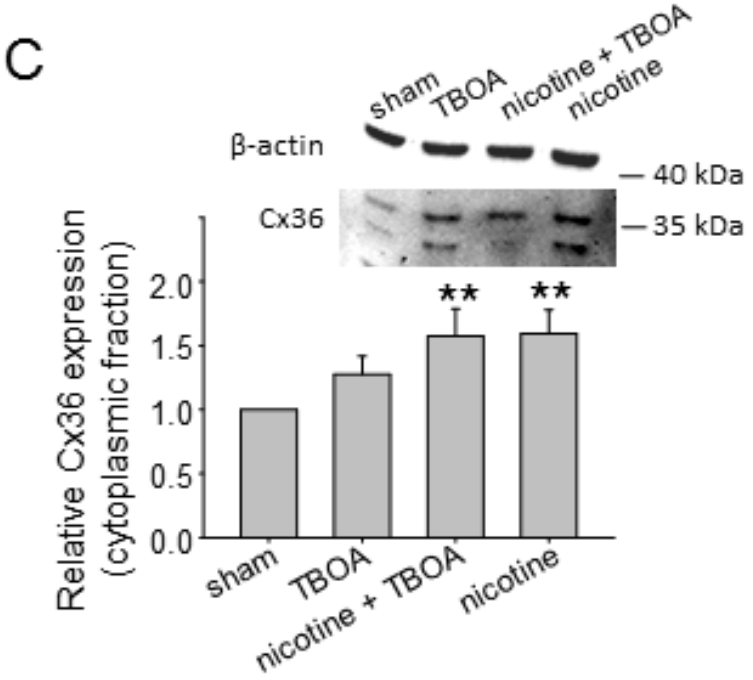
C
sham
TBOA
nicotine + TBOA
nicotine
β-actin
— 40 kDa
Cx36
— 35 kDa
Relative Cx36 expression
(cytoplasmic fraction)
2.0
1.5
1.0
0.5
0.0
**
**
sham
TBOA
nicotine + TBOA
nicotine

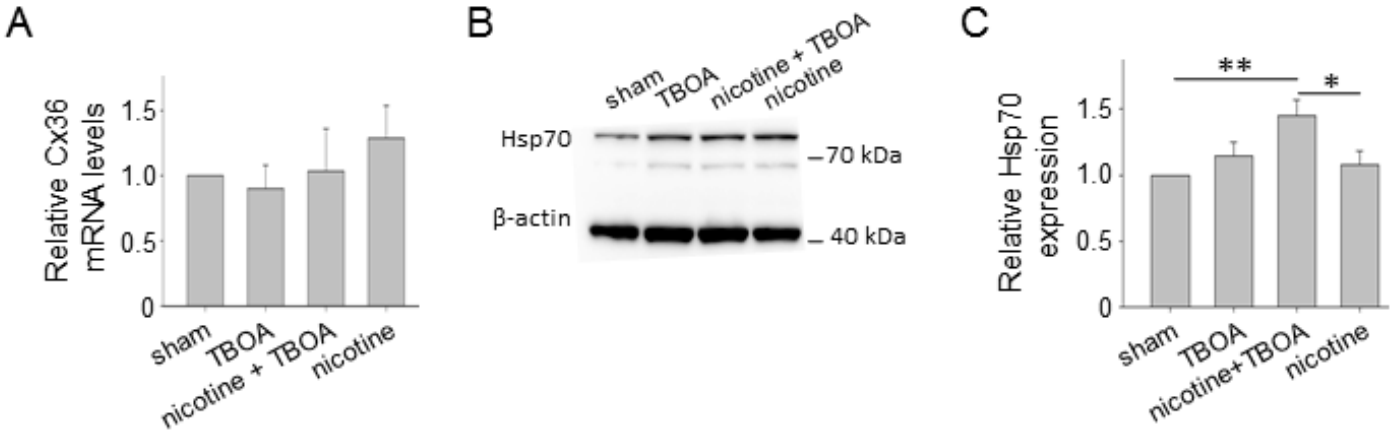
A
Relative Cx36 mRNA levels
1.5
1.0
0.5
0
sham
TBOA
nicotine + TBOA
nicotine
B
sham
TBOA
nicotine + TBOA
nicotine
Hsp70
β-actin
70 kDa
40 kDa
C
Relative Hsp70 expression
**
*
1.5
1.0
0.5
0
sham
TBOA
nicotine+TBOA
nicotine

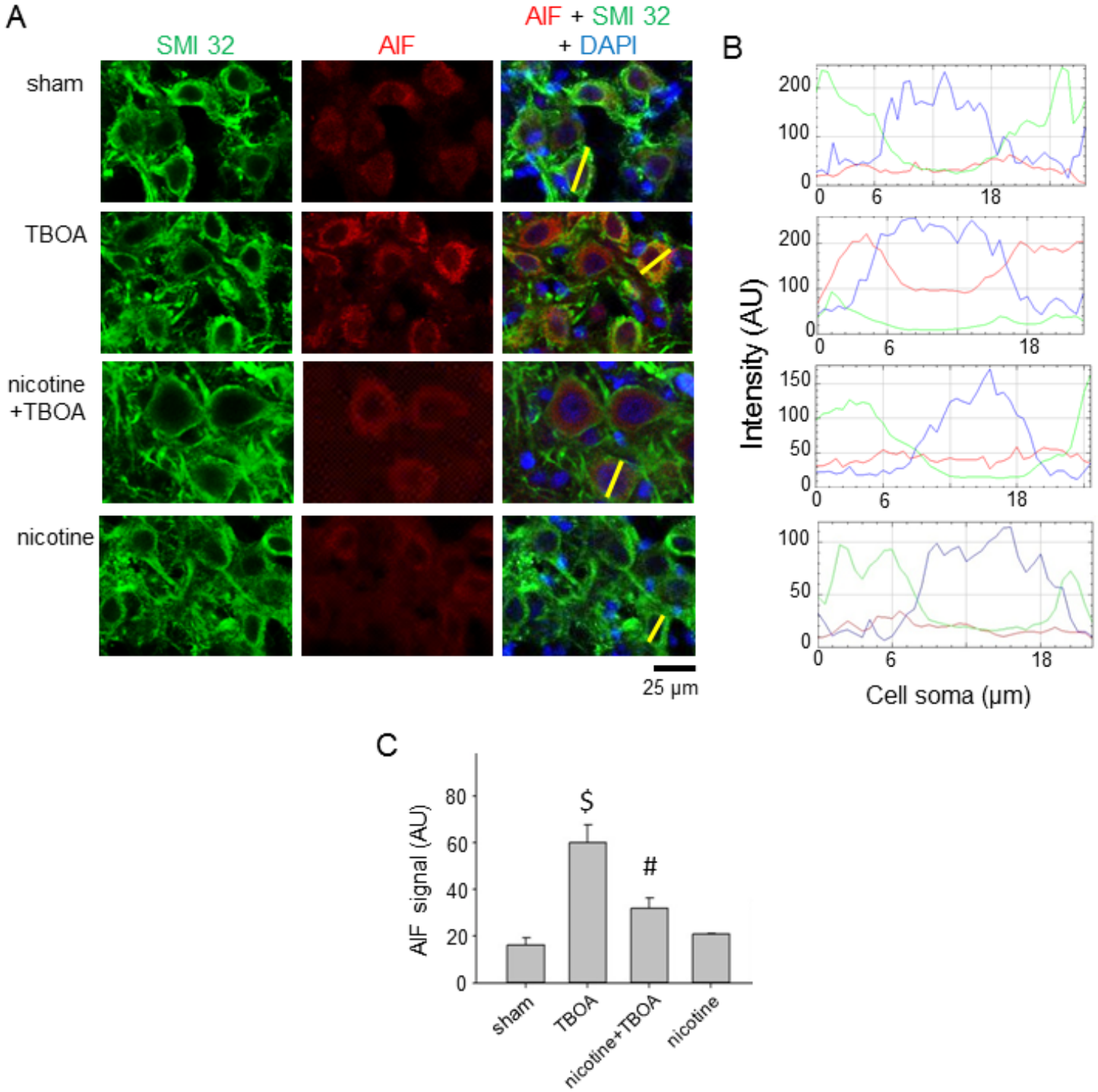
A
SMI 32
AIF
AIF + SMI 32
+ DAPI
sham
TBOA
nicotine
+TBOA
nicotine
25 µm
B
Intensity (AU)
Cell soma (µm)
C
AIF signal (AU)
$
#
sham
TBOA
nicotine+TBOA
nicotine

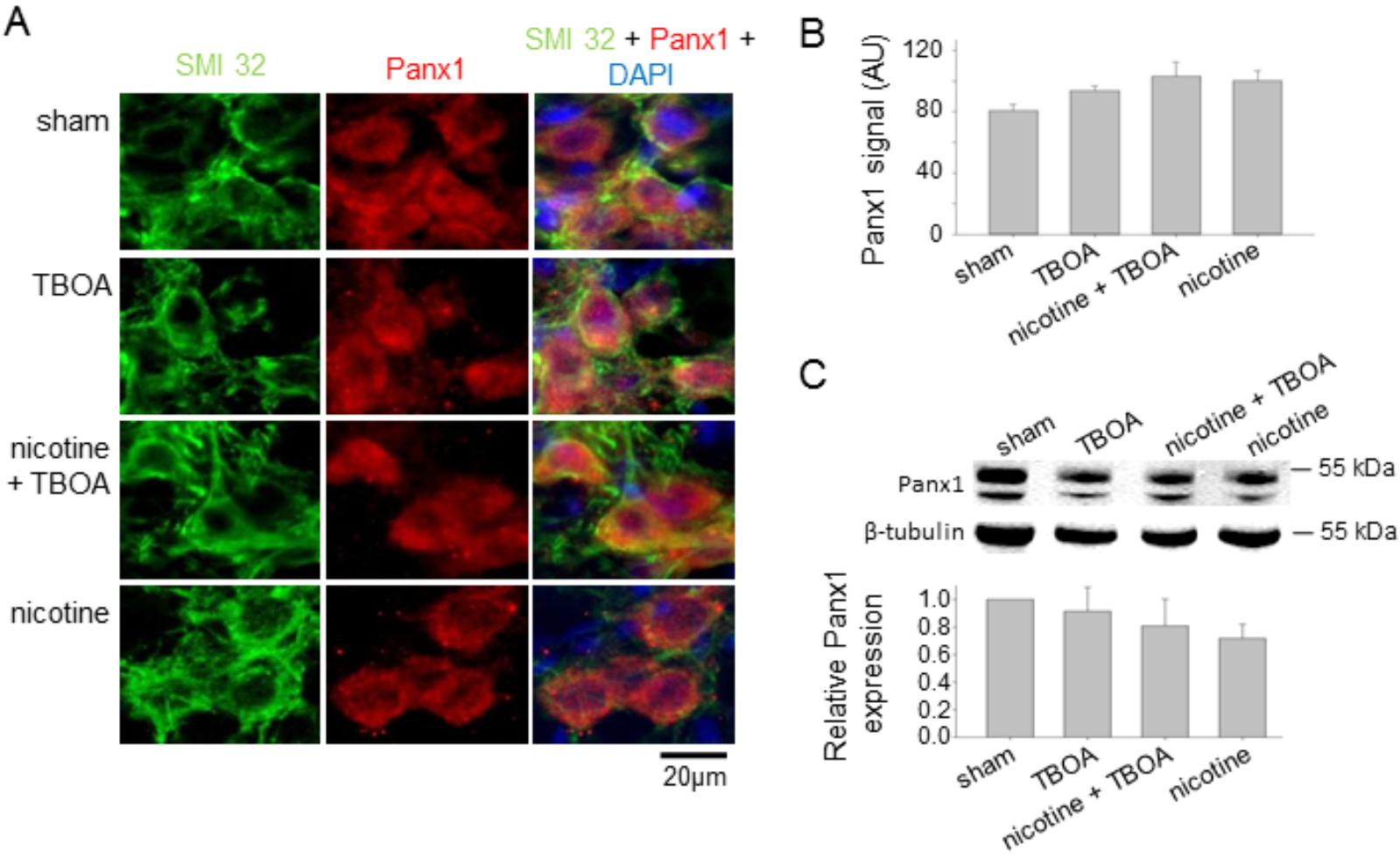
A
SMI 32
Panx1
SMI 32 + Panx1 + DAPI
sham
TBOA
nicotine + TBOA
nicotine
20μm
B
Panx1 signal (AU)
120
80
40
0
sham
TBOA
nicotine + TBOA
nicotine
C
sham
TBOA
nicotine + TBOA
nicotine
Panx1
55 kDa
β-tubulin
55 kDa
Relative Panx1 expression
1.0
0.8
0.6
0.4
0.2
0.0
sham
TBOA
nicotine + TBOA
nicotine

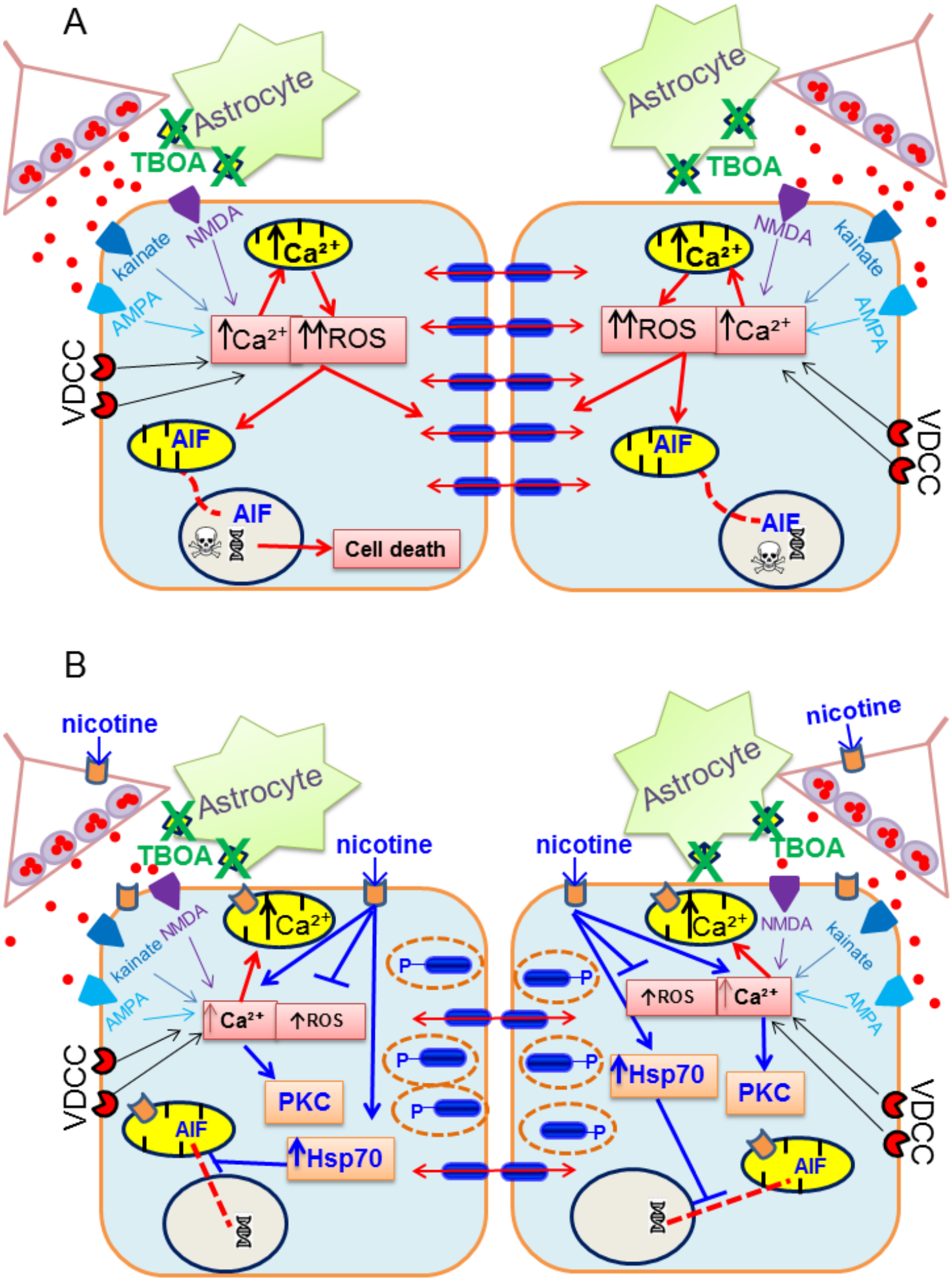
A
Astrocyte
TBOA
kainate
NMDA
AMPA
VDCC
Ca2+
ROS
AIF
Cell death
B
nicotine
PKC
Hsp70
P

Table 1. List of primers used for Real time-PCR

Gene	Primer sequence (5’ – 3’)	Reference
Cx36	Fw:ATACAGGTGTGAATGAGGGAGGATG Rv:TGGAGGGTGTTACAGATGAAAGAGG	(64)
Actb	Fw:GTGGGGCGCCCCGGCACCA Rv:CTCCTTAATGTCACGCACGATTT	(65)
Hprt	Fw:TCCTCATGGACTGATTATGGACA Rv:TAATCCAGCAGGTCAGCAAAGA	(66)
Rpl13A	Fw:TCCTCATGGACTGATTATGGACA Rv:TAATCCAGCAGGTCAGCAAAGA	(66)

Discussions

The pathways illustrated in Fig. 10 are common cell death mechanisms involved in a range of neurological disorders, although in case of ALS they have been derived from studies undertaken mainly using the mutant mouse model SOD1 (Turner et al., 2013).

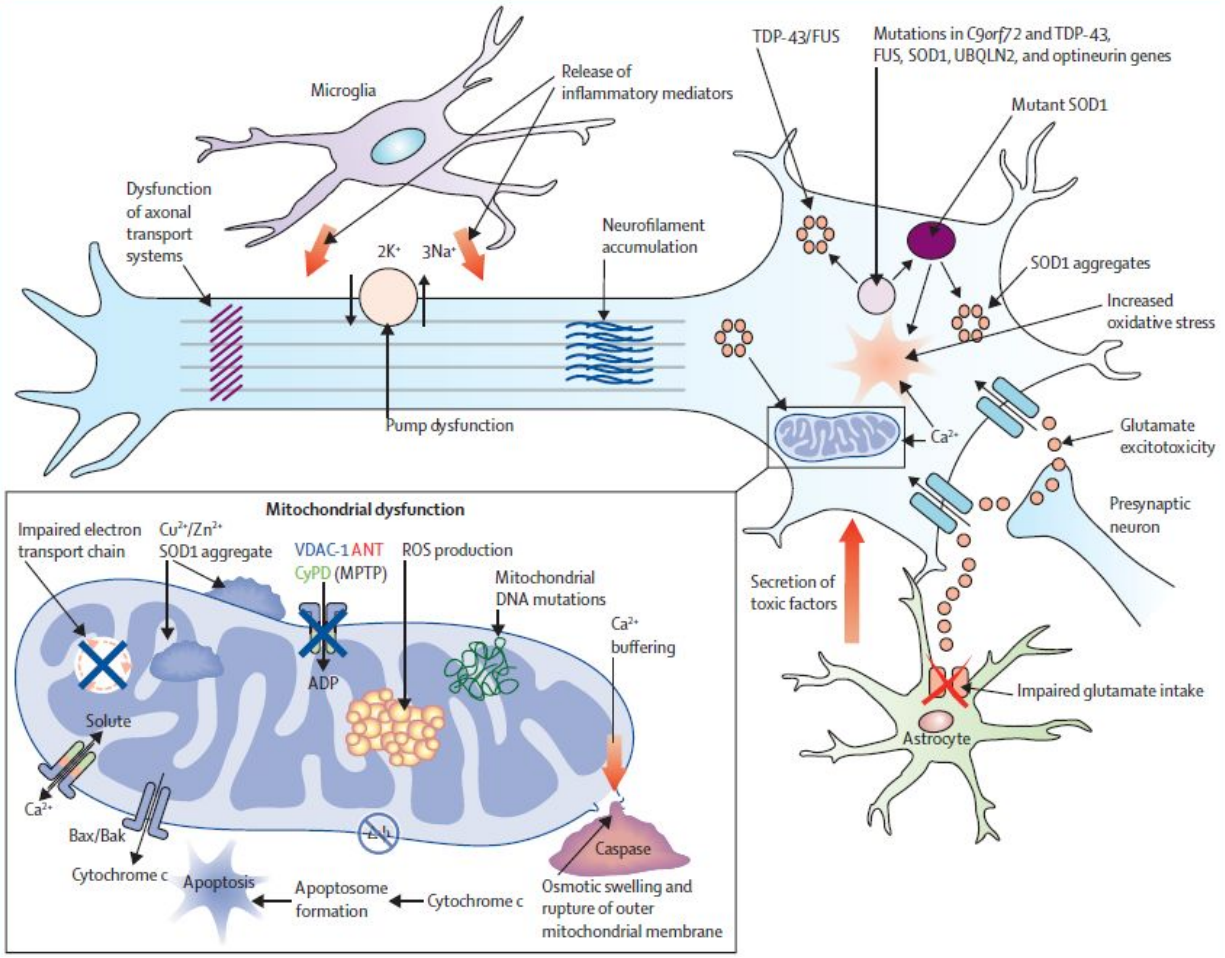

Figure 10: Proposed mechanisms underlying neurodegeneration in ALS. (from Turner et al., 2013)

Neurodegeneration in ALS might reflect combination of glutamate-mediated excitotoxicity, free radical generation, mitochondrial dysfunction and disruption of axonal transport processes via the accumulation of neurofilament intracellular aggregates. Intracellular aggregates, which are harmful to neurons, are associated with mutations in several ALS-related genes. Mithochondrial dysfunction, associated with increased production of ROS, facilitates susceptibility to glutamate excitotoxicity, perturbations in motoneuronal energy production, and apoptosis. Moreover, the activation of microglia results in secretion of proinflammatory cytokines resulting in further toxicity (Calvo et al., 2014; Orsini et al., 2015; Turner et al., 2013; Vucic and Kiernan, 2010; Wijesekera and Leigh, 2009; Zarei et al., 2015). In this framework, the present study is consistent with this scenario and suggested nAChRs as candidate for the prevention of HM degeneration. Principal results are depicted in fig. 12 and listed below.

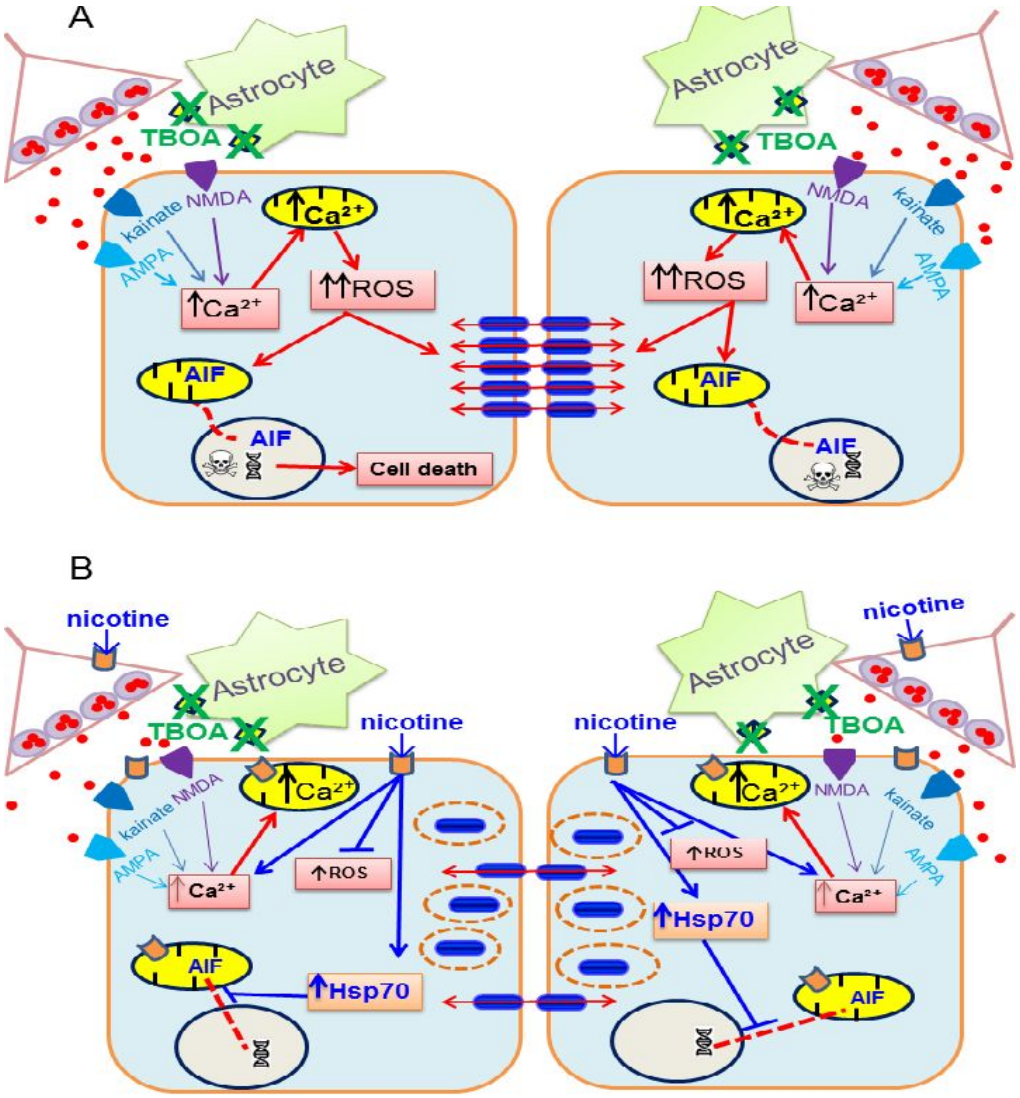

Figure 11. Idealized diagram to explain the toxic effects induced by TBOA and their antagonism by nicotine on HMs. (A) Inhibition of the excitatory aminoacid transporters by TBOA leads to the intensification of AMPA, kainate, and NMDA receptor activation by glutamate (filled red circles). This results in an increase of intracellular free Ca^{2+} which acts on mitochondria and favors ROS production, AIF release and DNA damage. The process is highly amplified by the bidirectional (red arrows) operation by gap junctions (in particular Cx36; filled blue cylinders) which may propagate damaging signals from injured to uninjured close neighbor HMs, with deleterious consequences on cell survival. (B) The neurotoxic effect of TBOA is largely attenuated in the presence of nicotine. It exerts multiple effects via nAChRs located on presynaptic terminal (decreasing glutamate release), HM membrane and even mitochondria. Nicotine reduces ROS production and promotes Hsp70 production, which blocks AIF nuclear migration. Moreover, nicotine strongly decreases motoneuronal coupling via gap junctions through the redistribution of Cx36 subunits, disjoining HMs from their collective excitatory behavior.

In summary, the present project obtained the following results:

1. On bursting HMs, nAChR activation rapidly contrasted excitotoxic burst activity induced by selective block of glutamate uptake, and modulated synaptic transmission (inhibition of glutamatergic tone and enhancement of synaptic transmission). Conversely, in non-bursting HMs, application of the antagonists for the α4- and α7-containing nAChRs unmasked bursts. These results suggest a pivotal role of the cholinergic tone, in particular via α4β2 and α7 nAChRs, to circumscribe bursting activity during excitotoxic stress.

2. After prolonged exposure to excitotoxic stress (up to 4 h), the motoneuron number significantly decreased. Nicotine, which *per se* exerted no cell toxic action, prevented HM loss caused by TBOA. Cell death was combined with an increase in intracellular free oxygen radicals (already highly expressed at 2 h), mitochondrial dysfunction (at 4 h), and protein misfolding associated with endoplasmic reticulum stress (4 h). Nicotine was able to prevent all the above mentioned stress factors, whereas nAChR antagonists co-application with TBOA did not change the increase in ROS level or the reduction in formazan production.

3. Neighbouring cells were more prone to bursting recruitment as observed with Ca^{2+} transients. Nicotine, and the gap junction blocker carbenoxolone, reduced the number of cells manifesting Ca^{2+} transients and the number of such events. Prolonged exposure to nicotine or carbenoxolone induced downregulation of connexin36 expression, and changes in the relative distribution of this protein (decreased in the membrane fraction and rise in the cytoplasmic fraction). Similar results were not obtained when analyzing the expression level of pannexin1.

4. Histochemical studies demonstrated that TBOA significantly increased the expression level of the apoptotic factor AIF. Nicotine both prevented the increase in the expression of this apoptosis inducing protein and increased intracellular levels of Hsp70, an important biomarker against cell stress factors.

These results were systematically discussed in the “discussion” sections of the enclosed papers. Here, I will review the limitation of the current models used in ALS research and suggest future experiments to translate our results to a human clinical setting.

1. Outlook for present and future studies

Although SOD1, the first ALS associated gene was discovered almost 20 years ago, the disease etiopathology remains poorly understood. Researchers have focused their attention to recapitulating the human disease in animal models, which has resulted in the identification of riluzole as the single drug approved for ALS treatment (Bensimon et al., 1994). However, the sole benefit of riluzole is to extend the lifespan by an average of a few months (Shamshiri et al., 2016; Wijesekera and Leigh, 2009). Over the past decade, all human clinical trials, of new drugs based on data collected using animal models have failed to demonstrate therapeutical efficacy (DeLoach et al., 2015). Thus, improvement of ALS experimentation will need directing focus toward innovative approaches.

1.1. Current animal model in use

To study ALS, various species have been use to developed models, from invertebrates to vertebrates, but all of them possess limitation in their ability to recapitulate the disease phenotype (Liu et al., 2013; McGoldrick et al., 2013; Philips and Rothstein, 2015). The ‘ideal’ model should reproduce human symptoms, with the same induction, progression, and neurobiological mechanism of action, allowing the evaluation of the possible therapeutic intervantions in humans.

1.1.1. Canine neurodegenerative myelopathy

Humans are the only known species that naturally developed ALS; however, dogs may develop similar neuromuscular disease with some common clinical features. The canine degenerative myelopathy is an age related, fatal disease with progressive loss of motoneurons and subsequent muscle degeneration caused by two SOD1 mutations. Although the role of SOD1 expression remains unclear, oxidative stress and ubiquitine-positive inclusion bodies appear to play a crucial role in the induction of the disease (Nardone et al., 2016). However, ALS and the canine

neurodegenerative myelopathy manifest significant differences and sick dogs are early euthanized in disease progression due to deterioration of quality of life (Clerc et al., 2016).

1.1.2. Transgenic animals

Rodents, and in particular mice, are the most used animal models for ALS studies due to their complex central nervous system associated with availability and short time to manifest disease-like phenotype. Concerning the phylogenetic similarity with humans, also non-human primate models have been developed (Uchida et al., 2012); though their use has significant disadvantages such as time, space, funding, and ethical concerns. Other models in use to study disease phenotype and progression are zebrafish, C. elegans and Drosophila (Guerrero et al., 2016; Liu et al., 2013; Philips and Rothstein, 2015).

Since 1993, when the gene SOD1 was associated with ALS (Rosen et al. 1993), a number of transgenic mutant human (h)SOD1 overexpression models have been created in mouse, C. elegans, Drosophila, and zebrafish (McGoldrick et al., 2013; Philips and Rothstein, 2015). Although SOD1 mutations account only for a small percentage of sALS cases (1-3%; Orsini et al., 2015), there is the general assumption that studying the fALS could provide insight into the sporadic form of the disease, inasmuch the two forms manifest many similiraties which may develop through the same neuronal degeneration pathway. However, the validity of these assumptions has been questioned (McGoldrick et al., 2013). In fact, the pathogenesis of sALS implicates TDP-43 aggregations, which are absent in SOD1 mutation models (Mackenzie et al., 2007), leading us to hypothesize that motoneuron degeneration may result from a set of different mechanisms and SOD1 models may better represent the phenotype of patients with this mutations, but not the remaining 98% of sALS which do not express SOD1 mutations.

The association between TARDBP (TAR DNA binding proteins, TDP-43) and ALS (3-5% of fALS and 2% of sALS; Calvo et al., 2014; Philips and Rothstein, 2015) was discovered in 2008. Since then, (h)TARDBP was overexpressed in C. elegans, Drosophila, zebrafish, rodents, and non-human primate (Guerrero et al., 2016; Liu et al., 2013). Mouse overpression models seem to replicate human ALS phenotypes exhibiting neuronal ubiquitin-positive inclusions, motoneuron and axon degeneration, motor loss, paralysis, and death (Guerrero et al., 2016; Stallings et al.,

2010). This model is relatively new, and there is a lack of characterization of the ALS phenotype of human TARDBP. Available studies are controversial because some publications report that 50 mutations of TARDBP involved with ALS, wheres others report that those mutations are rare in ALS (Gendron et al., 2013; Mackenzie et al., 2010).

The FUS mutated form was associated with 5% of fALS and 1% of sALS cases in 2009 (Calvo et al., 2014; Guerrero et al., 2016). Also for this gene a model has been created in C. elegans, Drosphila, zebrafish, and rodents (Guerrero et al., 2016). Even if mutants overespressing hFUS manifest many similar characteristics with ALS patients, such as protein aggregation, neurodegeneration, and muscle atrophy (Mackenzie et al., 2010), it seems that the overexpression of FUS induces different phenotypes depending on the species. Moreover, recent studies have reported cognitive defects in aged animals overexpressing FUS without motor phenotype or spinal cord pathology (Clerc et al., 2016).

To delineate the fundamental molecular disease pathway or integrate the complex genomic landscape, researches are performed also on cell and tissue models, such as yeast and induced pluripotent stem cells (Thomsen et al., 2014).

1.2. Limitations of the current models

The present study used a simple in vitro model obtained from neonatal rat motoneurons, which by its nature has certain limitations. Firstly, it is interesting to evaluate if the results obtained are reproducible in adult rodents, even if it is exceptionally difficult to applicate the patch-clamp technique to brainstem slices of adults (Jaiswal and Keller, 2009). Second, because of the viability of *in vitro* brainstem slices limited to a few hours, we are unable to follow up the evolution of the excitotoxicity over a long period (days). Nevertheless, our first aim was to investigate how motoneurons are damaged by early pathological mechanisms related to excitotoxic stress, which would reproduce the putative ALS-related rise in endogenous glutamate rather than a more aggressive and widespread excitotoxicity using direct agonist of glutamatergic receptors such as glutamate, AMPA, or kainate. We were able to show how nicotine was able to block or prevent motoneuronal damage activated by the impairment of glutamate reuptake. This process started from the early signs of distress and prevented delayed cell loss.

Another aspect of our research is the co-application of nicotine and TBOA. In many studies, potential drugs or compounds are usually tested before the onset of first symptoms. This approach is clearly unsuitable to clinical trials inasmuch it is impossible to start treating patients presymptomatically.

ALS is a complex disease with a wide spectrum of phenotypes that could represent several related disorders with different causes but similar phenotypes (Wijesekera and Leigh, 2009). Unfortunately, until now there is no effective model to represent the disease in all ALS features, thus, making it difficult to research and assess of new therapies. Future perspectives for the neuroprotective role of nicotine against excitotoxicity should lead to test nAChR agonists on a time extendent model. A possible strategy could be to test nicotine effects on organotipic colture of spinal cord, which may survive for a few weeks (Cifra et al., 2012 and 2013). As previously reported, ALS is a multifactorial disease (Turner et al., 2013), so its protective role on a model of excitotoxicity is not sufficient to justify clinical trials. A parallel study should be carried on ALS related mutant animals, to evaluate if the protective activity of nicotine could be replicated on various phenotypes. Lastly, given the wide spectrum of nicotine actions and its ability to permeate cell membranes and activate a series of intracellular pathways (Henderson and Lester, 2015), it should be interesting to analyze specific positive allosteric modulators of nAChRs.

1.2.1. nAChR positive allosteric modulators

Because nAChRs are involved in a wide range of functions, including modulation of synaptic transmission, organization of sleep, drug reinforcement, and cognitive processes (Changeux, 2010; Gotti and Clementi, 2004), the use of full- or partial- agonists may induce several side effects beyond neuroprotection. The same consideration should be applied to the use of ACh or acetylcholinerase inhibitors leading to ACh accumulation in the synaptic cleft and beyond. In the past years attention has been turned on the nAChR positive allosteric modulators (PAMs; Grupe et al., 2015; Pandya and Yakel, 2013; Williams et al., 2011). An allosteric modulator is a substance that indirectly modulates the effects of an agonist on a target protein, such as a receptor. It binds at sites other than the orthosthetic site where ACh binds. In particular, PAMs induce an amplification of the agonist effects, but are inactive in the absence of the orthosteric ligand. Moreover, they are divided into two groups concerning whether they decrease receptor

desensitization (type II) or not (type I; Chatzidaki and Millar, 2015). Thus, allosteric modulators provide an additional approach to manipulate nAChR fuction by increasing the effectiveness of endogenous ACh and strengthening the cholinergic tone without directly activating nicotinic receptors. The use of PAMs may prevent receptor desensitization its effect remains under the strict control of the released ACh, thus restricting drug effects to the areas where the neurotransmitter is released (Chatzidaki and Millar, 2015; Williams et al., 2011). Since α7 and α4β2 nAChRs are the more widespread forms in the nervous system and are highly connected to neurological diseases (Gotti and Clementi, 2004), PAMs for these receptors hold therapeutic potentials. This notion should, promising of course, be first tested with *in vivo* and *in vitro* animal models.

1.3. Concluding remarks

In the simple *in vitro* model used in our laboratory where excitotoxicity is induced by TBOA, nicotine has shown the potential to be a candidate for the prevention of motoneuron degeneration: this should might open new perpectives for ALS therapy. The short life span of our model and the lack of an appropriate animal model for studying ALS make the clinical translation from animals to human currently complex. However, our model may be useful to replicate the early pathological mechanisms involved in ALS and to be a starting point to develop new drug therapies.

References

Albuquerque, E.X., Pereira, E.F.R., Alkondon, M., and Rogers, S.W. (2009). Mammalian Nicotinic Acetylcholine Receptors: From Structure to Function. Physiol. Rev. *89*, 73–120.

Aldes, L.D. (1995). Subcompartmental organization of the ventral (protrusor) compartment in the hypoglossal nucleus of the rat. J. Comp. Neurol. *353*, 89–108.

Alkondon, M., Pereira, E.F.R., Eisenberg, H.M., and Albuquerque, E.X. (1999). Choline and Selective Antagonists Identify Two Subtypes of Nicotinic Acetylcholine Receptors that Modulate GABA Release from CA1 Interneurons in Rat Hippocampal Slices. J. Neurosci. *19*, 2693–2705.

Anderson, Christopher M., Bridges, R.J., Chamberlin, A.R., Shimamoto, K., Yasuda-Kamatani, Y., and Swanson, R.A. (2001). Differing effects of substrate and non-substrate transport inhibitors on glutamate uptake reversal. J. Neurochem. *79*, 1207–1216.

Arroyo-Jiménez, M. del M., Bourgeois, J.-P., Marubio, L.M., Sourd, A.-M.L., Ottersen, O.P., Rinvik, E., Fairén, A., and Changeux, J.-P. (1999). Ultrastructural Localization of the α4-Subunit of the Neuronal Acetylcholine Nicotinic Receptor in the Rat Substantia Nigra. J. Neurosci. *19*, 6475–6487.

Barnard, E.A., Sutherland, M., Zaman, S., Matsumoto, M., Nayeem, N., Green, T., Darlison, M.G., and Bateson, A.N. (1993). Multiplicity, structure, and function in GABAA receptors. Ann. N. Y. Acad. Sci. *707*, 116–125.

Bayliss, D.A., Viana, F., Bellingham, M.C., and Berger, A.J. (1994). Characteristics and postnatal development of a hyperpolarization-activated inward current in rat hypoglossal motoneurons in vitro. J. Neurophysiol. *71*, 119–128.

Becchetti, A., Aracri, P., Meneghini, S., Brusco, S., and Amadeo, A. (2015). The role of nicotinic acetylcholine receptors in autosomal dominant nocturnal frontal lobe epilepsy. Membr. Physiol. Membr. Biophys. *6*, 22.

Bellingham, M.C., and Berger, A.J. (1996). Presynaptic depression of excitatory synaptic inputs to rat hypoglossal motoneurons by muscarinic M2 receptors. J. Neurophysiol. *76*, 3758–3770.

Belousov, A.B., and Fontes, J.D. (2014). Neuronal gap junction coupling as the primary determinant of the extent of glutamate-mediated excitotoxicity. J. Neural Transm. Vienna Austria 1996 *121*, 837–846.

Benowitz, N.L. (2009). Pharmacology of Nicotine: Addiction, Smoking-Induced Disease, and Therapeutics. Annu. Rev. Pharmacol. Toxicol. *49*, 57–71.

Bensimon, G., Lacomblez, L., and Meininger, V. (1994). A controlled trial of riluzole in amyotrophic lateral sclerosis. ALS/Riluzole Study Group. N. Engl. J. Med. *330*, 585-591.

Berger, A.J. (2000). Determinants of respiratory motoneuron output. Respir. Physiol. *122*, 259–269.

Berger, A.J., Bayliss, D.A., and Viana, F. (1992). Modulation of neonatal rat hypoglossal motoneuron excitability by serotonin. Neurosci. Lett. *143*, 164–168.

Berger, A.J., Dieudonné, S., and Ascher, P. (1998). Glycine Uptake Governs Glycine Site Occupancy at NMDA Receptors of Excitatory Synapses. J. Neurophysiol. *80*, 3336–3340.

Blokhuis, A.M., Groen, E.J.N., Koppers, M., van den Berg, L.H., and Pasterkamp, R.J. (2013). Protein aggregation in amyotrophic lateral sclerosis. Acta Neuropathol. (Berl.) *125*, 777–794.

Boone, T.B., and Aldes, L.D. (1984). The ultrastructure of two distinct neuron populations in the hypoglossal nucleus of the rat. Exp. Brain Res. *54*, 321–326.

Borke, R.C., Nau, M.E., and Ringler Jr., R.L. (1983). Brain stem afferents of hypoglossal neurons in the rat. Brain Res. *269*, 47–55.

Boulter, J., O'Shea-Greenfield, A., Duvoisin, R.M., Connolly, J.G., Wada, E., Jensen, A., Gardner, P.D., Ballivet, M., Deneris, E.S., and McKinnon, D. (1990). Alpha 3, alpha 5, and beta 4: three members of the rat neuronal nicotinic acetylcholine receptor-related gene family form a gene cluster. J. Biol. Chem. *265*, 4472–4482.

Calvo, A.C., Manzano, R., Mendon&#xe7, A, D.M.F., Mu&#xf1, Oz, M., J, A., Zaragoza, P., Osta, R., Calvo, A.C., et al. (2014). Amyotrophic Lateral Sclerosis: A Focus on Disease Progression, Amyotrophic Lateral Sclerosis: A Focus on Disease Progression. BioMed Res. Int. BioMed Res. Int. *2014*, *2014*, e925101.

Carrì, M.T., Valle, C., Bozzo, F., and Cozzolino, M. (2015). Oxidative stress and mitochondrial damage: importance in non-SOD1 ALS. Front. Cell. Neurosci. *9*.

Champtiaux, N., Gotti, C., Cordero-Erausquin, M., David, D.J., Przybylski, C., Léna, C., Clementi, F., Moretti, M., Rossi, F.M., Novère, N.L., et al. (2003). Subunit Composition of Functional Nicotinic Receptors in Dopaminergic Neurons Investigated with Knock-Out Mice. J. Neurosci. *23*, 7820–7829.

Changeux, J.-P. (2010). Nicotine addiction and nicotinic receptors: lessons from genetically modified mice. Nat. Rev. Neurosci. *11*, 389–401.

Chatzidaki, A., and Millar., N.S. (2015). Allosteric modulation of nicotinic acetylcholine receptors. Biochem. Pharmacol. *97*, 408-417.

Chiurchiù, V., Orlacchio, A., and Maccarrone, M. (2016). Is Modulation of Oxidative Stress an Answer? The State of the Art of Redox Therapeutic Actions in Neurodegenerative Diseases. Oxid. Med. Cell. Longev. *2016*.

Ciechanover, A., and Kwon, Y.T. (2015). Degradation of misfolded proteins in neurodegenerative diseases: therapeutic targets and strategies. Exp. Mol. Med. *47*, e147.

Cifra, A., Nani, F., Sharifullina, E., and Nistri, A. (2009). A repertoire of rhythmic bursting produced by hypoglossal motoneurons in physiological and pathological conditions. Philos. Trans. R. Soc. B Biol. Sci. *364*, 2493–2500.

Cifra, A., Nani, F., and Nistri, A. (2011). Riluzole is a potent drug to protect neonatal rat hypoglossal motoneurons in vitro from excitotoxicity due to glutamate uptake block. Eur. J. Neurosci. *33*, 899–913.

Cifra, A., Mazzone, G.L., Nani, F., Nistri A., and Mladinic, M. (2012). Postnatal developmental profile of neurons and glia in motor nuclei of the brainstem and spinal cord, and its comparison with organotypic slice cultures. Dev. Neurobiol. *72*, 1140-1160.

Cifra, A., Mazzone, G.L., and Nistri, A. (2013). Riluzole: what it does to spinal and brainstem neurons and how it does it. Neuroscientist *19*, 137-144.

Clerc, P., Lipnick, S., and Willett, C. (2016). A look into the future of ALS research. Drug Discov. Today *21*, 939–949.

Clunes, L.A., Bridges, A., Alexis, N., and Tarran, R. (2008). In vivo versus in vitro airway surface liquid nicotine levels following cigarette smoke exposure. J. Anal. Toxicol. *32*, 201–207.

Cobb, S.R., Bulters, D.O., and Davies, C.H. (2000). Coincident activation of mGluRs and mAChRs imposes theta frequency patterning on synchronised network activity in the hippocampal CA3 region. Neuropharmacology *39*, 1933–1942.

Colombo, S.F., Mazzo, F., Pistillo, F., and Gotti, C. (2013). Biogenesis, trafficking and up-regulation of nicotinic ACh receptors. Biochem. Pharmacol. *86*, 1063–1073.

Cooper, M.H. (1981). Neurons of the hypoglossal nucleus of the rat. Otolaryngol.--Head Neck Surg. Off. J. Am. Acad. Otolaryngol.-Head Neck Surg. *89*, 10–15.

Cunningham, E.T., and Sawchenko, P.E. (2000). Dorsal medullary pathways subserving oromotor reflexes in the rat: implications for the central neural control of swallowing. J. Comp. Neurol. *417*, 448–466.

D'Amico, E., Factor-Litvak, P., Santella, R.M., and Mitsumoto, H. (2013). Clinical Perspective of Oxidative Stress in Sporadic ALS. Free Radic. Biol. Med. *65*.

Del Negro, C.A., Morgado-Valle, C., Hayes, J.A., Mackay, D.D., Pace, R.W., Crowder, E.A., and Feldman, J.L. (2005). Sodium and calcium current-mediated pacemaker neurons and respiratory rhythm generation. J. Neurosci. Off. J. Soc. Neurosci. *25*, 446–453.

DeLoach, A., Cozart, M., Kiaei, A., and Kiaei, M. (2015). A retrospective review of the progress in amyotrophic lateral sclerosis drug discovery over the last decade and a look at the latest strategies. Expert. Opin. Drug. Discov. *10*, 1099-1118.

Dineley, K.T., Pandya, A.A., and Yakel, J.L. (2015). Nicotinic ACh receptors as therapeutic targets in CNS disorders. Trends Pharmacol. Sci. *36*, 96–108.

Dobbins, E.G., and Feldman, J.L. (1995). Differential innervation of protruder and retractor muscles of the tongue in rat. J. Comp. Neurol. *357*, 376–394.

Donato, R., and Nistri, A. (2000). Relative Contribution by GABA or Glycine to Cl−-Mediated Synaptic Transmission on Rat Hypoglossal Motoneurons In Vitro. J. Neurophysiol. *84*, 2715–2724.

Donato, R., Lape, R., and Nistri, A. (2003). Pre and postsynaptic effects of metabotropic glutamate receptor activation on neonatal rat hypoglossal motoneurons. Neurosci. Lett. *338*, 9–12.

Dong, X., Wang, Y., and Qin, Z. (2009). Molecular mechanisms of excitotoxicity and their relevance to pathogenesis of neurodegenerative diseases. Acta Pharmacol. Sin. *30*, 379–387.

Doyle, K.M., Kennedy, D., Gorman, A.M., Gupta, S., Healy, S.J.M., and Samali, A. (2011). Unfolded proteins and endoplasmic reticulum stress in neurodegenerative disorders. J. Cell. Mol. Med. *15*, 2025–2039.

Essin, K., Nistri, A., and Magazanik, L. (2002). Evaluation of GluR2 subunit involvement in AMPA receptor function of neonatal rat hypoglossal motoneurons. Eur. J. Neurosci. *15*, 1899–1906.

Feldman, J.L., and Del Negro, C.A. (2006). Looking for inspiration: new perspectives on respiratory rhythm. Nat. Rev. Neurosci. *7*, 232–242.

Fluharty, M., Taylor, A.E., Grabski, M., and Munafò, M.R. (2016). The Association of Cigarette Smoking With Depression and Anxiety: A Systematic Review. Nicotine Tob. Res. ntw140.

Fukunaga, K., Shinoda, Y., and Tagashira, H. (2015). The role of SIGMAR1 gene mutation and mitochondrial dysfunction in amyotrophic lateral sclerosis. J. Pharmacol. Sci. *127*, 36–41.

Funk, G.D., Smith, J.C., and Feldman, J.L. (1993). Generation and transmission of respiratory oscillations in medullary slices: role of excitatory amino acids. J. Neurophysiol. *70*, 1497–1515.

García Del Caño, G., Millán, L.M., Gerrikagoitia, I., Sarasa, M., and Matute, C. (1999). Ionotropic glutamate receptor subunit distribution on hypoglossal motoneuronal pools in the rat. J. Neurocytol. *28*, 455–468.

Gendron, T.F., Rademakers, R., and Petrucelli, L. (2013). TARDBP mutation analysis in TDP-43 proteinopathies and deciphering the toxicity of mutant TDP-43. J. Alzheimers Dis. JAD *33 Suppl 1*, S35-45.

Gergalova, G., Lykhmus, O., Kalashnyk, O., Koval, L., Chernyshov, V., Kryukova, E., Tsetlin, V., Komisarenko, S., and Skok, M. (2012). Mitochondria express α7 nicotinic acetylcholine receptors to regulate Ca2+ accumulation and cytochrome c release: study on isolated mitochondria. PloS One *7*, e31361.

Gergalova, G., Lykhmus, O., Komisarenko, S., and Skok, M. (2014). α7 nicotinic acetylcholine receptors control cytochrome c release from isolated mitochondria through kinase-mediated pathways. Int. J. Biochem. Cell Biol. *49*, 26–31.

Gestreau, C., Dutschmann, M., Obled, S., and Bianchi, A.L. (2005). Activation of XII motoneurons and premotor neurons during various oropharyngeal behaviors. Respir. Physiol. Neurobiol. *147*, 159–176.

Ghezzi, F., Corsini, S., and Nistri, A. (2016). Electrophysiological characterization of the M-current in rat hypoglossal motoneurons. Neurosci. doi: 10.1016/j.neuroscience.2016.10.048

Giniatullin, R., Nistri, A., and Yakel, J.L. (2005). Desensitization of nicotinic ACh receptors: shaping cholinergic signaling. Trends Neurosci. *28*, 371–378.

Gotti, C., and Clementi, F. (2004). Neuronal nicotinic receptors: from structure to pathology. Prog. Neurobiol. *74*, 363–396.

Grupe, M., Grunnet, M., Bastlund, J.F., and Jensen, A.A. (2015). Targeting α4β2 nicotinic acetylcholine receptors in central nervous system disorders: perspectives on positive allosteric modulation as a therapeutic approach. Basic. Clin. Pharmacol. Toxicol. *116*, 187-200.

Guerrero, E.N., Wang, H., Mitra, J., Hegde, P.M., Stowell, S.E., Liachko, N.F., Kraemer, B.C., Garruto, R.M., Rao, K.S., and Hegde, M.L. (2016). TDP-43/FUS in motor neuron disease: complexity and challenges. Prog. Neurobiol. *145-146*, 78-97.

Haddad, G.G., Donnelly, D.F., and Getting, P.A. (1990). Biophysical properties of hypoglossal neurons in vitro: intracellular studies in adult and neonatal rats. J. Appl. Physiol. Bethesda Md 1985 *69*, 1509–1517.

Hay, M., McKenzie, H., Lindsley, K., Dietz, N., Bradley, S.R., Conn, P.J., and Hasser, E.M. (1999). Heterogeneity of metabotropic glutamate receptors in autonomic cell groups of the medulla oblongata of the rat. J. Comp. Neurol. *403*, 486–501.

Henderson, B.J., and Lester, H.A. (2015). Inside-out neuropharmacology of nicotinic drugs. Neuropharmacology *96*, 178–193.

Hermosura, M.C., and Garruto, R.M. (2007). TRPM7 and TRPM2—Candidate susceptibility genes for Western Pacific ALS and PD? Biochim. Biophys. Acta BBA - Mol. Basis Dis. *1772*, 822–835.

Hetz, C., Chevet, E., and Harding, H.P. (2013). Targeting the unfolded protein response in disease. Nat. Rev. Drug Discov. *12*, 703–719.

Huang, H., and Bordey, A. (2004). Glial glutamate transporters limit spillover activation of presynaptic NMDA receptors and influence synaptic inhibition of Purkinje neurons. J. Neurosci. Off. J. Soc. Neurosci. *24*, 5659–5669.

Huang, Y.H., Sinha, S.R., Tanaka, K., Rothstein, J.D., and Bergles, D.E. (2004). Astrocyte glutamate transporters regulate metabotropic glutamate receptor-mediated excitation of hippocampal interneurons. J. Neurosci. Off. J. Soc. Neurosci. *24*, 4551–4559.

Hughes, S.W., Cope, D.W., Blethyn, K.L., and Crunelli, V. (2002). Cellular mechanisms of the slow (<1 Hz) oscillation in thalamocortical neurons in vitro. Neuron *33*, 947–958.

Hurst, R., Rollema, H., and Bertrand, D. (2013). Nicotinic acetylcholine receptors: from basic science to therapeutics. Pharmacol. Ther. *137*, 22–54.

Jaiswal, M.K., and Keller, B.U. (2009). Cu/Zn Superoxide Dismutase Typical for Familial Amyotrophic Lateral Sclerosis Increases the Vulnerability of Mitochondria and Perturbs Ca2+ Homeostasis in SOD1G93A Mice. Mol. Pharmacol. *75*, 478–489.

Kabashi, E., and Durham, H.D. (2006). Failure of protein quality control in amyotrophic lateral sclerosis. Biochim. Biophys. Acta BBA - Mol. Basis Dis. *1762*, 1038–1050.

Kalb, R.G. (1994). Regulation of motor neuron dendrite growth by NMDA receptor activation. Development *120*, 3063–3071.

Kim, G.H., Kim, J.E., Rhie, S.J., and Yoon, S. (2015). The Role of Oxidative Stress in Neurodegenerative Diseases. Exp. Neurobiol. *24*, 325–340.

Krammer, E.B., Rath, T., and Lischka, M.F. (1979). Somatotopic organization of the hypoglossal nucleus: a HRP study in the rat. Brain Res. *170*, 533–537.

Kuryatov, A., Luo, J., Cooper, J., and Lindstrom, J. (2005). Nicotine Acts as a Pharmacological Chaperone to Up-Regulate Human α4β2 Acetylcholine Receptors. Mol. Pharmacol. *68*, 1839–1851.

Ladewig, T., Kloppenburg, P., Lalley, P.M., Zipfel, W.R., Webb, W.W., and Keller, B.U. (2003). Spatial profiles of store-dependent calcium release in motoneurones of the nucleus hypoglossus from newborn mouse. J. Physiol. *547*, 775–787.

Lamanauskas, N., and Nistri, A. (2006). Persistent rhythmic oscillations induced by nicotine on neonatal rat hypoglossal motoneurons in vitro. Eur. J. Neurosci. *24*, 2543–2556.

Lamanauskas, N., and Nistri, A. (2008). Riluzole blocks persistent Na+ and Ca2+ currents and modulates release of glutamate via presynaptic NMDA receptors on neonatal rat hypoglossal motoneurons in vitro. Eur. J. Neurosci. *27*, 2501–2514.

Lape, R., and Nistri, A. (1999). Voltage-activated K+ currents of hypoglossal motoneurons in a brain stem slice preparation from the neonatal rat. J. Neurophysiol. *81*, 140–148.

Lape, R., and Nistri, A. (2000). Current and voltage clamp studies of the spike medium afterhyperpolarization of hypoglossal motoneurons in a rat brain stem slice preparation. J. Neurophysiol. *83*, 2987–2995.

Lape, R., and Nistri, A. (2001). Characteristics of fast Na(+) current of hypoglossal motoneurons in a rat brainstem slice preparation. Eur. J. Neurosci. *13*, 763–772.

Laslo, P., Lipski, J., Nicholson, L.F., Miles, G.B., and Funk, G.D. (2001). GluR2 AMPA receptor subunit expression in motoneurons at low and high risk for degeneration in amyotrophic lateral sclerosis. Exp. Neurol. *169*, 461–471.

Lewerenz, J., and Maher, P. (2015). Chronic Glutamate Toxicity in Neurodegenerative Diseases—What is the Evidence? Neurodegeneration 469.

Li, Y.Q., Takada, M., Kaneko, T., and Mizuno, N. (1997). Distribution of GABAergic and glycinergic premotor neurons projecting to the facial and hypoglossal nuclei in the rat. J. Comp. Neurol. *378*, 283–294.

Lindstrom, J., Anand, R., Peng, X., Gerzanich, V., Wang, F., and Li, Y. (1995). Neuronal Nicotinic Receptor Subtypes. Ann. N. Y. Acad. Sci. *757*, 100–116.

Liu, Y.C., Chiang, P.M., and Tsai, K.J. (2013). Disease animal models of TDP-43 proteinopathy and their pre-clinical applications. Int. J. Mol. Sci. *14*, 20079-20111.

Lowe, A.A. (1980). The neural regulation of tongue movements. Prog. Neurobiol. *15*, 295–344.

Lykhmus, O., Gergalova, G., Koval, L., Zhmak, M., Komisarenko, S., and Skok, M. (2014). Mitochondria express several nicotinic acetylcholine receptor subtypes to control various pathways of apoptosis induction. Int. J. Biochem. Cell Biol. *53*, 246–252.

Mackenzie, I.R., Rademakers, R., and Neumann, M. (2010). TDP-43 and FUS in amyotrophic lateral sclerosis and frontotemporal dementia. Lancet Neurol. *9*, 995–1007.

Mackenzie, I.R.A., Bigio, E.H., Ince, P.G., Geser, F., Neumann, M., Cairns, N.J., Kwong, L.K., Forman, M.S., Ravits, J., Stewart, H., et al. (2007). Pathological TDP-43 distinguishes sporadic amyotrophic lateral sclerosis from amyotrophic lateral sclerosis with SOD1 mutations. Ann. Neurol. *61*, 427–434.

Marchetti, C., Pagnotta, S., Donato, R., and Nistri, A. (2002). Inhibition of spinal or hypoglossal motoneurons of the newborn rat by glycine or GABA. Eur. J. Neurosci. *15*, 975–983.

Marchi, M., Risso, F., Viola, C., Cavazzani, P., and Raiteri, M. (2002). Direct evidence that release-stimulating alpha7* nicotinic cholinergic receptors are localized on human and rat brain glutamatergic axon terminals. J. Neurochem. *80*, 1071–1078.

Marder, E., and Calabrese, R.L. (1996). Principles of rhythmic motor pattern generation. Physiol. Rev. *76*, 687–717.

Martínez-Lozada, Z., and Ortega, A. (2015). Glutamatergic Transmission: A Matter of Three. Neural Plast. *2015*.

Martin-Ruiz, C.M., Lee, M., Perry, R.H., Baumann, M., Court, J.A., and Perry, E.K. (2004). Molecular analysis of nicotinic receptor expression in autism. Brain Res. Mol. Brain Res. *123*, 81–90.

Marubio, L.M., del Mar Arroyo-Jimenez, M., Cordero-Erausquin, M., Léna, C., Le Novère, N., de Kerchove d'Exaerde, A., Huchet, M., Damaj, M.I., and Changeux, J.P. (1999). Reduced antinociception in mice lacking neuronal nicotinic receptor subunits. Nature *398*, 805–810.

Matta, S.G., Balfour, D.J., Benowitz, N.L., Boyd, R.T., Buccafusco, J.J., Caggiula, A.R., Craig, C.R., Collins, A.C., Damaj, M.I., Donny, E.C., et al. (2006). Guidelines on nicotine dose selection for in vivo research. Psychopharmacology (Berl.) *190*, 269–319.

Matus, S., Valenzuela, V., Medinas, D.B., and Hetz, C. (2013). ER Dysfunction and Protein Folding Stress in ALS. Int. J. Cell Biol. *2013*, 674751.

McClung, J.R., and Goldberg, S.J. (2000). Functional anatomy of the hypoglossal innervated muscles of the rat tongue: a model for elongation and protrusion of the mammalian tongue. Anat. Rec. *260*, 378–386.

McGoldrick, P., Joyce, P.I., Fisher, E.M.C., and Greensmith, L. (2013). Rodent models of amyotrophic lateral sclerosis. Biochim. Biophys. Acta. *1832*, 1421-1436.

Medina, L., Figueredo-Cardenas, G., Rothstein, J.D., and Reiner, A. (1996). Differential Abundance of Glutamate Transporter Subtypes in Amyotrophic Lateral Sclerosis (ALS)-Vulnerable versus ALS-Resistant Brain Stem Motor Cell Groups. Exp. Neurol. *142*, 287–295.

Miladinovic, T., Nashed, M.G., and Singh, G. (2015). Overview of Glutamatergic Dysregulation in Central Pathologies. Biomolecules *5*, 3112–3141.

Mosfeldt Laursen, A., and Rekling, J.C. (1989). Electrophysiological properties of hypoglossal motoneurons of guinea-pigs studied in vitro. Neuroscience *30*, 619–637.

Mukherjee, J., Kuryatov, A., Moss, S.J., Lindstrom, J.M., and Anand, R. (2009). Mutations of cytosolic loop residues impair assembly and maturation of alpha7 nicotinic acetylcholine receptors. J. Neurochem. *110*, 1885–1894.

Muller, E., Triller, A., and Legendre, P. (2004). Glycine receptors and GABAA receptor α1 and γ2 subunits during the development of mouse hypoglossal nucleus. Eur. J. Neurosci. *20*, 3286–3300.

Nakamura, Y., and Katakura, N. (1995). Generation of masticatory rhythm in the brainstem. Neurosci. Res. *23*, 1–19.

Nani, F., Cifra, A., and Nistri, A. (2010). Transient oxidative stress evokes early changes in the functional properties of neonatal rat hypoglossal motoneurons in vitro. Eur. J. Neurosci. *31*, 951–966.

Nardone, R., Höller, Y., Taylor, A.C., Lochner, P., Tezzon, F., Golaszewski, S., Brigo, F., and Trinka, E. (2016). Canine degenerative myelopathy: a model of human amyotrophic lateral sclerosis. Zool. Jena Ger. *119*, 64–73.

Netter, F. H. (2006). Atlas of Human Anatomy. 4th. Saunders Elsevier.

Niedzielska, E., Smaga, I., Gawlik, M., Moniczewski, A., Stankowicz, P., Pera, J., and Filip, M. (2015). Oxidative Stress in Neurodegenerative Diseases. Mol. Neurobiol. 1–32.

O'Brien, J.A., Isaacson, J.S., and Berger, A.J. (1997). NMDA and non-NMDA receptors are co-localized at excitatory synapses of rat hypoglossal motoneurons. Neurosci. Lett. *227*, 5–8.

Orsini, M., Oliveira, A.B., Nascimento, O.J.M., Reis, C.H.M., Leite, M.A.A., de Souza, J.A., Pupe, C., de Souza, O.G., Bastos, V.H., de Freitas, M.R.G., et al. (2015). Amyotrophic Lateral Sclerosis: New Perpectives and Update. Neurol. Int. *7*.

Pagnotta, S.E., Lape, R., Quitadamo, C., and Nistri, A. (2005). Pre- and postsynaptic modulation of glycinergic and gabaergic transmission by muscarinic receptors on rat hypoglossal motoneurons in vitro. Neuroscience *130*, 783–795.

Palomo, G.M., and Manfredi, G. (2015). Exploring new pathways of neurodegeneration in ALS: The role of mitochondria quality control. Brain Res. *1607*, 36–46.

Pandya, A.A., and Yakel, J.L. (2013). Effects of neuronal nicotinic acetylcholine receptor allosteric modulators in animal behavior studies. Biochem. Pharmacol. *86*, 1054-1062.

Parkis, M.A., Bayliss, D.A., and Berger, A.J. (1995). Actions of norepinephrine on rat hypoglossal motoneurons. J. Neurophysiol. *74*, 1911–1919.

Paton, J.F., and Richter, D.W. (1995). Role of fast inhibitory synaptic mechanisms in respiratory rhythm generation in the maturing mouse. J. Physiol. *484 (Pt 2)*, 505–521.

Peever, J.H., Shen, L., and Duffin, J. (2002). Respiratory pre-motor control of hypoglossal motoneurons in the rat. Neuroscience *110*, 711–722.

Perez-Lloret, S., and Barrantes, F.J. (2016). Deficits in cholinergic neurotransmission and their clinical correlates in Parkinson's disease. Npj Park. Dis. *2*, 16001.

Philips, T., and Rothstein, J.D. (2015). Rodent models of amyotrophic lateral sclerosis. Curr. Protoc. Pharmacol. *69*, 1-21.

Pollari, E., Goldsteins, G., Bart, G., Koistinaho, J., and Giniatullin, R. (2014). The role of oxidative stress in degeneration of the neuromuscular junction in amyotrophic lateral sclerosis. Front. Cell. Neurosci. *8*.

Pomierny-Chamioło, L., Rup, K., Pomierny, B., Niedzielska, E., Kalivas, P.W., and Filip, M. (2014). Metabotropic glutamatergic receptors and their ligands in drug addiction. Pharmacol. Ther. *142*, 281–305.

Potter, A.S., Schaubhut, G., and Shipman, M. (2014). Targeting the nicotinic cholinergic system to treat attention-deficit/hyperactivity disorder: rationale and progress to date. CNS Drugs *28*, 1103–1113.

Quick, M.W., and Lester, R.A.J. (2002). Desensitization of neuronal nicotinic receptors. J. Neurobiol. *53*, 457–478.

Quik, M., and Wonnacott, S. (2011). α6β2* and α4β2* nicotinic acetylcholine receptors as drug targets for Parkinson's disease. Pharmacol. Rev. *63*, 938–966.

Quik, M., Zhang, D., Perez, X.A., and Bordia, T. (2014). Role for the nicotinic cholinergic system in movement disorders; therapeutic implications. Pharmacol. Ther. *144*, 50–59.

Quitadamo, C., Fabbretti, E., Lamanauskas, N., and Nistri, A. (2005). Activation and desensitization of neuronal nicotinic receptors modulate glutamatergic transmission on neonatal rat hypoglossal motoneurons. Eur. J. Neurosci. *22*, 2723–2734.

Rekling, J.C. (1990). Excitatory effects of thyrotropin-releasing hormone (TRH) in hypoglossal motoneurons. Brain Res. *510*, 175–179.

Rekling, J.C., Funk, G.D., Bayliss, D.A., Dong, X.-W., and Feldman, J.L. (2000). Synaptic Control of Motoneuronal Excitability. Physiol. Rev. *80*, 767–852.

Roda, F., Gestreau, C., and Bianchi, A.L. (2002). Discharge Patterns of Hypoglossal Motoneurons During Fictive Breathing, Coughing, and Swallowing. J. Neurophysiol. *87*, 1703–1711.

Rosen, D.R., Siddique, T., Patterson, D., Figlewicz, D.A., Sapp, P., Hentati, A., Donaldson, D., Goto, J., O'Regan, J.P., Deng, H.-X., et al. (1993). Mutations in Cu/Zn superoxide dismutase gene are associated with familial amyotrophic lateral sclerosis. Nature *362*, 59–62.

Rosenberg, M.M., Blitzblau, R.C., Olsen, D.P., and Jacob, M.H. (2002). Regulatory mechanisms that govern nicotinic synapse formation in neurons. J. Neurobiol. *53*, 542–555.

Rothstein, J.D., Tsai, G., Kuncl, R.W., Clawson, L., Cornblath, D.R., Drachman, D.B., Pestronk, A., Stauch, B.L., and Coyle, J.T. (1990). Abnormal excitatory amino acid metabolism in amyotrophic lateral sclerosis. Ann. Neurol. *28*, 18–25.

Rothstein, J.D., Martin, L.J., and Kuncl, R.W. (1992). Decreased Glutamate Transport by the Brain and Spinal Cord in Amyotrophic Lateral Sclerosis. N. Engl. J. Med. *326*, 1464–1468.

Rothstein, J.D., Van Kammen, M., Levey, A.I., Martin, L.J., and Kuncl, R.W. (1995). Selective loss of glial glutamate transporter GLT-1 in amyotrophic lateral sclerosis. Ann. Neurol. *38*, 73–84.

Rowland LP (2001). How amyotrophic lateral sclerosis got its name: The clinical-pathologic genius of jean-martin charcot. Arch. Neurol. *58*, 512–515.

Rukhadze, I., and Kubin, L. (2007). Mesopontine cholinergic projections to the hypoglossal motor nucleus. Neurosci. Lett. *413*, 121–125.

Sallette, J., Pons, S., Devillers-Thiery, A., Soudant, M., Prado de Carvalho, L., Changeux, J.-P., and Corringer, P.J. (2005). Nicotine Upregulates Its Own Receptors through Enhanced Intracellular Maturation. Neuron *46*, 595–607.

Salminen, O., Murphy, K.L., McIntosh, J.M., Drago, J., Marks, M.J., Collins, A.C., and Grady, S.R. (2004). Subunit Composition and Pharmacology of Two Classes of Striatal Presynaptic Nicotinic Acetylcholine Receptors Mediating Dopamine Release in Mice. Mol. Pharmacol. *65*, 1526–1535.

Sasaki, S., and Iwata, M. (2007). Mitochondrial Alterations in the Spinal Cord of Patients With Sporadic Amyotrophic Lateral Sclerosis. J. Neuropathol. Exp. Neurol. *66*, 10–16.

Sasaki, S., Komori, T., and Iwata, M. (2000). Excitatory amino acid transporter 1 and 2 immunoreactivity in the spinal cord in amyotrophic lateral sclerosis. Acta Neuropathol. (Berl.) *100*, 138–144.

Sawczuk, A., Powers, R.K., and Binder, M.D. (1995). Spike frequency adaptation studied in hypoglossal motoneurons of the rat. J. Neurophysiol. *73*, 1799–1810.

Scarr, E. (2012). Muscarinic Receptors: Their Roles in Disorders of the Central Nervous System and Potential as Therapeutic Targets. CNS Neurosci. Ther. *18*, 369–379.

Schon, E.A., and Przedborski, S. (2011). Mitochondria: the next (neurode)generation. Neuron *70*, 1033–1053.

Shamshiri, H., Fatehi, F., Abolfazil, R., Harirchian, M.H., Sedighi, B., Zamani, B., Roudbari, A., Razazian, N., Khamseh, F., and Nafissi, S. (2016) Trends of quality of life changes in amyotrophic lateral sclerosis patients. J. Neurol. Sci. *15*, 35-40.

Sharifullina, E., and Nistri, A. (2006). Glutamate uptake block triggers deadly rhythmic bursting of neonatal rat hypoglossal motoneurons. J. Physiol. *572*, 407–423.

Sharifullina, E., Ostroumov, K., and Nistri, A. (2004). Activation of group I metabotropic glutamate receptors enhances efficacy of glutamatergic inputs to neonatal rat hypoglossal motoneurons in vitro. Eur. J. Neurosci. *20*, 1245–1254.

Sharifullina, E., Ostroumov, K., and Nistri, A. (2005). Metabotropic glutamate receptor activity induces a novel oscillatory pattern in neonatal rat hypoglossal motoneurones. J. Physiol. *563*, 139–159.

Sharifullina, E., Ostroumov, K., Grandolfo, M., and Nistri, A. (2008). N-methyl-D-aspartate triggers neonatal rat hypoglossal motoneurons in vitro to express rhythmic bursting with unusual Mg^{2+} sensitivity. Neuroscience *154*, 804–820.

Shaw, P.J. (2005). Molecular and cellular pathways of neurodegeneration in motor neurone disease. J. Neurol. Neurosurg. Psychiatry *76*, 1046–1057.

Singer, J.H., and Berger, A.J. (2000). Development of inhibitory synaptic transmission to motoneurons. Brain Res. Bull. *53*, 553–560.

Singer, J.H., Talley, E.M., Bayliss, D.A., and Berger, A.J. (1998). Development of Glycinergic Synaptic Transmission to Rat Brain Stem Motoneurons. J. Neurophysiol. *80*, 2608–2620.

Sokoloff, A.J. (2000). Localization and contractile properties of intrinsic longitudinal motor units of the rat tongue. J. Neurophysiol. *84*, 827–835.

Sommer, B., Köhler, M., Sprengel, R., and Seeburg, P.H. (1991). RNA editing in brain controls a determinant of ion flow in glutamate-gated channels. Cell *67*, 11–19.

Soriani, M.-H., and Desnuelle, C. (2009). Épidémiologie de la SLA. Rev. Neurol. (Paris) *165*, 627–640.

Srinivasan, R., Pantoja, R., Moss, F.J., Mackey, E.D.W., Son, C.D., Miwa, J., and Lester, H.A. (2011). Nicotine up-regulates α4β2 nicotinic receptors and ER exit sites via stoichiometry-dependent chaperoning. J. Gen. Physiol. *137*, 59–79.

Stallings, N.R., Puttaparthi, K., Luther, C.M., Burns, D.K., and Elliott, J.L. (2010). Progressive motor weakness in transgenic mice expressing human TDP-43. Neurobiol. Dis. *40*, 404–414.

Steenland, H.W., Liu, H., and Horner, R.L. (2008). Endogenous Glutamatergic Control of Rhythmically Active Mammalian Respiratory Motoneurons In Vivo. J. Neurosci. *28*, 6826–6835.

Suzue, T. (1984). Respiratory rhythm generation in the in vitro brain stem-spinal cord preparation of the neonatal rat. J. Physiol. *354*, 173–183.

Takasu, N., and Hashimoto, P.H. (1988). Morphological identification of an interneuron in the hypoglossal nucleus of the rat: A combined Golgi-electron microscopic study. J. Comp. Neurol. *271*, 461–471.

Takasu, N., Nakatani, T., Arikuni, T., and Kimura, H. (1987). Immunocytochemical localization of gamma-aminobutyric acid in the hypoglossal nucleus of the macaque monkey, Macaca fuscata: a light and electron microscopic study. J. Comp. Neurol. *263*, 42–53.

Takata, M. (1993). Two types of inhibitory postsynaptic potentials in the hypoglossal motoneurons. Prog. Neurobiol. *40*, 385–411.

Thomsen, G.M., Gowing, G., Svendsen, S., and Svendsen, C.N. (2014). The past, present and future of stem cell clinical trials for ALS. Exp. Neurol. *262*, 127-137.

Traynelis, S.F., Wollmuth, L.P., McBain, C.J., Menniti, F.S., Vance, K.M., Ogden, K.K., Hansen, K.B., Yuan, H., Myers, S.J., and Dingledine, R. (2010). Glutamate Receptor Ion Channels: Structure, Regulation, and Function. Pharmacol. Rev. *62*, 405–496.

Tsetlin, V., Kuzmin, D., and Kasheverov, I. (2011). Assembly of nicotinic and other Cys-loop receptors. J. Neurochem. *116*, 734–741.

Turner, M.R., Hardiman, O., Benatar, M., Brooks, B.R., Chio, A., de Carvalho, M., Ince, P.G., Lin, C., Miller, R.G., Mitsumoto, H., et al. (2013). Controversies and priorities in amyotrophic lateral sclerosis. Lancet Neurol. *12*, 310–322.

Uchida, A., Sasaguri, H., Kimura, N., Tajiri, M., Ohkubo, T., Ono, F., Sakaue, F., Kanai, K., Hirai, T., Sano, T., et al. (2012). Non-human primate model of amyotrophic lateral sclerosis with cytoplasmic mislocalization of TDP-43. Brain J. Neurol. *135*, 833–846.

Umemiya, M., and Berger, A.J. (1994). Properties and function of low- and high-voltage-activated Ca2+ channels in hypoglossal motoneurons. J. Neurosci. Off. J. Soc. Neurosci. *14*, 5652–5660.

Van Den Bosch, L., Van Damme, P., Bogaert, E., and Robberecht, W. (2006). The role of excitotoxicity in the pathogenesis of amyotrophic lateral sclerosis. Biochim. Biophys. Acta BBA - Mol. Basis Dis. *1762*, 1068–1082.

Vehviläinen, P., Koistinaho, J., and Gundars, G. (2014). Mechanisms of mutant SOD1 induced mitochondrial toxicity in amyotrophic lateral sclerosis. Front. Cell. Neurosci. *8*.

Viana, F., Bayliss, D.A., and Berger, A.J. (1993a). Multiple potassium conductances and their role in action potential repolarization and repetitive firing behavior of neonatal rat hypoglossal motoneurons. J. Neurophysiol. *69*, 2150–2163.

Viana, F., Bayliss, D.A., and Berger, A.J. (1993b). Calcium conductances and their role in the firing behavior of neonatal rat hypoglossal motoneurons. J. Neurophysiol. *69*, 2137–2149.

Viana, F., Bayliss, D.A., and Berger, A.J. (1994). Postnatal changes in rat hypoglossal motoneuron membrane properties. Neuroscience *59*, 131–148.

Viana, F., Bayliss, D.A., and Berger, A.J. (1995). Repetitive firing properties of developing rat brainstem motoneurones. J. Physiol. *486 (Pt 3)*, 745–761.

Vinsant, S., Mansfield, C., Jimenez-Moreno, R., Moore, V.D.G., Yoshikawa, M., Hampton, T.G., Prevette, D., Caress, J., Oppenheim, R.W., and Milligan, C. (2013). Characterization of early pathogenesis in the SOD1 ^{G93A} mouse model of ALS: part I, background and methods. Brain Behav. *3*, 335–350.

Vivekanandarajah, A., Chan, Y.L., Chen, H., and Machaalani, R. (2016). Prenatal cigarette smoke exposure effects on apoptotic and nicotinic acetylcholine receptor expression in the infant mouse brainstem. NeuroToxicology *53*, 53–63.

Vucic, S., and Kiernan, M.C. (2010). Upregulation of persistent sodium conductances in familial ALS. J. Neurol. Neurosurg. Psychiatry *81*, 222–227.

Whittington, M.A., Traub, R.D., and Jefferys, J.G. (1995). Synchronized oscillations in interneuron networks driven by metabotropic glutamate receptor activation. Nature *373*, 612–615.

Wijesekera, L.C., and Leigh, P.N. (2009). Amyotrophic lateral sclerosis. Orphanet J. Rare Dis. *4*, 3.

Williams, D.K., Wang, J., Papke, R.L. (2011). Positive allosteric modulators as an approach to nicotinic acetylcholine receptor-targeted therapeutics: advantages and limitations. Biochem. Pharmacol. *82*, 915-930.

Williams, T.L., Ince, P.G., Oakley, A.E., and Shaw, P.J. (1996). An immunocytochemical study of the distribution of AMPA selective glutamate receptor subunits in the normal human motor system. Neuroscience *74*, 185–198.

Wilson-Pauwels, L., Akesson, E.J., and Stewart, P.A. (2002). Cranial Nerves in Health and Disease (PMPH-USA).

Witzemann, V., Barg, B., Criado, M., Stein, E., and Sakmann, B. (1989). Developmental regulation of five subunit specific mRNAs encoding acetylcholine receptor subtypes in rat muscle. FEBS Lett. *242*, 419–424.

Woolf, N.J. (1991). Cholinergic systems in mammalian brain and spinal cord. Prog. Neurobiol. *37*, 475–524.

Yasuda, K., Robinson, D.M., Selvaratnam, S.R., Walsh, C.W., McMorland, A.J., and Funk, G.D. (2001). Modulation of hypoglossal motoneuron excitability by NK1 receptor activation in neonatal mice in vitro. J. Physiol. *534*, 447–464.

Yu, C.R., and Role, L.W. (1998). Functional contribution of the alpha7 subunit to multiple subtypes of nicotinic receptors in embryonic chick sympathetic neurones. J. Physiol. *509 (Pt 3)*, 651–665.

Zarei, S., Carr, K., Reiley, L., Diaz, K., Guerra, O., Altamirano, P.F., Pagani, W., Lodin, D., Orozco, G., and Chinea, A. (2015). A comprehensive review of amyotrophic lateral sclerosis. Surg. Neurol. Int. *6*.

Zoli, M. (2000). Neuronal Nicotinic Acetylcholine Receptors in Development and Aging. In Neuronal Nicotinic Receptors, P.D.F. Clementi, D.D. Fornasari, and D.C. Gotti, eds. (Springer Berlin Heidelberg), pp. 213–246.

Zoli, M., Pistillo, F., and Gotti, C. (2015). Diversity of native nicotinic receptor subtypes in mammalian brain. Neuropharmacology *96, Part B*, 302–311.